

New Synthetic Strategies to Tethered Bilayer Lipid Membranes

Dissertation zur Erlangung des Grades
'Doktor der Naturwissenschaft'

am Fachbereich Chemie und Pharmazie
der Johannes Gutenberg Universität Mainz

Catherine Breffa
Geboren in Strasbourg, Frankreich

Mainz, November 2005

Die vorliegende Arbeit wurde unter Betreuung von Herrn Prof. Dr. W. Knoll im Zeitraum zwischen Oktober 2002 bis November 2005 am Max Planck Institut für Polymerforschung, Mainz, Deutschland angefertigt.

"Don't worry about what anybody else is going to do.

The best way to predict the future is to invent it."

Alan Kay

Contents

1. Introduction.....	1
1.1. A biological membrane.....	1
1.2. Model membranes.....	3
1.2.1. Vesicles and liposomes.....	3
1.2.2. Black lipid membranes.....	4
1.2.3. Membranes on solid supports.....	4
1.2.3.1. Supported Bilayer Lipid Membranes (sBLM).....	5
1.2.3.2. Tethered Lipid Bilayer Membranes (tBLM).....	5
1.3. Motivation.....	6
2. Characterization methods.....	7
2.1. Structural information and purification.....	7
2.1.1. Nuclear magnetic Resonance (NMR).....	7
2.1.2. Mass Spectrometry.....	11
2.1.2.1. FD-MS.....	11
2.1.2.2. Maldi-ToF.....	12
2.1.3. Chromatography.....	12
2.1.3.1. General principle of chromatography.....	12
2.1.3.2. Size Exclusion Chromatography.....	13
2.2. Characterization of the bilayer.....	15
2.2.1. Contact angle.....	15
2.2.2. Surface Plasmon Resonance.....	17
2.2.2.1. Total reflection.....	17
2.2.2.2. Surface Plasmons.....	18
2.2.2.3. Measuring method.....	20
2.2.2.4. Experimental setup.....	23
2.2.3. Electrochemical Impedance Spectroscopy.....	24
2.2.3.1. Concept of complex impedance.....	24
2.2.3.2. Equivalent circuit.....	26
2.2.3.3. Measurements.....	28
3. Synthesis of longer spacers.....	29
3.1. Synthesis of DPTL in industry.....	29
3.1.1. DPTL description.....	30
3.1.1.1. Lipid headgroup.....	30
3.1.1.2. Hydrophilic spacer.....	30
3.1.1.3. Anchor group.....	30
3.1.2. DPTL synthesis at the industrial level.....	31
3.1.2.1. Experimental.....	32
3.1.2.2. Results and discussion.....	35
3.1.2.3. Conclusion.....	38
3.2. Synthesis of longer spacers.....	39
3.2.1. Motivation.....	39

3.2.2. Polymerization.....	39
3.2.2.1. Anionic polymerisation.....	40
3.2.2.2. Synthesis of oligoethyleneglycol via anionic polymerisation.....	41
3.2.2.3. Experimental.....	44
3.2.2.4. Conclusion.....	45
3.2.3. Synthesis of defined heterofunctionalized oligoethyleneglycols..	46
3.2.3.1. Experimental.....	47
3.2.3.2. Results and discussion.....	48
3.2.3.3. Conclusion.....	50
3.2.4. Precursor synthesis.....	51
3.2.4.1. Experimental.....	52
3.2.4.2. Results and discussion.....	54
3.2.4.3. Conclusion.....	55
4. Membrane formation, characterization and protein incorporation.....	57
4.1. How to build the system.....	57
4.2. Procedures.....	58
4.2.1. The substrate.....	58
4.2.2. Monolayer formation.....	59
4.2.3. Bilayer formation.....	64
4.2.4. Incorporation of proteins.....	65
4.3. Membrane formation with our systems.....	67
4.3.1. Polymer membranes.....	67
4.3.1.1. Monolayer formation.....	67
4.3.1.2. Conclusion.....	73
4.3.2. Tether molecules from defined synthesis.....	74
4.3.2.1. Monolayer and bilayer formation.....	74
4.3.2.2. Protein incorporation.....	79
4.3.2.3. Comparison between the different systems.....	83
4.4. Conclusion.....	85
5. Conclusion & Outlook.....	87
Literature.....	89
Appendix.....	93
Materials and Buffers.....	93
NMR and FD-MS spectra.....	94
Curriculum vitae.....	105
Acknowledgements.....	107

Abbreviations

CDCL ₃	Deuterated Chloroform
DCM	Dichloromethane
DPhyPC	DiPhytanyl Phosphatidyl Choline
DPHL	2,3,di-O-phytanyl-sn-glycerol-hexaethyleneglycol-lipoic acid ester lipid
DPOL	2,3,di-O-phytanyl-sn-glycerol-octaethyleneglycol-lipoic acid ester lipid
DPTL	2,3,di-O-phytanyl-sn-glycerol-tetraethyleneglycol-lipoic acid ester lipid
DPTDL	2,3,di-O-phytanyl-sn-glycerol-tetradecaethyleneglycol-lipoic acid ester lipid
EDC	1-Ethyl-3-(3-Dimethylaminopropyl)Carbodiimide
EE	Ethylacetate
EG	ethyleneglycol
EIS	Electrochemical Impedance Spectroscopy
EtOH	Ethanol
f	frequency
FD-MS	Field Desorption Mass Spectrometry
GPC	Gel Permeation Chromatography
HEPES	4-(2-HydroxyEthyl)-1-PiperazineEthaneSulfonic acid
HOBT	1-HydrOxyBenzotriazole
LB	Langmuir Blodgett
MALDI-ToF	Matrix Assisted Laser Desorption/Ionization Time-of-Flight
MHz	MegaHertz
MPOL	monophytanyl-octaethyleneglycol- α lipoic acid ester lipid
MPTL	monophytanyl-tetraethyleneglycol- α lipoic acid ester lipid
NMR	Nuclear Magnetic Resonance
PEG	polyethyleneglycol
R	gas constant
SA	Self Assembly
SAM	Self Assembled Monolayer
sBLM	supported Bilayer Lipid Membranes
SE	Solvent Exchange
SEC	Size Exclusion Chromatography
SPR	Surface Plasmon Resonance
T	Tesla
tBLM	tethered Bilayer Lipid Membranes
THP	tetrahydropyran
TLC	Thin Layer Chromatography
TMAC	Tetramethylammonium Chloride
TMA ⁺	Tetramethylammonium
TSG	Template Stripped Gold
VF	Vesicle Fusion
ω	angular frequency

1. Introduction

1.1. The biological membrane

Membranes play a central role in both the structure and function of all cells, prokaryotic and eukaryotic, plant and animal. Membranes basically define compartments, each membrane being associated with an inside and an outside. Membranes also determine the nature of all communication between the inside and the outside, as well as between two different cells. This may take the form of the actual passage of ions or molecules between the two compartments (in and out), or may be in the form of information, transmitted through conformational changes induced in the membrane components. Most of the fundamental biochemical functions in a cell involve a membrane at some point, which makes it a crucial part of the cell.

Even if they have very different functions, the basic structure is the same for all membranes. It mainly involves lipids and proteins, held together in a 2D matrix by non covalent interactions. Figure 1 represents the most commonly used model for a cell membrane, the fluid mosaic model, developed by Singer & Nicolson.^[1]

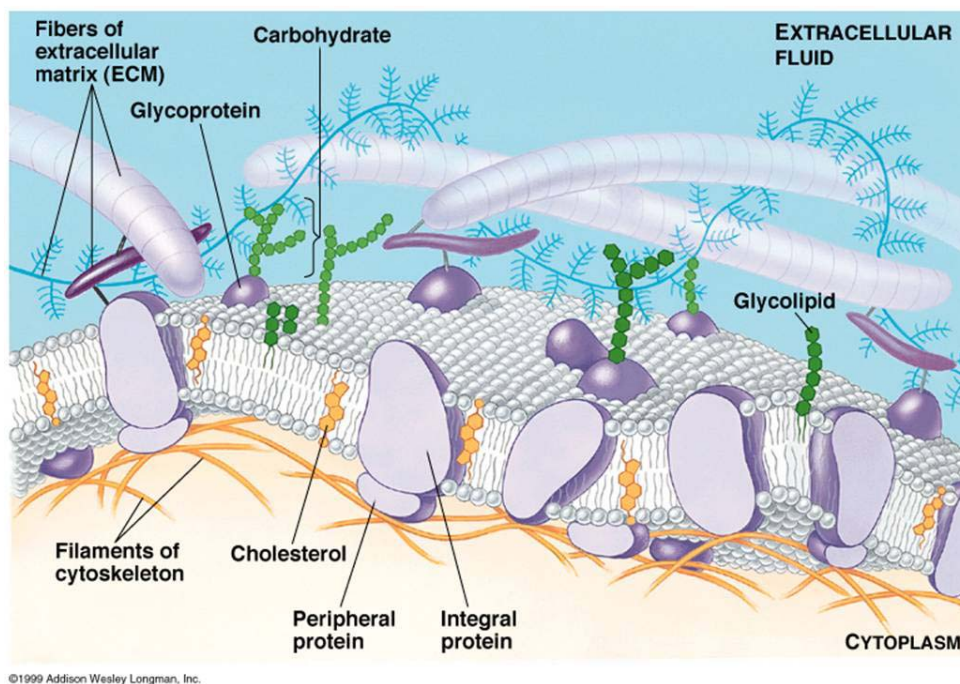


Figure 1: The fluid mosaic model described by Singer & Nicolson

The membrane is composed of proteins, which can be thought of as shifting tiles. The space between the tiles is filled with fluid-like phospholipids. Phospholipids consist of a hydrophilic head, which points towards the outside environment and the cytoplasm, and hydrophobic tails that repel the water and point in. Thus, as shown in Figure 2, the phospholipids form a bilayer that acts like a barrier between the cell and the environment. The phospholipid bilayer also contains cholesterol, which makes the bilayer stronger, more flexible and more permeable.

There are different types of membrane proteins: e.g. receptor proteins, which deal with communication across the cell membrane; recognition and transport proteins that regulate the transport of water and soluble molecules through the membrane. The protein amounts varies between 18% for nerve membranes and 70-80% for bacteria membranes, which must perform complex enzymatic and transport functions.^[2, 3] The density of a membrane is directly proportional to the amount of protein in the membrane (lipid = 80 Da, Protein = 100 000 Da).

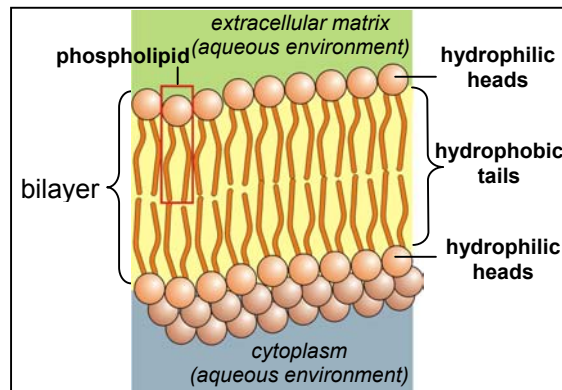


Figure 2: Details of a lipid bilayer

The complexity of the system and the number of parameters involved has made the membrane an extensive and exciting field of study for the past decades. Not only does the study of basic interaction mechanisms that are responsible for the structure and function of biological membranes trigger the attention of many research groups, but the study of membrane proteins should lead also to a better understanding of the complex correlations of metabolic processes.

Moreover, membrane proteins, such as channels or carriers, are responsible for the mass transport across the membrane. Therefore, membranes are a promising candidate for a platform for biosensing devices. Indeed, a membrane should provide a very reliable interface between the biological processes and the electronic recording system.

Because of the high complexity of the system, there is a need for a simplified model system. Here, we briefly present the models developed and the latest achievements and challenging fields of research for the next decades.

1.2. Model membranes

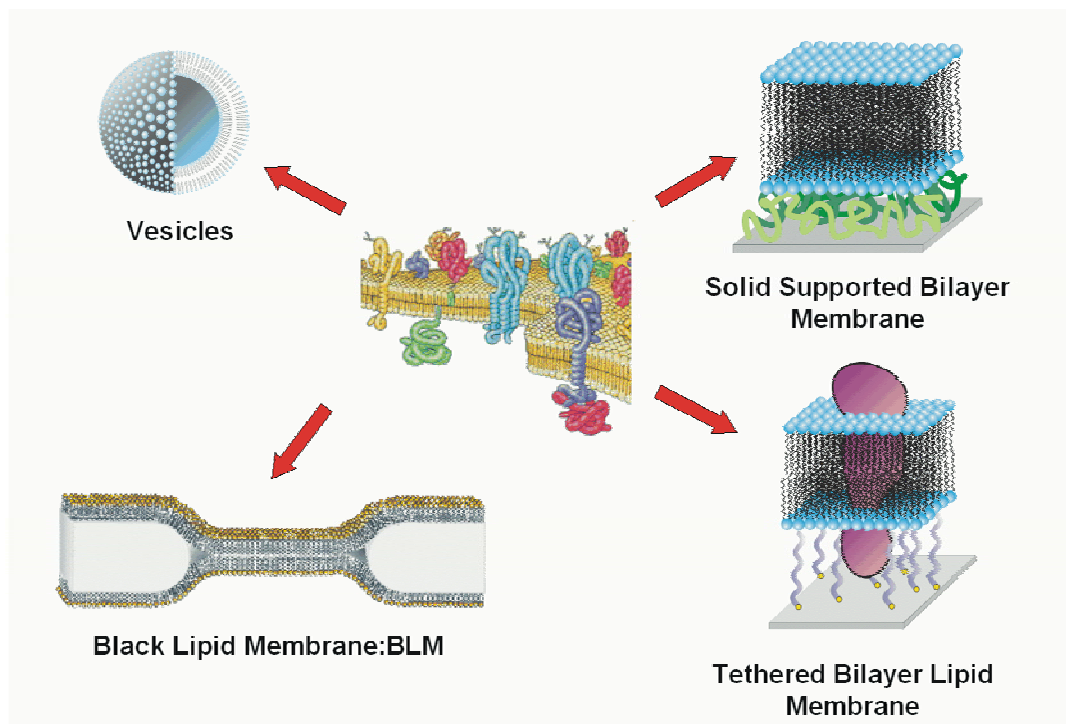


Figure 3: The biological membrane and its model systems.

To enable the study of the complex system of a membrane, as well as the functionality of single proteins, a series of different model systems was implemented. They have given enormous insight into the structure and function of biomembranes. Moreover, most of these systems are also optimised to provide an efficient platform for biosensors.

The strategy here is biomimesis: the model should mimic the membrane environment, but in a simplified manner, to decrease the number of parameters that come into play. The different models depicted in Figure 3 will be described in the next paragraphs.

1.2.1. Vesicles and liposomes

Phospholipids, when dispersed in water, spontaneously form a heterogeneous mixture of vesicular structures, which contain multiple bilayers forming a series of concentric shells. Of greater utility are unilamellar vesicles, which can be prepared by a variety of methods (e.g. extrusion, sonication, etc...).

Liposomes are of great use as model membranes, in which proteins are incorporated and measured via the patch clamp technique.^[4] It is also very common to encapsulate solutes in vesicles for use as drug delivery systems. Furthermore, vesicles of lipid mixtures allow for example to determine the phase transition temperature of the mixture.

The major drawback of these systems is the lack of stability. Vesicles aggregate to form liposomes, so they only have a definite size distribution for a few days. Moreover, they are very fragile when used for the patch clamp experiment.

However, polymer chemists got interested in this area and Meier et al^[5] obtained triblock copolymer vesicles bearing a high stability and reasonable biocompatibility. It was possible to observe the binding and uptake of such vesicles functionalised with a specific ligand by cells bearing the corresponding receptor.^[6] Moreover, the incorporation of membrane proteins was successfully performed in these vesicles^[7, 8], and a triblock copolymer ABC could even keep the orientation of the asymmetric membrane protein Aquaporin 0.^[9]

But these promising experiments cannot be generalized, and may seem too exotic to be used in applications requiring biocompatible materials. Therefore, the planar bilayer lipid membrane was developed.

1.2.2. Black lipid membranes

Traditionally, planar membranes are produced by painting a concentrated solution of phospholipids in a solvent, such as decane over a small hole (1 mm diameter) in a nonpolar partition (e.g. polystyrene) separating two chambers containing aqueous buffer. Much of the excess solvent disperses in the medium and under appropriate conditions the lipids spontaneously form a bilayer across the small hole. These membranes are frequently called bimolecular lipid membranes or BLMs. Because of the lack of light reflectance, they are also called black lipid membranes.

Such a setup allowed to measure the electrical properties of a pure lipid bilayer for the first time. It is possible to simulate the bilayer as a RC equivalent circuit, (see chapter 2.2.3.2.) with the following values, $R > 10^6 \Omega\text{cm}^2$, and $C \sim 0,5 \mu\text{Fcm}^{-2}$.

This system is particularly valuable for studying pores, channels or carriers that facilitate or catalyse the transfer of charges across the bilayer from one compartment to the other^[10, 11], using electrochemical measurements. High sealing properties are needed when it comes to single molecule measurements and BLMs provide this.

However, planar membranes formed in this way have the disadvantage of containing an unknown amount of residual solvent. Moreover, being spanned over this hole, mechanical constraints in the bilayer lower its stability, increase the probability of rupture and hinder the incorporation of proteins.

These first two model systems allowed the collection of useful information on the pure lipid bilayers and are still used today for many studies, for example translocation of molecules through a pore^[12]. However, the lack of stability makes these systems tedious to use.

The development of the new surface analysis techniques favored the development of new bilayer models on surfaces.

1.2.3. Membranes on solid supports

The major advantage of solid supported membranes is that numerous surface analysis methods such as AFM, SPR, QCM or FRAP can be applied.

1.2.3.1. Supported Bilayer Lipid Membranes (sBLM)

Sackmann was the first to develop the concept of supported bilayer lipid membranes (sBLM).^[13] Phospholipid bilayers can be formed on solid hydrophilic supports (glass, oxidized silicon wafer and others) by the sequential transfer of two monolayers from an air water interface or by vesicle fusion^[14-16]. A water layer (1-2 nm) is formed between the support and the lipid headgroups. The bilayers obtained are stable for a couple of hours, and are very convenient for physico-chemical studies of lipids and the study of proteins, ion channels as well as integral proteins^[17-19].

The inclusion of a hydrophilic polymer cushion between the bilayer and the solid support provides a soft deformable layer that can facilitate protein insertion and mobility.^[20, 21] Reconstitution of small membrane peptides was also achieved in S-proteins supported bilayers^[22, 23].

These supported membranes can also be used as a platform to tether vesicles.^[24, 25] This architecture proves to be very useful for studying membranes and integral membrane proteins, as well as their interaction with each other and the components in solution under conditions that approach a native environment. To increase stability, the lipids in the bilayers were polymerised, which yields a robust bilayer without adversely affecting the activity of the incorporated protein.^[26, 27]

However, this system presents disadvantages: the lifetime is still too short for practical sensing purposes, and the distance between the support and the membrane surface does not provide enough space for some proteins to sufficiently reconstitute. Moreover, the intrinsic sealing properties of vesicles of BLMs are not valid for sBLMs. It is believed that these drawbacks will be solved by tethered bilayers.

1.2.3.2. Tethered Bilayer Lipid Membranes (tBLM)

The tethered system is composed of a first monolayer attached covalently to the surface and a second monolayer of free lipids. The proximal layer is decoupled from the surface by a spacer group, mostly ethylene glycol, which provides space for incorporation of proteins bearing outer membrane parts, but also an ionic reservoir for the storage of ions underneath the membrane. The tethering system guarantees a mechanically and chemically robust attachment of the lipid bilayer to the support, but it also decouples the two elements sufficiently so as to allow the bilayer to remain in a fluid state.^[17] The membrane can then be used to incorporate membrane proteins.

The work of Cornell et al.^[28], Vogel et al.^[29] and Schiller et al.^[30, 31], show very promising results for tethered lipids as biosensing devices on gold surfaces. Similar systems were also attached on different electrodes such as mercury^[32] via thiol bonding, or silicon^[33] and glass^[34] using the silane chemistry, and show a functional incorporation of proteins.

Hybrid systems were developed to combine the advantages of different models. Steinem et al ^[35, 36] for example, developed the concept of nanoBLMs, where the membrane is formed on a porous substrate, namely alumina or silica. Lipid bilayers are suspended over the pores, whereas part of the membrane is supported on gold evaporated on the substrate. This system exhibits high stability as well as high resistances, and allows the incorporation of many different proteins.

Bushby et al ^[37] report on pseudo tethered vesicles utilizing a cholesterol tether, whereas Giess et al ^[38] describe a protein-tethered membrane, where the protein remains functional.

1.3. Motivation

In the frame of this project, tethered bilayer membranes were designed to form a generic platform suitable for transport membrane proteins. The system developed previously in our group ^[30, 31] allows the incorporation of several membrane proteins in combination with excellent electrical properties. However, the incorporation of large proteins, as well as of proteins with large submembrane parts, is still very difficult and therefore, further optimisation of the system is necessary. The right balance is required between a high packing of the membrane (high density to avoid defects and provide good sealing properties) and a good fluidity (to allow the incorporation of the protein).

This work is divided in two sections. Starting first from the previously synthesized architecture, a synthetic pathway was introduced to obtain a family of thiolipids with longer spacer lengths and different lipid headgroups. In chapter 3, we report on the different strategies developed to synthesize these molecules, first via polymerisation, then via defined synthesis using protected oligoethyleneglycols.

The thiolipids were then assembled on gold substrates via different methods and characterized for bilayer formation, as well as protein incorporation, using mainly electrochemical impedance spectroscopy (EIS). These experimental results are reported in chapter 4.

2. Investigation methods

This chapter is divided in two sections: the first one dedicated to the methods of investigation on the structure of the molecules synthesized and their purification. The second one is a short introduction to the methods used for the study of the membrane systems on surfaces.

In the first chapter, NMR (Nuclear Magnetic Resonance), FD-MS (Field Desorption Mass Spectrometry) and chromatography techniques are described. In the second chapter, Contact Angle, Surface Plasmon Resonance (SPR) and Electrochemical impedance Spectroscopy (EIS) are introduced. These explanations are not meant to be extensive but should give in a nutshell some basic principles of the techniques to get a better general understanding of them.

2.1. Structural information and purification

2.1.1. Nuclear Magnetic Resonance (NMR)

Nuclear magnetic resonance spectroscopy (NMR) is the most powerful tool available for organic structure determination. Experiments are performed on the nuclei of atoms, and the chemical environment of specific nuclei is deduced from the information obtained. NMR is a non invasive method and can be used with a very small amount of material. Here we will give a very brief description of the NMR phenomenon^[39].

- *Nuclear spin and the splitting of energy levels in a magnetic field.*

Electrons, protons and neutrons possess a fundamental property called spin. In many atoms, (such as ¹²C), these spins are paired against each other such that the nucleus of the atom has no overall spin. However, in some atoms (such as ¹H and ¹³C) the nucleus does possess an overall spin. In nuclear magnetic resonance, those nuclei with unpaired nuclear spins are of importance.

¹H NMR uses proton nuclei for measurements:

When placed in a magnetic field of strength B, a nucleus with the spin ½ has two possible orientations, i.e. energy states as can be seen in Figure 4. The particle can undergo a transition between the two energy states by the absorption of a photon of frequency ν . The frequency depends on the gyromagnetic ratio γ of the particle.

$$\nu = \gamma B$$

(for hydrogen, $\gamma = 42.58$ MHz/T)

The energy being related to the frequency by the Planck constant, $E = h \nu$. The energy of the photon needed to cause a transition between the two spin states is $E = h \gamma B$.

When the energy of the photon matches the energy difference between the two spin states, absorption of energy occurs.

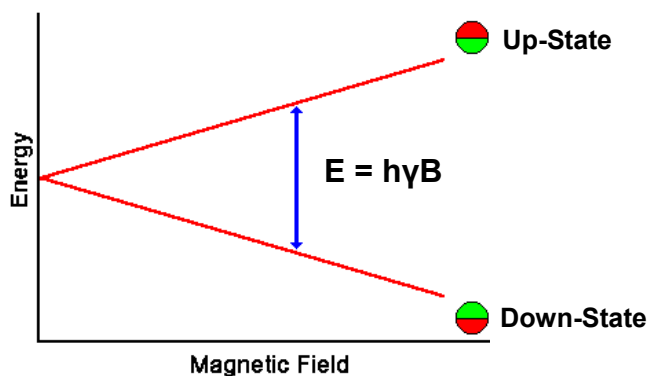


Figure 4: When a magnetic field is applied, the nucleus has two possible orientations. An absorption will occur if the energy of the photon matches the energy difference of the two states.

Macroscopically, when a group of spins is placed in a magnetic field, each spin aligns in one of the two possible orientations. The magnetic field due to the spins can be represented by a magnetization vector and is proportional to the population difference between the states. The signal in NMR is proportional to this population difference, which makes it a rather sensitive spectroscopy.

Motions in solution, which result in time fluctuations of the magnetic field, cause spin relaxation. There are two different relaxation processes, the spin-lattice relaxation defined by the time constant T_1 , and the spin-spin relaxation, defined by the time constant T_2 .

- *^1H NMR spectroscopy*

When an atom is placed in a magnetic field, its electrons circulate about the direction of the applied magnetic field. This circulation causes a small magnetic field at the nucleus which opposes the externally applied field. The magnetic field at the nucleus (the effective field) is therefore generally less than the applied field.

The electron density around each nucleus in a molecule varies according to the types of nuclei and bonds in the molecules. The opposing field and therefore the effective field at each nucleus will vary. This is called the chemical shift phenomenon.

The chemical shift is defined as nuclear shielding/applied magnetic field. The chemical shift is function of the nucleus and its environment. It is measured relative to a reference compound. For ^1H NMR, the reference is usually tetramethylsilane, $\text{Si}(\text{CH}_3)_4$.

Nuclei experiencing the same chemical environment or chemical shift are called equivalent. Nuclei, which are close to one another exert an influence on each other's effective magnetic field, this effect can be observed in the NMR spectrum when the distance between non-equivalent nuclei is less or equal to three bond lengths. This effect is called spin-spin coupling, or J coupling, and results in the splitting of the peaks. The complexity of the splitting pattern increases as the number of equivalent nuclei increases. (number of equivalent protons in neighbouring atom +1)

In pulsed NMR spectroscopy, the magnetization of the sample will induce a current in a coil of wire located around the X axis. Plotting current as a function of time gives a sine wave. This wave will decay with the time constant T_2^* due to dephasing of the spin packets. This signal is called a free induction decay (FID) and shown in Figure 5. This signal can then be Fourier transformed into a frequency domain spectrum.

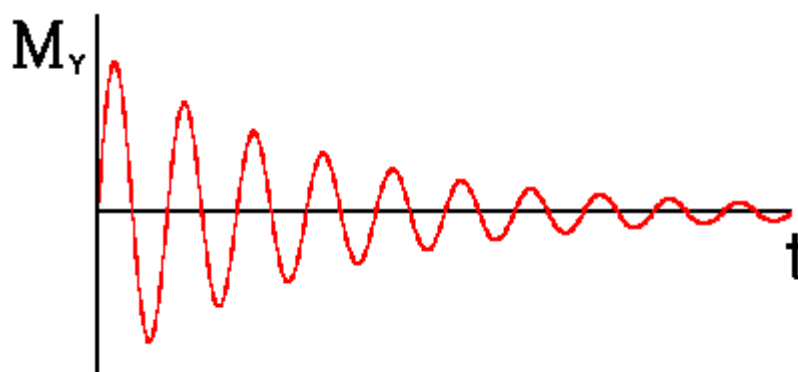


Figure 5: Signal collected by an NMR spectrometer: the free induction decay (FID)

Based on the number of allowed absorptions due to chemical shifts and spin-spin couplings of the different nuclei in a molecule, an NMR spectrum may contain many different frequency lines.

In addition to chemical shift and spin-spin coupling, there is one supplementary piece of information which one can use in determining the structure of a molecule. This information is the relative area of absorption peaks in the spectrum. The peak area is proportional to the number of a given type of spins in the molecule in the sample.

- *Practical considerations*

The samples used in this work were measured with a Bruker Biospin 250 MHz spectrometer using an automated software for the recording of the spectrum, ICON NMR 3.1.8.

The processing of the spectra was done with WinNMR and MestreC softwares.

In Figure 6, a typical ^1H NMR spectrum is shown. The areas of interest for the molecules described in this work are the following: around 1 ppm for all the methylene groups of the phytanyl chains (orange block), between 3 and 4 ppm, where the peaks for ethyleneglycol can be found (green block), and around 7 ppm for our protected molecules where the peaks of the benzyl group appear (blue area, but no peak present in this case).

If not otherwise stated, the samples were measured in CDCl_3 , which gives a peak at 7,24 ppm.

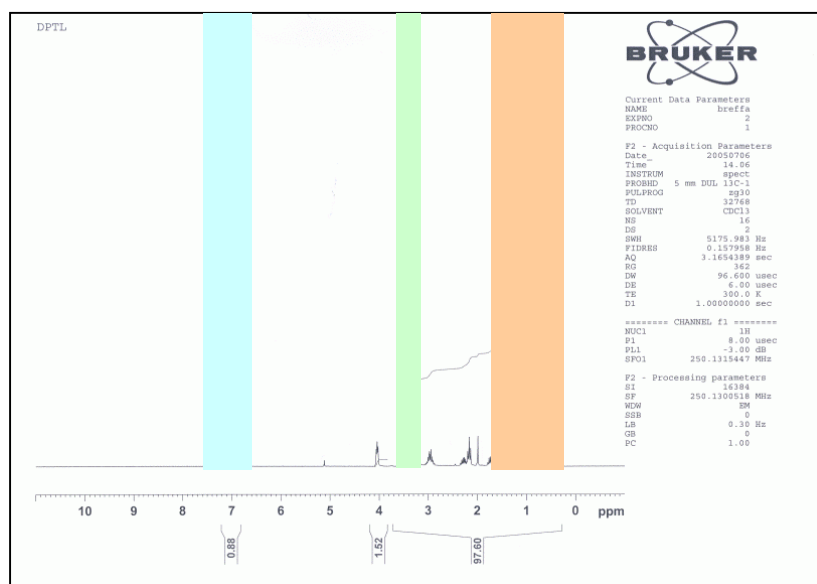


Figure 6: ^1H NMR spectrum of DPTL. The colored blocks show the areas of interest for our synthesis.

2.1.2. Mass spectrometry

Mass spectrometry provides the molecular weight and valuable information about the molecular formula, using very small amounts of material^[40].

A mass spectrometer ionises molecules in a high vacuum, sorts the ions according to their masses, and records the abundance of ions of each mass on a mass spectrum. There are many types of mass spectrometers and sample introduction techniques, which allow a wide range of analysis. The discussion here will focus on mass spectrometry as FD-MS for the study of low molecular weight molecules and as MALDI for the study of polymers.

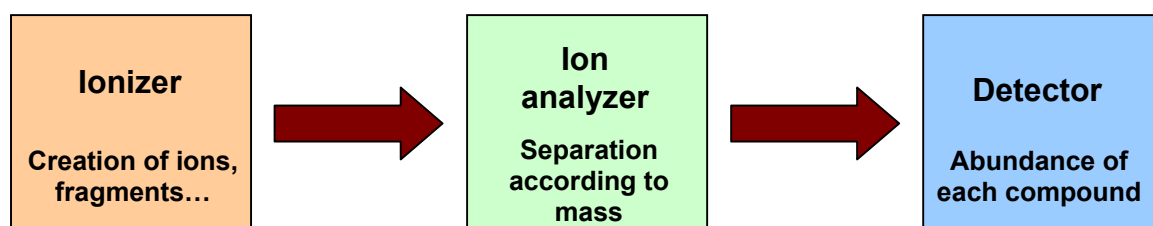


Figure 7: A general schematic of a mass spectrometer.

As depicted in Figure 7, all mass spectrometers consist of three distinct regions: the ionizer, the ion analyser and the detector.

In the ionizer, the analysed molecules are ionized. In the ion analyser, the ions are sorted via different methods, and finally, listed according to their mass and abundance by the detector.

2.1.2.1. Field Desorption Mass Spectrometry (FD-MS)

A spectrometer VG ZAB2-SE-FPD Spectrofield was used for the detection of molecules with low molecular weight.

The principle of field desorption is described in the literature^[41]. In our case, the sample, usually dissolved in CHCl_3 or acetone, is spread on graphite needles on a microscopic wire. This wire is then introduced in the ionisation chamber and a high potential (8kV) is applied. Ions are formed in the gas phase in the presence of this high electrical field and separated by a magnetic field. The abundance of the different compounds present in the sample is recorded by a photomultiplier.

This type of spectrometer can detect samples with masses in the range of 250 to 3500 g/mol, which allows one to use this method for all of the compounds synthesized via defined synthesis in this work.

2.1.2.2. Maldi-ToF

Matrix Assisted Laser Desorption/Ionization Time-of-Flight (MALDI-TOF) is a technique that offers a quick and easy method of mass analysis using a minimal amount of sample. The principles involved in the MALDI mass analysis can be seen in Figure 8.

For the determination of polymer molecular weights, a MALDI spectrometer was used. The important feature of this method lies in the sample preparation, which allows one to measure very fragile samples.

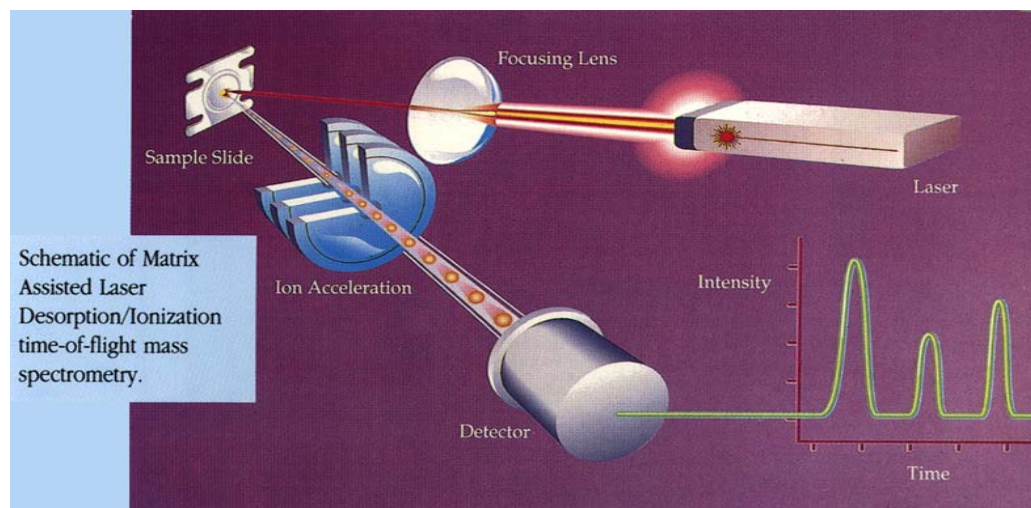


Figure 8: Principle of MALDI TOF

In fact, the sample is dispersed in a large excess of matrix material, which will strongly absorb the incident light. The matrix contains chromophores tuned to the laser light and since the matrix is in a large molar excess it will absorb essentially all of the laser radiation. The matrix isolates the sample molecules in a chemical environment, which enhances the probability of ionization without fragmentation. Short pulses of laser light focused onto the sample spot cause sample and matrix to volatilize.

2.1.3. Chromatography

2.1.3.1. General principle of chromatography^[42]

Chromatographic separation is a two phase separation method. It is a consecutive equilibrium process of analytes transitioning between a mobile phase and a stationary phase. A variety of chromatography methods exists and they are categorized according to the nature of the equilibrium process, which is essentially determined by the choice of the mobile and the stationary phase. The equilibrium constant K is a function of two thermodynamic parameters, ΔH° and ΔS° , associated with the solute partition process, solute in the mobile phase and solute in the stationary phase.

$$K = \frac{C_s}{C_m} = \exp\left(-\frac{\Delta G^\circ}{RT}\right) = \exp\left(-\frac{\Delta H^\circ}{RT} + \frac{\Delta S^\circ}{R}\right)$$

(Analyte concentration in mobile phase: C_m , stationary phase: C_s)

In this work, chromatography was used in two different cases, first for the purification of molecules and second to determine the molecular weight distribution of the polymers.

For the purification of the synthesized compounds, silica gel chromatography was used to separate the products from impurities using eluent gradients. According to the separation observed on the TLC (Thin Layer Chromatography) and to the amount of crude material to separate, different column sizes were used.

2.1.3.2. Size Exclusion Chromatography (SEC)

Size Exclusion Chromatography (SEC), also named Gel Permeation Chromatography (GPC), is commonly used in polymer chemistry to measure a molecular weight distribution. It is a separation method, which can, with the help of a calibration curve, determine the molecular weight distribution of a polymer.

Exclusion chromatography separates molecules on the basis of size, that is the hydrodynamic volume of the macromolecule, and not its molecular weight.

A column is filled with semi-solid beads of a polymeric gel that will admit ions and small molecules into their interior but do not accept large ones as is depicted in Figure 9.

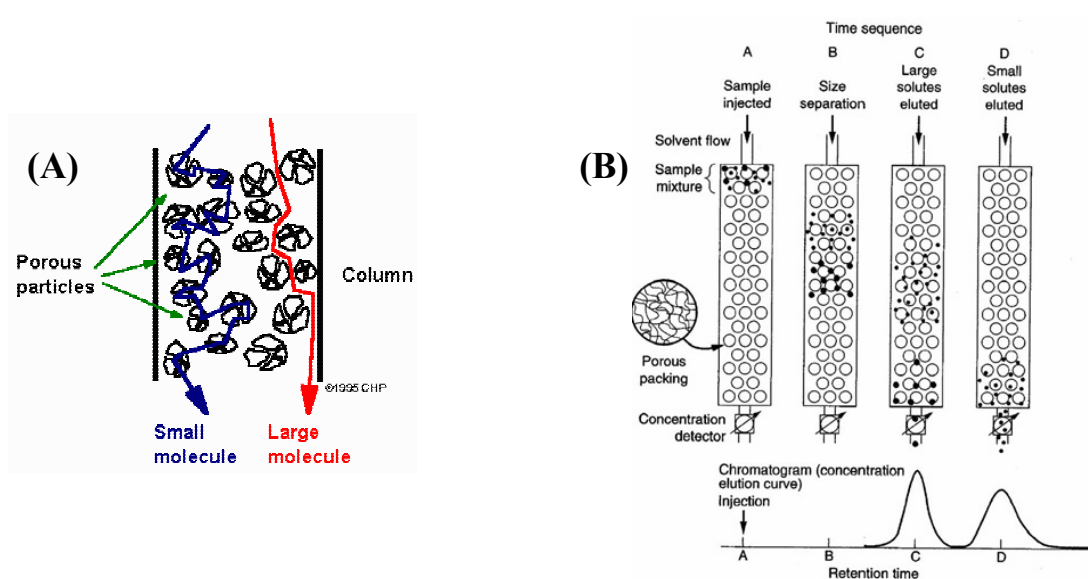


Figure 9: Chromatography method. A) Details of the polymeric gel and how the particles are separated according to their size. B) The process of separation in practice.

When a mixture of molecules and ions dissolved in a solvent, is applied to the top of the column, the smaller molecules (and ions) are distributed over a larger volume of solvent than is available to the large molecules. Consequently, the large molecules move more rapidly through the column, and in this way the mixture can be separated (fractionated) into its components as can be seen in Figure 9. The elution time of the polymer is governed by the time that it spends in the pores. Hence, larger molecules that spend less time in the pores elute first, and smaller molecules elute later.

The apparent molecular weight of polymer samples is determined by comparison of the chromatogram of a sample to that of standards with known molecular weight.

In practice, Polystyrene was used as calibration for our measurements because it was soluble in THF just like our compound. Polystyrene is not directly comparable to our polymer, but the spectra obtained give an idea about the molecular weight distribution of the sample.

2.2. Characterization of the membrane

2.2.1. Contact angle

Contact angle measurements consist of the analysis of the shape of a droplet on a surface. This method reveals information about the hydrophilicity of surfaces.

The theoretical description of contact arises from the consideration of a thermodynamic equilibrium between three phases^[43, 44]: the liquid phase (L) of the droplet, the solid phase (S) of the substrate, and the gas/vapor phase (V) of the ambient (which will be a mixture of ambient atmosphere and an equilibrium concentration of the liquid vapor). At equilibrium, the chemical potential in the three phases should be equal. It is convenient to frame the discussion in terms of interfacial energies. With the solid-vapor interfacial energy γ_{SV} , the solid-liquid interfacial energy γ_{SL} , and the liquid-vapor energy (i.e. the surface tension) γ , the Young equation describes the following equilibrium condition:

$$\gamma_{SV} = \gamma_{SL} + \gamma \cos \theta$$

Where θ is the experimental contact angle.

The measurement of the contact angle of a surface gives information about the hydrophilic character of the surface, as can be seen in Figure 10. On extremely hydrophilic surfaces, a water droplet will completely spread (an effective contact angle of 0°). This occurs for surfaces that have a large affinity for water (including material that adsorb water). On many hydrophilic surfaces, water droplets will exhibit contact angles of 10° to 30° . On highly hydrophobic surfaces, which are incompatible with water, one observes a large contact angle ($>90^\circ$). The contact angle thus directly provides information on the interaction energy between the surface and the liquid.

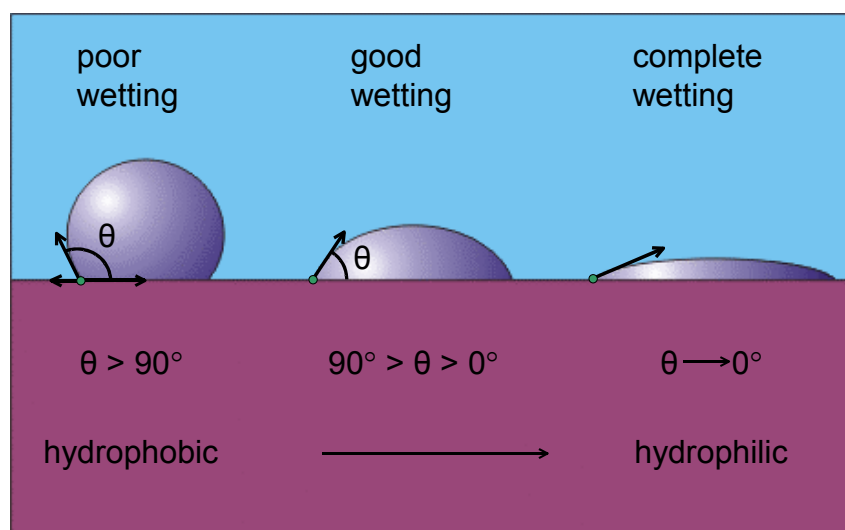


Figure 10: Three different situations for the contact angle

There are several methods to measure a contact angle. The method used in this work, is the sessile drop method. It is an optical contact angle method. This method is used to estimate wetting properties of a localized region on a solid surface. The angle between the baseline of the drop and the tangent at the drop boundary is measured, as can be seen in Figure 11.

Ideally, the droplet should be as small as possible because the force of gravity can actually change the contact angle. The shape of the droplet is determined by the Laplace equation. The contact angle plays the role of a boundary condition.

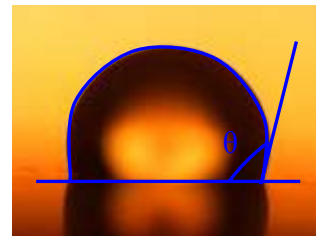


Figure 11: a sessile drop

The measurement of the static contact angle will help define the properties of the monolayer: it is a first insight into the quality of the monolayer and determines which strategy to use to form a bilayer. Typically, it is only possible to obtain a vesicle fusion on an highly hydrophobic surface ($\theta > 80^\circ$).

Experimentally, a 5 μl drop is recorded with a camera, while standing on the surface. The experimental setup, DSA 10 from Krüss CA, Germany, is depicted in Figure 12. The shape of the droplet is simulated with the software, Drop Shape analysis v1.5, and gives the static contact angle as a mean value of the angle of each side of the droplet.

In average, 5 measurements were used per slide to obtain a mean value of the contact angle.

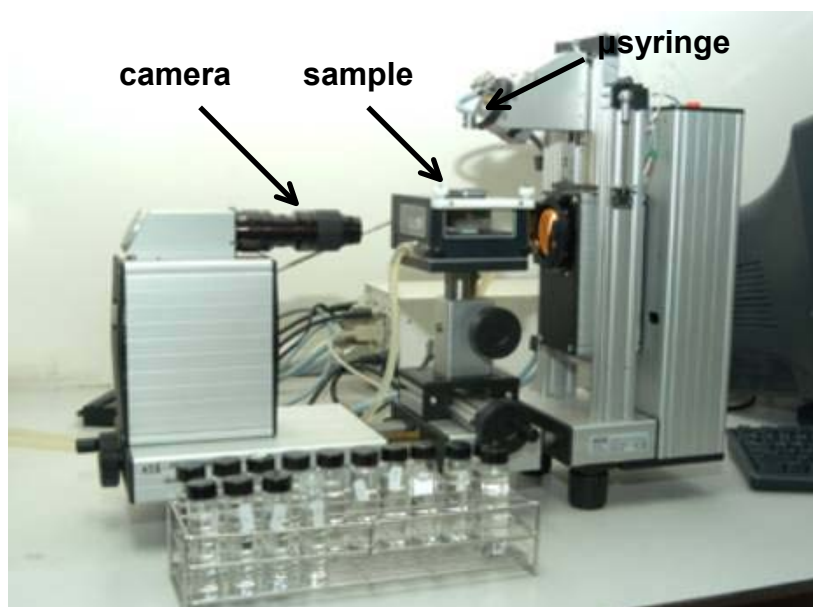


Figure 12: Picture of our contact angle setup.

2.2.2. Surface Plasmon Resonance

In the past years, surface plasmon resonance spectroscopy (SPR) has gained importance for the analysis of thin organic films. This method is especially well suited for the study of ultrathin dielectric layers.^[45, 46] In the following chapter the fundamentals about the method and the measurement principle will be described.

2.2.2.1. Total reflection

If a light beam reaches a surface dividing two media with different refractive indices n_1 and n_2 , a part of the incident light is transmitted and the other part is reflected. (see Figure 13) The angle of the incident light is equal to the angle of the reflected light.

If the transmission occurs from a medium with a high refractive index to a medium with a low refractive index, the angle of the transmitted light is higher than the angle of the incoming light. This phenomenon is described by Snell's law

$$n_1 \sin \theta_1 = n_2 \sin \theta_2$$

The critical angle, θ_c , is the angle where θ_2 , the angle of the transmitted light, reaches 90° . This angle is the limit of total reflection.

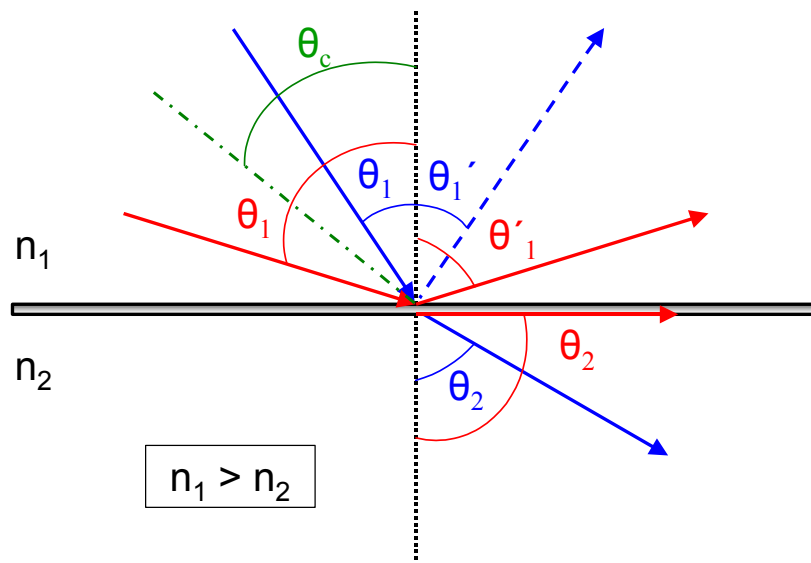


Figure 13: Reflection at the glass/dielectric interface. The angle of incidence or reflection is defined as the angle between the corresponding light beam and the normal to the surface.

This angle can be calculated according to Snell's law

$$\sin \theta_c = \frac{n_2}{n_1} \quad \theta_c = \text{critical angle}$$

According to Maxwell's theory, above θ_c , the optical E-field along the propagation direction, E_x , has the usual oscillatory character of an electromagnetic mode. The component perpendicular to the interface, E_z , however, does not fall to zero abruptly, but decays exponentially with a decay length l , which is a function of the angle of incidence.

$$l = \frac{\lambda}{2\pi\sqrt{(n \cdot \sin \theta)^2 - 1}} \quad \theta > \theta_c$$

Such an electromagnetic field distribution is called an evanescent field. The decay length is in the order of the wavelength of the incoming light.

2.2.2.2. Surface plasmons

If the beam reaches a metal surface in contact with a dielectric, then as described in the previous paragraph, a part will be reflected and a part of it will be transmitted. Additionally, it can lead to an interaction between the light and the electrons in the metal. This produces a collective movement of the nearly free electron gas of the metal, as shown in Figure 14. Because of their charge, the electrons of the free electron gas keep a certain distance from each other, and a pseudo lattice is created. The electrons can only move in a collective manner in this lattice.^[47] These collective excitation states of the quasi free electron gas of the metal are described as Surface Plasmon Polaritons.

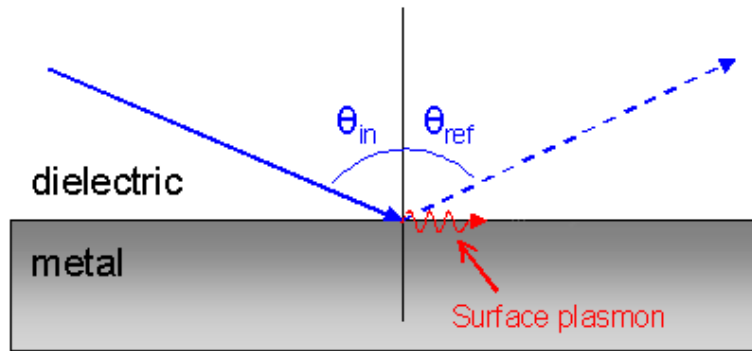


Figure 14: Reflection at an interface of a metal and dielectric. Surface plasmons are the collective oscillation of free electrons at the metal surface.

From the dispersion of plasmons along the metal/dielectric interface the following relation arises between the x component of the wave vector of the plasmon $k_{plasmon}$, and the dielectric functions of metal and dielectric medium, ϵ_M and ϵ_D .

$$k_{plasmon} = \frac{\omega}{c} \sqrt{\frac{\epsilon_M(\omega) \cdot \epsilon_D(\omega)}{\epsilon_M(\omega) + \epsilon_D(\omega)}}$$

To achieve the plasmon resonance with photons, the energy and momentum should be conserved. The wave vector of the photon k_{photon} in the dispersion direction has to be adapted to the wave vector of the plasmon k_{plasmon} to obtain a resonance.

Indeed, as can be seen in Figure 15, the dispersion curve of the plasmon and the photon in air do not intersect. This means that the momentum of a photon in air is too small to excite a plasmon. For a resonance, the momentum of light needs to be increased.

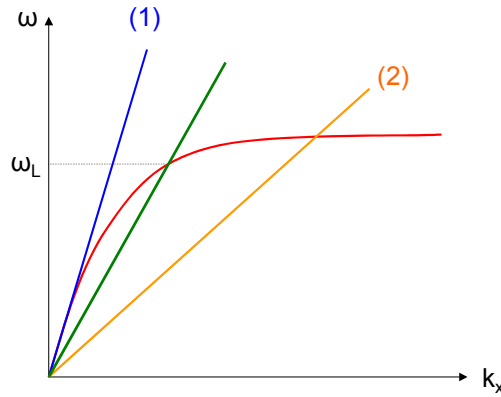


Figure 15: Dispersion relation of the photon (1) and the surface plasmon. The lines do not intersect. For a higher refractive index, there is an intersection (2), but which does not have the same frequency as the laser. Only if the angle is varied (3), there is a possibility to match the right frequency and then excite the resonance of the surface plasmon.

This is feasible with the increase of the dielectric constants, that is, by using a dielectric with a higher refractive index, for example a prism.

In prism coupling, the momentum of photons p is increased by the passage of the beam through a medium with a refractive index higher than 1. But only after the variation of the incoming angle it is possible to tune the wave vector in such a way that it matches the k_{plasmon} , as shown in Figure 16. When these two are equal, there is plasmon resonance. The evanescent field close to the surface causes a very intensive and sensitive interaction with the surface. Therefore, the surface plasmon spectroscopy is a suitable tool for the investigation of optical properties of thin films and layers.^[45]

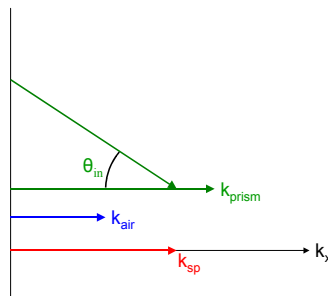


Figure 16: Representation of the prism coupling. The wave vector of a photon in air k_{air} is too short. Through coupling with the prism, it is possible to increase the wave vector. The wave vector of the prism is too long though. With the variation of the angle θ_{in} of the incoming light, the wavevector k_{prism} turns to match with the wavevector of the plasmon. At this angle, the plasmon resonance occurs.

Another option to match the two wave vector is to use grating coupling.^[48] The spectra obtained in this work were all measured with prism coupling, using the Kretschmann configuration.

In the Kretschmann configuration (Figure 17), the light is reflected at the basis of the prism. The evanescent field $E(z)$ enters into the thin metal film here (approx. 50 nm). At the accurate incoming angle, resonance occurs. The excited plasmon results in an electric field in the dielectric medium, which decays exponentially in the x and z axis.

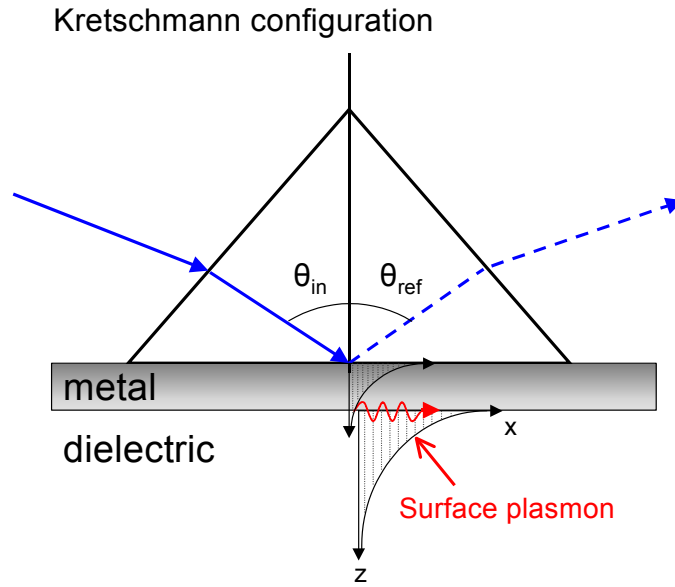


Figure 17: Schematic representation of the prism coupling in the Kretschmann configuration.

2.2.2.3. Measuring method

Reflection mode

As shown in Figure 18, in SPR spectroscopy, the reflectivity is detected as a function of the angle of the incoming light. The reflected intensity is constant until the so-called critical angle. At the critical angle θ_c , total reflection occurs while θ_0 denotes the resonance angle.

If a thin dielectric layer is adsorbed on the surface, the dispersion relation changes and the resonance angle will be shifted. The shift between the two angles is proportional to the optical thickness, which is the product of the difference between the two refractive indices and the film thickness d .^[49]

$$\Delta\theta = \theta_1 - \theta_0 \propto (N_{film} - N_{dielectric}) \cdot d$$

The relationship between the refractive index N and the complex dielectric constant ε is the following

$$\varepsilon = N^2 = (n + ik)^2 = n^2 + 2ikn - k^2 = \varepsilon' + i\varepsilon''$$

with n = real part of the refractive index

k = imaginary part of the refractive index (corresponds to the absorption)

ε' = real part of the dielectric constant ($\varepsilon' = n^2 + k^2$)

ε'' = imaginary part of the dielectric constant ($\varepsilon'' = 2kn$)

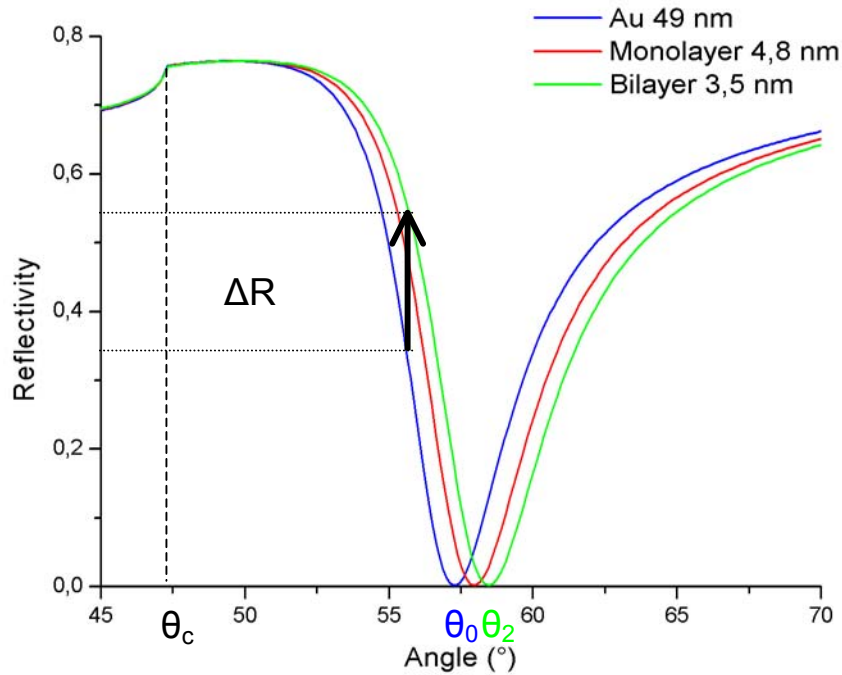


Figure 18: Simulated reflectivity curve of the surface plasmon resonance. θ_c is the critical angle of the total reflection. The minimum of reflectivity at the angle θ_0 shows the existence of a surface plasmon at the interface metal / dielectric.

If the layer on the metal surface is non absorbing, then the imaginary part disappears (is equal to zero) and the dielectric constant is $\varepsilon' = n^2$. For known refractive index, Fresnel equations translate a shift of angle to a thickness of the layer. This relation represents the fundamentals of the plasmon spectroscopy, but also shows the difficulty in this method. Refractive index and thickness are related to each other. Therefore, one of the two quantities needs to be determined by another method or known from an independent source.

In our case, the refractive indices used for the different components of our system are the following:

LASFN9: prism $n = 1,84$

Au: $n = 0,178$; $k = 3,07$ (www.sopra-sa.com), values which are then fit to the gold thin layers

Dielectric layer(lipids): $n = 1,45$

In this work, all reflection curves were fit with the help of the Winspall software, developed in the Max Planck Institute. The software calculates the Fresnel coefficients of the layer system with a recursion formalism.^[50]

Because reference slides are used for the gold parameters for slides of the same batch, only relative thicknesses can be determined. Indeed, the monolayer is formed on the slide without measuring the parameters before, to avoid any contamination of the gold surface.

Kinetic mode

In a kinetic measurement, the change in intensity of the reflected light is measured at constant angle.^[49, 51] The formation of a new layer results in an increase ΔR in intensity of the reflected light as shown in Figure 18. This increase in intensity corresponds to a shift of the resonance angle θ_0 .

A typical kinetic curve is shown in Figure 19. After a specific time, there are only very slight changes in reflectivity until the curve reaches a plateau.

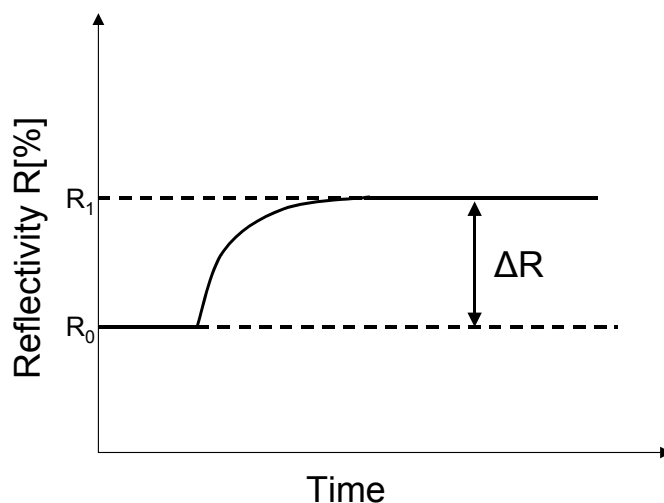


Figure 19: Change in the plasmon resonance with time. The increase in intensity of the reflected light is measured at a constant angle.

Kinetic measurements allow the investigation of adsorption processes. Moreover, qualitative aspects of the adsorption can be observed. A fast adsorption, for example, results in a very sharp slope.

In our case, the kinetic measurements allow us to observe vesicle fusion on our monolayers. An increase of approximately 4 nm is expected.

2.2.2.4. Experimental setup

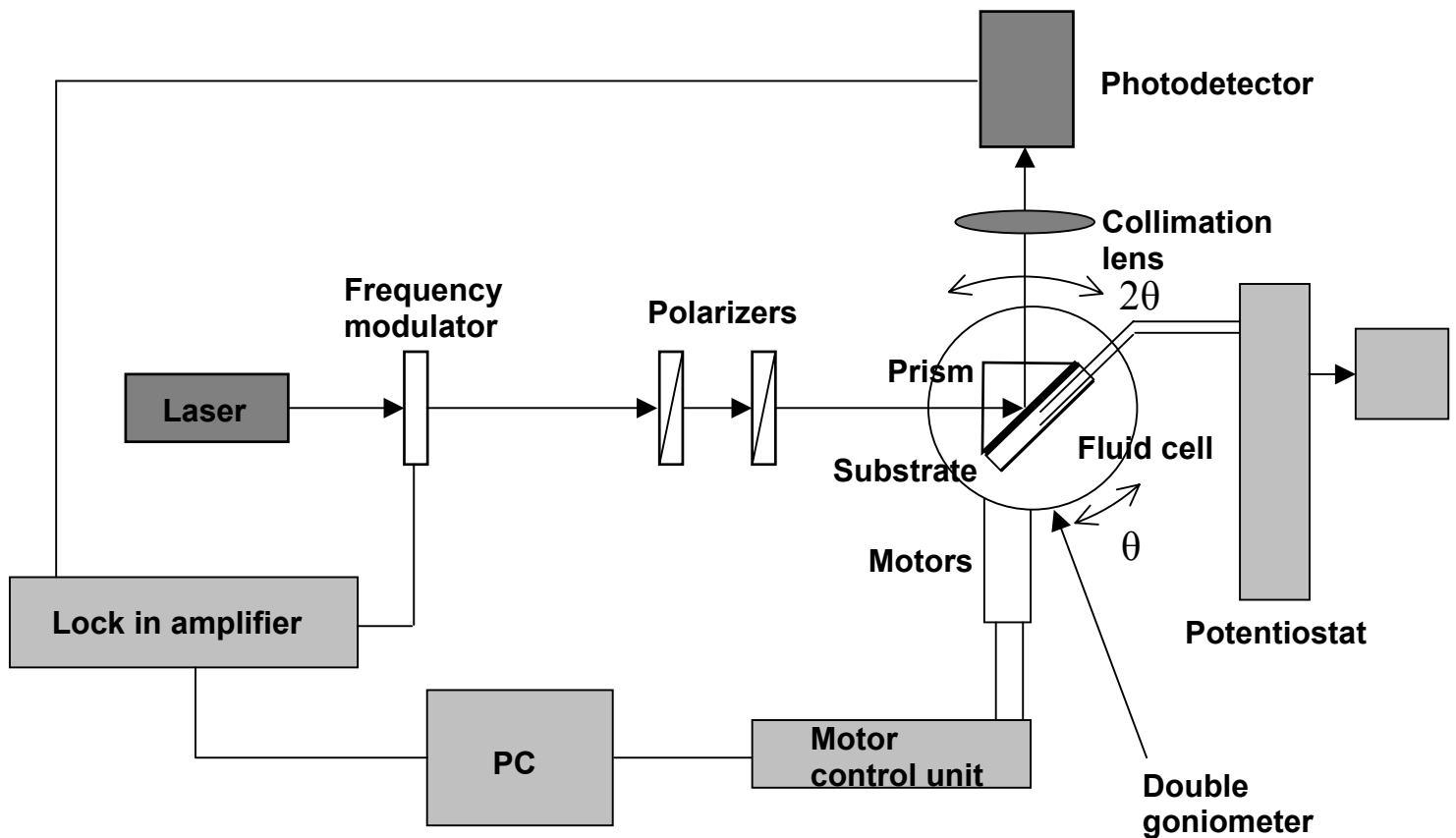


Figure 20: Experimental setup coupled with EIS.

The experimental setup used in our study allows the simultaneous recording of SPR and EIS spectra. The scheme represented in Figure 20 shows the setup for the plasmon spectroscopy, where the reflectivity of a multilayer system is determined. The beam of the HeNe Laser ($\lambda = 632,8 \text{ nm}$) is periodically modulated by a frequency modulator. This frequency is transmitted to the Lock-in amplifier as a reference signal to filter noise.

The beam passes two polarizers, to tune the intensity and to set the polarization. Finally, the beam reaches a 90° prism (LaSFN9, a high refractive index glass), which is optically matched to our glass substrate with the help of a matching oil ($n = 1,7$).

On the other side of the substrate, there is template stripped gold (see chapter 4.2.2.), on which surface plasmons can be excited, and a flow cell. This system (prism/substrate/cell) is mounted on a goniometer, which can be moved with two precise motors.

The reflected light is collimated with the help of a biconvex lens on a Si photodiode. The outgoing voltage is proportional to the intensity of the reflected light.

2.2.3. Electrochemical Impedance Spectroscopy

Impedance spectroscopy is especially suitable for the determination of the electrical properties of complex systems. In many aspects, this is the method of choice for the characterization of materials whose electrical properties are governed by a variety of coupled processes, with different time constants^[52]. More recently, impedance spectroscopy gained importance in biophysics, since it enables the characterization of dielectric biomaterials or to transduce signals from organic systems for sensoric applications.^[28] Several studies of organic molecules that are attached to solid supports or lipid membranes containing proteins have been reported.^[13, 53, 54] Impedance spectroscopy is a non-invasive and label-free technique, and biological systems can be analysed in their natural environment^[55-57]. Therefore this method is particularly suited for the study of ion transport through bilayer membranes.

2.2.3.1. Concept of complex impedance

The concept of electrical resistance is well known and is defined by Ohm's law. Resistance is the ability of a circuit element to resist the flow of electrical current, mathematically expressed as $R = E/I$, where R is the resistance in ohms, E is voltage in volts, and I is current in amperes.

However, this relationship is limited to only one circuit element, the ideal resistor. An ideal resistor has several simplifying properties: it follows Ohm's law at all current and voltage levels. Its resistance value is independent of frequency and AC current and voltage signals through a resistor are in phase with each other.

The real world contains circuit elements that exhibit much more complex behaviour. Impedance is a more general circuit parameter. Similar to resistance, impedance is a measure of the ability of a circuit to resist the flow of electrical current. Unlike resistance, impedance is not limited by the simplifying properties listed above.

Electrochemical impedance is usually measured by applying an AC potential to an electrochemical cell and by measuring the current flow through the cell. The current response to a sinusoidal potential will be a sinusoid at the same frequency but shifted in phase, as can be seen in Figure 21.

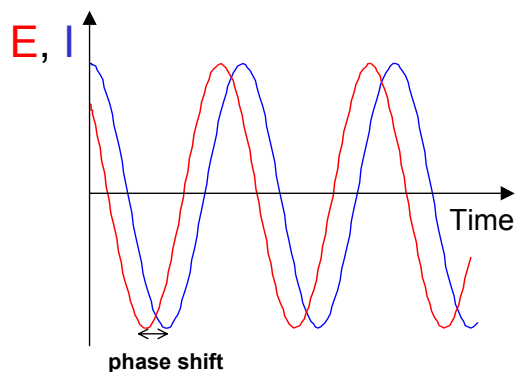


Figure 21: Current and voltage as a function of time. The current response is shifted in time.

The excitation signal, expressed as a function of time has the form $E(t) = E_0 \cos(\omega t)$
 $E(t)$ is the potential at time t , E_0 is the amplitude of the signal, and ω is the radial frequency ($\omega = 2\pi f$)

In a linear system, the response signal $I(t)$ is shifted in phase and has a different amplitude I_0 .

$$I(t) = I_0 \cos(\omega t - \phi)$$

An expression analogous to Ohm's law allows us to calculate the impedance of the system as

$$Z = \frac{E(t)}{I(t)} = \frac{E_0 \cos(\omega t)}{I_0 \cos(\omega t - \phi)} = Z_0 \frac{\cos(\omega t)}{\cos(\omega t - \phi)}$$

The impedance is therefore expressed in terms of a magnitude, Z_0 and a phase shift ϕ .

Using Euler's relationship, it is possible to express the impedance as a complex function. The potential described as $E(t) = E_0 \exp(j\omega t)$ and the current response as $I(t) = I_0 \exp(j\omega t - j\phi)$, the impedance is then represented as a complex number

$$Z = \frac{E}{I} = Z_0 \exp(j\phi) = Z_0 (\cos \phi + j \sin \phi) \quad \text{with } j^2 = -1.$$

There are two different major principles to obtain impedance spectra $Z(\omega)$. The measurements can be performed in the time domain or as in this work, in the frequency domain. The frequency domain, or harmonic measuring method, applies a sinusoidal voltage signal $E(t)$ causing a current response $I(t)$. Here the polar coordinates for a certain frequency are $Z_0(\omega) = E_0(\omega)/I_0(\omega)$ and $\phi(\omega)$. The perturbation amplitude E_0 should be small in order to maintain a linear response of the system, in general in the range of the thermodynamic fluctuations of 25 mV. The spectra are obtained by sequential measurements of $E(t)$ and $I(t)$ for different frequencies over a certain amount of periods.

The obtained impedance spectra are plotted in the so-called Bode plot, where the absolute value $Z(\omega)$ and the phase shift $\phi(\omega)$ is presented as a function of frequency, as can be seen in Figure 22.

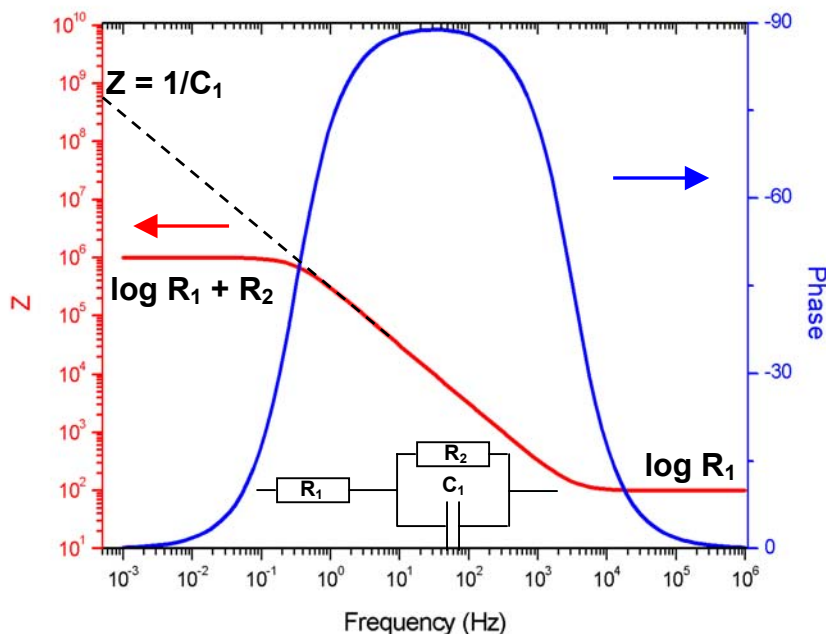


Figure 22: Bode plot for a simple electrochemical system

The Bode plot has some distinct advantages over other representations. Since frequency appears as one of the axes, it is easy to understand from the plot how the impedance depends on the frequency. The plot uses the logarithm of frequency to allow a very wide frequency range to be plotted on one graph. The Bode plot also shows the magnitude (Z) on a log axis so that wide impedance ranges can be easily plotted on the same set of axes. This is an advantage for the identification of small impedances in the presence of large ones.

2.2.3.2. Equivalent circuit

In order to quantify the electrical properties of the system under investigation, it is necessary to construct a theoretical model circuit consisting of electrical components, and exhibiting the same impedance behavior.

With these so-called equivalent circuits, the evaluated impedance data can be converted into physical understanding^[52]. It should be mentioned that any model circuit must be understood as simplification of the real system, since many minor contributions can not be resolved and must be neglected. In addition, the circuits are not imperatively unique, especially if the amount of consisting elements becomes large. Theoretical and experimental impedance spectra were fit using a non-linear curve fitting algorithm.

The equivalent circuit elements used throughout this work are summarized in Table 1. In order to analyze the obtained impedance spectra, different circuits composed of only a small number of these elements are developed later in the chapter.

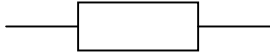
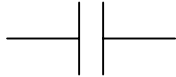
Resistance R		$Z_R(\omega) = R$
Capacitance C		$Z_C(\omega) = -j / \omega C$

Table 1: Different equivalent circuit elements used throughout this work. The symbols are given together with their names and the complex impedance as a function of frequency ω .

Even if the amount of elements is kept small, the equivalent circuits provide a large amount of information about the complex hybrid system under study. Resistances and capacitances are denoted as ideal elements, since they assume ideal properties of the system. For real systems, it is possible to introduce special, so-called distributed elements taking into account for example the size restriction, the finite permeability or inhomogeneity.

However, to keep it simple, an approach using equivalent systems composed of ideal elements was considered. With this approach, it was possible to evaluate electrical parameters of the multilayer system.

Indeed, the Bode plot contains all information needed to determine the values of the equivalent circuit. In a Bode plot representing the simple equivalent circuit (see Figure 22), the $\log Z$ vs. $\log \omega$ curve can yield values of R_1 and R_2 . At the highest frequencies shown in Figure 22, the ohmic resistance dominates the impedance and $\log R_1$ can be read from the high frequency horizontal plateau. At the lowest frequencies, polarization resistance also contributes, and $\log (R_1 + R_2)$ can be read from the low frequency horizontal plateau. At intermediate frequencies, this curve should be a straight line with a slope of -1 . Extrapolating this line to the $\log Z$ axis at $\omega = 1$ yields the value of the capacitor C from the relationship $Z = 1/C$.

The Bode plot format also shows the phase angle, θ . At the high and low frequency limits, where the behavior of the circuit is resistor-like, the phase angle is nearly zero. At intermediate frequencies, θ increases as the imaginary component of the impedance increases. The ZVIEW software allows to determine the values of the equivalent circuit using a simulation/fitting curve.

The equivalent circuits used to describe our system are of two kinds, as depicted in Figure 23.

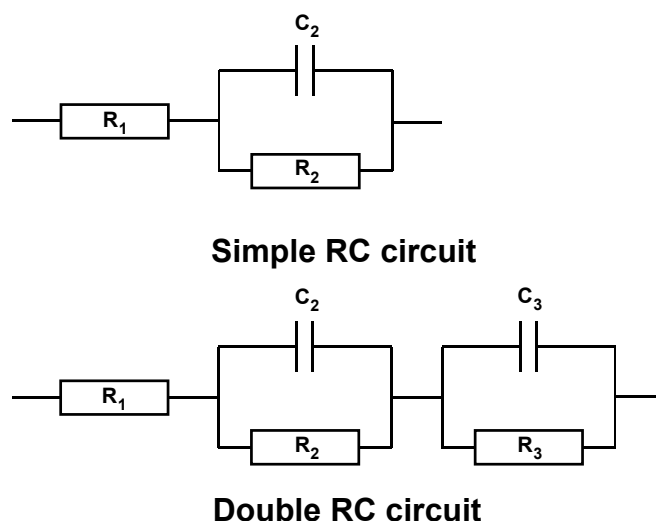


Figure 23: Equivalent circuits used in this work

The first one is a simple circuit, which is often used to describe the electrical properties of a self-assembled monolayer.^[30] In this reference, the circuit was also used to describe bilayer formation as well as protein incorporation. Physically, the resistance R_1 corresponds to the feed resistance of the solvent, with a typical value of around 100Ω , whereas the RC element corresponds to the membrane part, and bears values similar to natural membranes. However, it was not possible to use this circuit in our case. There was a need to introduce a second RC element to have a more faithful description of the system. In this case, the bilayer contribution is split into two RC elements, the first attributed to the spacer part of the tBLM system and the second due to the lipid double layer. Even with this circuit, it was not always possible to obtain a very good fit, but it allowed to compare the values obtained for the different stages of the construction of the system, and also to compare the different systems.

2.2.3.3. Measurements

The impedance spectra throughout this work were recorded in the frequency domain, using an Autolab PGSTAT 12 impedance spectrometer with the FRA (Frequency Response Analysis) software.

Typical spectra were recorded with 40 different frequencies between 1 MHz and 0,002 mHz using a perturbation amplitude of $E_0 = 10$ mV. Raw data were analysed using the ZVIEW software package (version 2.70, Scribner Associates).

Three electrodes measurements were performed in Teflon cells with the substrates as the working electrode, a coiled platinum wire as the counter electrode and DRIREF-2 reference electrodes from World Precision Instruments. The in-house Teflon cells have a buffer volume of 0,5 mL and an open electrode area of 0,385 cm² (SPR-EIS cell) or 0.2 cm² (EIS cell). The obtained values for the equivalent circuit are normalized to the electrode surface area.

3. Synthesis of longer spacers

The investigation of tethered bilayers is a new field of research, which is still in its infancy. The search for an ideal model membrane involves the optimisation of existing molecules and of the bilayer formation (e.g. with respect to the best electrical properties). Nevertheless, commercial products have their limitations and therefore, there is a need for new molecules designed especially for that purpose and fulfilling the required criteria.

First, the synthesis of a new family of tethered bilayer lipids will be described, and the strategies investigated to achieve this purpose. The synthetic goal of this thesis was to obtain a range of molecules that could be investigated for membrane formation on surfaces. The proof of principle is the important factor that is driving us in this study. To be able to perform a series of electrical measurements, only a small amount of compound is needed. Therefore, different synthetic pathways were investigated, and the molecules obtained were tested for membrane formation. This allowed us to tune the requirements to obtain the best compound.

In 2003, a molecule was synthesized in our group^[30, 31] that can form tBLMs which fulfill most of the criteria that describe a good membrane. In a collaboration with Diverchim (www.diverchim.com), the modification of the synthetic route has been investigated in order to scale up the synthesis to an industrial format. The first part of this chapter will describe this scale up synthesis. The following chapters will show our attempts to prepare a new family of thiolipids based on the model of DPTL, using polymerisation first, then changing to defined synthesis, using heterofunctionalized ethylene glycol chains and a step by step synthesis, with a monoprotected tetraethylene glycol precursor.

3.1. Synthesis of DPTL in industry

DPTL was first synthesized in our group some years ago^[31]. The good electrochemical characteristics of DPTL allowed for the incorporation and the study of different proteins such as channels, ion carriers etc...^[30, 31] To protect this new type of molecules, a patent was issued (27726P). To give an opportunity to exploit this patent, as well as to supply our group (and the market) with a reasonable amount of the product, I went to Diverchim, a small research company in Montataire, France. My target was to synthesize the molecule with the lab equipment available and to transfer the know-how.

3.1.1. DPTL

DPTL is a thiolipid that is composed of three distinct parts as shown in Figure 24: a lipid head, a hydrophilic spacer and an anchor group. Each of these parts has to fulfil certain criteria, always with respect to its influence on the membrane formation processes or on the membrane properties.

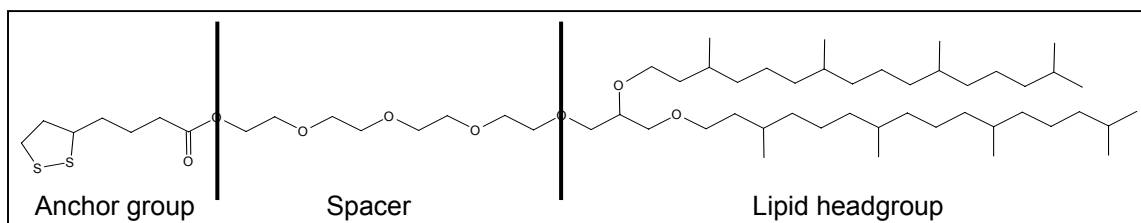


Figure 24: The DPTL molecule 2,3,di-*O*-phytanyl-*sn*-glycerol-1-tetraethylene-glycol-*D,L*- α lipoic acid ester lipid

3.1.1.1. Lipid headgroup

The lipid headgroup helps to form the proximal lipid monolayer according to Van der Waals interactions between the hydrocarbon tails. The lipids used in this work are based on archaea analogue models (isoprenoid tails linked by glycerol). The archaea type bacteria possess membranes keeping a high fluidity under very harsh conditions of pressure, pH or temperature^[58]. Moreover, these membranes are in the fluid state at room temperature, due to the methyl side groups which hinder crystallization. Lipid headgroups with phytanyl chains were used in different model thiolipids.^[28, 29] A single phytanyl chain, however, does not form stable membranes.

3.1.1.2. Hydrophilic spacer

The spacer, as noted in the introduction, should decouple the membrane from the surface and provide a submembrane space. Moreover, to mimic a bilayer membrane in a more realistic way, the spacer should provide an ion reservoir underneath the membrane, similar to the cytosol of a real cell. In DPTL, the ion reservoir is made of four ethylene glycol units. This oligomer has a fully stretched helical structure in contrast to longer polymers having a mushroom like conformation. Studies of PEG (polyethyleneglycol) are reported in the literature showing that polymer cushions under the membranes are very good ionic reservoirs.^[20, 21]

3.1.1.3. Anchor group

The anchor group provides stability of the proximal layer of the membrane through the covalent bonding of the thiol group with gold. Lipoic acid, which was used in the case of DPTL, provides a disulfide bridge, which is more stable than a simple thiol bond. After the adsorption on the Au surface, a tilted monolayer is formed.^[59]

The all ether bonds (except for lipoic acid) provide a higher stability than ester bonds which can be hydrolyzed.

3.1.2.1. Experimental

Reaction a: Hydrogenation of Phytol according to Bendavid et al ^[60]

Phytol (25 g, 87.6 mmol, 296.5g/mol) was introduced in a 200 ml autoclave with 60 ml ethanol and purged 3x with N₂. Then, Raney Nickel (8 g, 10 %wgt, 58.69 g/mol) was introduced, and the autoclave was purged 3x with N₂ and 2x with H₂. A hydrogen pressure of 2 bars was applied and the reactor was left stirring overnight. The end of the reaction was determined by ¹H NMR.

The mixture was filtered over a Celite plug to remove the catalyst, and the filter residues were rinsed thoroughly to dissolve the product in the filtrate. The solvent was removed under reduced pressure. The product **1** is a colorless oil.

M = 25,5 g (ρ = 100%)

Ref NMR : **1** (Figure 69)

Notes :

Care should be taken with Raney Nickel, 50% slurry in water. Because of ignition, the reaction should be performed under inert atmosphere !

A 1 M HCl solution is used to deactivate the Nickel catalyst. Due to the building of a Nickel-Chloride complex, the solution becomes light green.

Reaction b: Opening of the epoxide ring

Glycidyl tosylate (20g, 87.6 mmol, 1 eq, 228,27 g/mol) was introduced in a 500ml 3 necked round flask under N₂ and diluted in 300 ml DCM. Then **1** (28.8g, 96.5 mmol, 1.1 eq, 298.5 g/mol) was added. Boron etherate (800 μl, 5 mol%) was added dropwise with the help of a syringe, the mixture turns to light orange and the reaction mixture was left stirring overnight.

The next morning, a TLC check showed the reaction was over.

Eluent : Heptane/Ethylacetate

Ratio : 1/1

Developer : KMnO₄

300 ml water were added and the two phases separated. The aqueous phase was extracted 3x with DCM. The organic phases were dried over MgSO₄ and filtered. The solvent was removed under vacuum.

A purification via column chromatography in Heptane/Ethylacetate starting with 95/5, gave a colorless oil.

M = 32,3 g (ρ = 70%)

Ref NMR **2** (Figure 70)

Notes : Care should be taken with BF₃.Et₂O, it is a very corrosive Lewis acid.

Reaction c: Formation of an epoxide

2 (6g, 11.39 mmol, 1 eq, 526.83g/mol) was introduced in a 250 ml 3 necked round bottom flask under N₂, and 120 ml methanol was added. The mixture was cooled to 0°C. Then, K₂CO₃ (3.15g, 2 eq) was added in small amounts, and the mixture was left stirring for 3 h at 0°C.

A TLC check showed the reaction is finished.

Eluent : Heptane/Ethylacetate

Ratio : 7/3

Developer : Phosphomolybdic acid

The reaction mixture was poured in saturated NH₄Cl, then Et₂O was added. The phases were separated and the aqueous phase was extracted 3x with Et₂O. The organic layers were washed with brine until the aqueous phase reached pH 7.

The organic phases were collected and dried over MgSO₄. The solvent was removed under vacuum, to give a colorless oil used without further purification.

M = 3,8 g ($\rho = 94\%$)
Ref NMR **3** (Figure 71)

Notes:

If all the base is not neutralized, it will lead to an opening of the epoxide ring by methanol during evaporation of the solvent!

A column chromatography can be used in case of incomplete reaction.

Reaction d: Monoprotection of a tetraethyleneglycol moiety

Tetraethylene glycol (70 ml, 79.1g, 407 mmol, 4 eq, 194.2 g/mol), NaOH 50% in H₂O (17 ml) and Benzyl Bromide (12,2 ml, 17.4g, 102 mmol, 1 eq, 171.04 g/mol) were introduced in a 3 necked bottom flask and refluxed for 24h at 100°C. ($T_{\text{bath}} = 130^{\circ}\text{C}$)

After 24h, the mixture was cooled, then H₂O was added and the aqueous layer was extracted 4x with Et₂O. The organic layers were dried over MgSO₄ and filtered. The solvent was removed under vacuum.

The product was purified via flash chromatography with Heptane/Ethylacetate as eluent to give a slightly yellow oil.

M = 19,2 g ($\rho = 66\%$)
Ref NMR **4** (Figure 72)

Reaction e: Opening of the epoxide ring with a TEG moiety

3 (5g, 14.1 mmol, 1 eq, 354.6 g/mol) was introduced in a 3 necked round flask and diluted in 100 ml DCM. Then **4** (4.4g, 15.47 mmol, 1.1 eq, 284.3 g/mol) was added. Boron etherate (100 μl , 5 mol%) was added dropwise with the help of a syringe, the mixture turned to dull orange and the reaction mixture was left stirring overnight.

The next morning, a TLC check showed the reaction was over.

Eluent : Heptane/Ethylacetate

Ratio : 1/1

Developer : PhosphoMolybdic acid

The crude product was dissolved in water and extracted 3x with DCM. The organic phases were collected and dried over MgSO₄. Then the solvent was removed under vacuum to give a yellow oil.

A column chromatography was performed in Heptane/Ethylacetate to give a light yellow oil.

M = 3,32 g ($\rho = 37\%$)
Ref NMR **5** (Figure 74)

Reaction f: Obtention of Phytol Iodide according to patent n° US 2,315,580 (1940) Germany 321067 (1939)

A mixture of Phytol (15 g, 50.6 mmol, 296.5 g/mol) and 150 ml HI was stirred vigorously overnight.

A TLC check showed the reaction is over.

Eluent : Heptane

Developer : KMnO₄

The organic layer was washed several times with ice water and then it was dried over MgSO₄ with a small amount of DCM, filtered and evaporated, to give a dark pink oil, which was used without further purification.

M = 29,4 g ($\rho = 100\%$)
Ref NMR **6** (Figure 75)

Notes: Phytol Iodide is not very stable. Therefore, this compound should be prepared only a few hours before use. Another option is to prepare the bromide, and substitute it with NaI at the very last moment.

Reaction g: Substitution of Phytol Iodide

The reactants **5** (4.6 g, 7.22 mmol, 1 eq, 636.98 g/mol), **6** (15 g, 36 mmol, 5 eq, 406.44 g/mol) and TBABr (234 mg, 0.72 mmol, 0.1 eq, 322.36 g/mol) were introduced in a flask with DCM/NaOH and stirred vigorously via a mechanic stirrer during one night.

A TLC check was performed the next day.

Eluent : Heptane/Ethylacetate

Ratio : 1/1

Developer : KMnO₄

NH₄Cl (5-10 ml) was added to the reaction mixture then the two phases were separated. The aqueous phase was extracted with DCM and the organic layers were washed with brine. They were then dried over MgSO₄ and filtered. The solvent was removed under vacuum.

The mixture was purified via column chromatography with Heptane/Ethylacetate as eluent to give a yellow oil.

M = 3,2 g ($\rho = 50\%$)

Ref NMR **7** (Figure 76)

Reaction h : Hydrogenation and deprotection of **7**

7 (3.2 g, 3.5 mmol, 1eq, 917.5 g/mol) and 40 ml acetic acid were introduced in a 200 ml autoclave and rinsed 3x with N₂. Then the catalyst Pd/C (0.32 g, 10 w%) was added, and the autoclave was purged 3x with N₂. Then it was purged 2x with H₂ and finally the pressure was set around 8 bars.

The reaction was followed by ¹H-NMR.

When the reaction was over, the reaction mixture was filtered over a Celite plug to remove the catalyst. New catalyst was added and the reaction was started again. (Pressure around 8 bars)

When the pressure stabilizes, the reaction is stopped, the reaction mixture was filtered over a Celite plug to remove the catalyst, and the catalyst was rinsed many times to get all the product dissolved in the filtrate. The solvent was removed under reduced pressure. A coevaporation with toluene helps to remove the acetic acid. The product is a white gel, which is used without further purification.

M = 3,6 g ($\rho = 100\%$)

Ref NMR **8** (Figure 77)

Reaction i : Coupling with lipoic acid

Lipoic acid (1.49 g, 2.41 mmol, 1 eq, 829.39 g/mol) was dissolved in 40 mL DCM in a 100 ml 3 neck bottom flask under N₂ to give a yellow solution. DIEA (2.33 g, 18.08 mmol, 2.5 eq, 129.25 g/mol) was added, and then the solution turned to transparent yellow. HOBT (1.075 g, 7.96 mmol, 1.1 eq, 135.13 g/mol) is added and then slowly EDC (1.526 g, 7.96 mmol, 1.1 eq, 191.71 g/mol). The mixture was left stirring for 30 min.

Then, the lipid (2g, 2.41 mmol, 0.33 eq, 829.39 g/mol) dissolved in a minimum of DCM was added to the mixture, and it was left stirring over night.

A TLC check showed that the reaction was over.

Eluent : Heptane/Ethylacetate

Ratio : 7/3

Developer : KMnO₄

40 ml DCM were added and the organic layer was washed 3x with sat. K₂CO₃ then 3x with brine. The organic phases were collected and dried over MgSO₄ and filtered. The solvent was removed under vacuum.

The product was purified via column chromatography DCM/MeOH to give a yellow oil.

M = 1,6 g ($\rho = 65\%$)

Ref NMR **9** (Figure 78)

3.1.2.2. Results and discussion

The starting point for this synthesis was to use the available glycidyl tosylate as a base to attach the different chains. The epoxide reactivity allows one to functionalize the three available oxygen atoms selectively.

In the following section, I will give a description of the reaction mechanisms and the synthetic strategies used in this project.

Hydrogenation of phytol to phytanol

In the first step, the hydrogenation of phytol to phytanol was performed, using Raney Nickel as a catalyst (in EtOH).

Mechanism.^[61]

The hydrogenation is a heterogeneous catalytic reaction, which happens at the surface of the catalyst as shown in Figure 26. Hydrogen gas is adsorbed onto the surface of the catalyst, and the catalyst weakens the H-H bond. A phytol molecule adsorbs at the surface of the catalyst, at the place of the double bond. Then the available hydrogen atoms insert into the π bond at the catalyst surface. The molecule is released from the surface of the catalyst, allowing another molecule to come and start the process again.

Because the two hydrogens add from a solid surface, they add with syn stereochemistry. Both hydrogen atoms add to the face of the double bond that is complexed with the catalyst. Contamination of the catalyst will hinder the reaction.

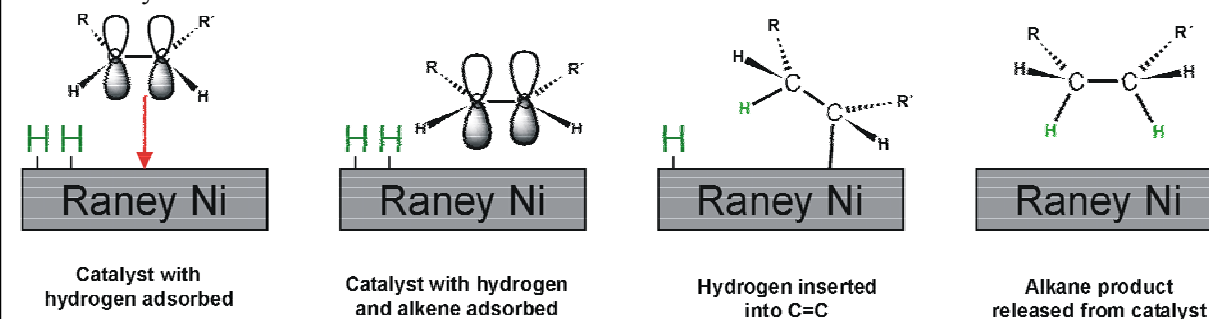


Figure 26: Hydrogenation reaction with Raney Nickel as a catalyst. Raney Nickel adds two hydrogen atoms to the same face of the π -bond (syn stereochemistry)

The reaction can be followed by NMR. The peaks corresponding to the C-C double bond should disappear completely when the reaction is complete as can be seen in Figure 69. Yields around 100% can be obtained. The use of Raney Nickel instead of PtO₂ decreases the reaction times and is more reliable.

The ease of use of Raney Nickel catalyst makes it the catalyst of choice for our reaction. However, care should be taken that it never becomes dry, otherwise the very reactive Ni atoms may ignite.

Opening of an epoxide with an alcohol

The second and fourth steps involve the opening of the epoxide ring with nucleophiles catalysed by $\text{BF}_3 \cdot \text{Et}_2\text{O}$.

Epoxides have served as important synthetic intermediates because of their high chemical reactivity, ease of preparation, and availability in optically active forms. In our case, an epoxide allows to selectively functionalize each oxygen atom of the glycerol moiety separately. Therefore, a method developed by Bittman was used^[62, 63]. $\text{BF}_3 \cdot \text{Et}_2\text{O}$ is described as the material of choice to perform the double opening of the epoxide.

Mechanism

BF_3 is a Lewis acid and provides the opening of the epoxide by attracting electrons from the oxygen atom. Boron trifluoride has an empty orbital which will attract the free electrons of the oxygen. This weakens the bonds of the epoxide. Phytanol as a nucleophile (electrons of the oxygen atom) can then attack one of the carbon atoms neighboring the epoxide, see Figure 27. Usually, it is the less substituted, because there is less steric hindrance. The oxygen belonging to the epoxide is protonated. The BF_3 catalyst is then ready to be used again.

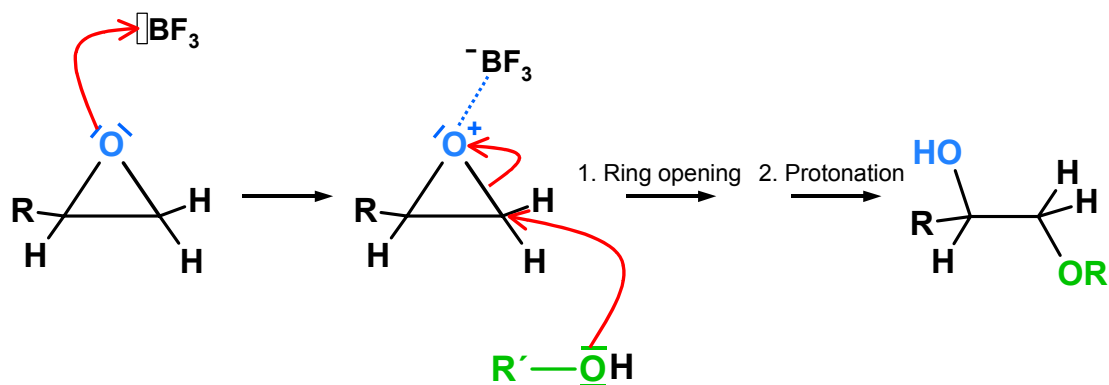


Figure 27: The opening of an epoxide

The second opening consists in the addition of a protected tetraethyleneglycol to the glycerol part. This is the critical part of the synthesis, different strategies were tested, including NaH as opening helper in different solvents and at different temperatures and $\text{BF}_3 \cdot \text{Et}_2\text{O}$ as catalyst. It was not possible to improve the yield more than 37%. Water contained in the protected tetraethyleneglycol may be one reason for deactivation of the catalyst, or formation of a side product, by opening the epoxide. Moreover, the intermediate species formed before protonation can act as a nucleophile to attack another epoxide and lead to another side product.

Formation of an epoxide

The third step is the formation of an epoxide ring using a base. This reaction is almost quantitative and very fast. Though, first trials according to literature^[62, 63] included a workup without neutralization of the base. In the presence of base, the methanol was nucleophilic enough to open the epoxide ring. The product obtained was a methoxyglycerol. To solve this problem, the reaction mixture was first neutralized with NH_4Cl and then extracted with ethylether and brine. The new workup allowed to obtain the expected product with very high yields, up to 95 %.

Mechanism, see Figure 28

An alkoxide ion and an appropriate leaving group are needed in this reaction. To obtain the alkoxide ion, the starting reagent is treated with base to remove the proton. If the alkoxide ion and the leaving group are located in the same molecule, the alkoxide may displace the leaving group and form a ring. Treatment of the alcohol with a base leads to an epoxide through internal S_N2 reaction.

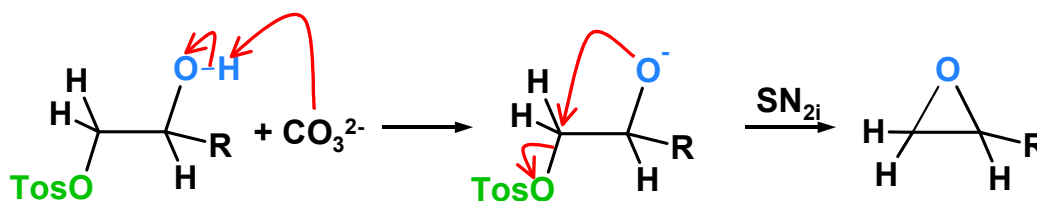


Figure 28: Base mediated formation of an epoxide

Usage of benzyl protection group

The Benzyl protecting group is a very convenient group because it is UV visible, so it is easy to track via TLC. Moreover, it has the advantage of being easily detected by NMR, since the signals of the benzyl group are significantly separated from the other signals of moieties present in the molecule.

A catalyst in the presence of acid was used to cleave the benzyl group. Pd/C is a catalyst commonly used for the cleavage of the benzyl group. In our case, it could simultaneously reduce the carbon double bond present in the molecule.

Phase transfer reaction to substitute the last free hydroxy group

The addition of phitylbromide or -iodide was tried with the usual NaH deprotonation scheme, but it was not successful, presumably because of the lack of availability of the OH group due to steric hindrance in the middle of the two chains. To overcome this problem, a phase transfer reaction was performed, which gives very good yields and is very convenient in practice.

As shown in Figure 29, this methodology consists in the use of a heterogeneous two-phase systems, one aqueous phase being a base for generation of organic anions, whereas organic reactants and catalysts (source of lipophilic cations) are located in the second, organic phase. The reacting anions are continuously introduced into the organic phase in the form of lipophilic ion-pairs with lipophilic cations supplied by the catalyst. Most often, tetraalkylammonium cations serve as phase transfer catalysts. ^[64]

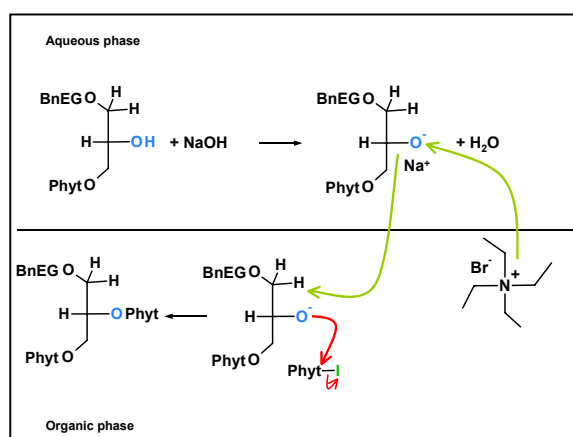


Figure 29: Phase transfer reaction

Ester coupling using activated esters

Finally, the functionalization with lipoic acid was performed using a peptide coupling agent, which can also be used for esterification. Indeed, the ester group can be prepared directly from the carboxylic acid using peptide coupling reagents like EDC/HOBT. EDC (1-ethyl-3-(3'-dimethylaminopropyl)carbodiimide) has been used as a coupling reagent for the last 15 years. In combination with HOBT, this reaction gave fair yields (> 65%).

Mechanism

The mechanism of the carbodiimide activation, which is complex and depends on the solvent, starts by a proton transfer, followed by addition of the carboxylate to form the O-acylisourea, as shown in Figure 30. This is the most reactive species that can attack the alcohol to give the corresponding peptide. However, this urea can undergo rearrangement and lead to many side products, which are not reactive. The HOBT reactive esters, formed by substitution of the carbodiimide group, are less reactive than the O-acylisourea, but are more stable and less prone to racemize. All these factors make the addition of benzotriazole derivatives almost mandatory to preserve the ester formation by carbodiimide formation of low yields and undesired side reactions.

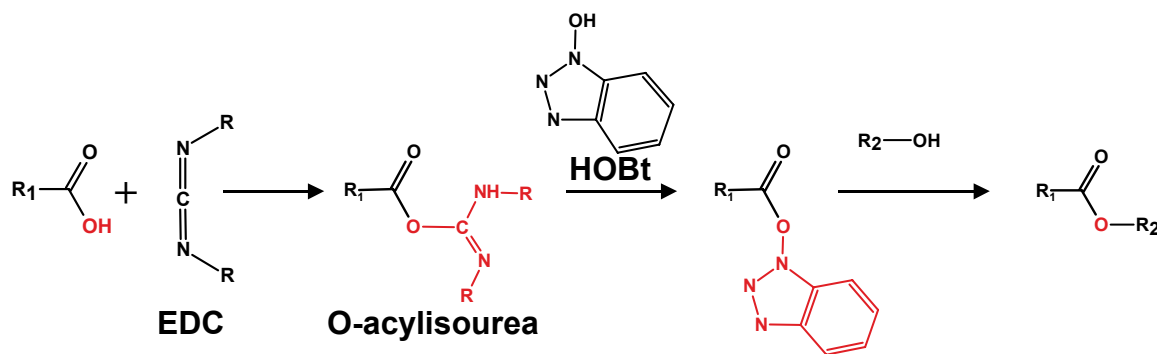


Figure 30: Esterification via EDC/HOBT

3.1.2.3. Conclusion

DPTL was successfully synthesized in a decigram scale using a different pathway than reported in the literature, suitable for a larger industrial scale synthesis. Furthermore, this synthesis, compared to the previous one reported in the literature, allows to keep the optical activity of the glycerol part.

This period allowed the exploration of a new synthetic route, which can lead easily to a new range of compounds, for example, the synthesis of lipids with two different hydrocarbon tails, or the synthesis of translipids that may both be interesting components of a tethered membrane.

3.2. Synthesis of longer spacers

3.2.1. Motivation

DPTL is a very efficient molecule, allowing the formation of bilayers and the incorporation of different proteins.^[30] Though, larger proteins, especially those having a large submembrane part, often do not incorporate. Indeed, the submembrane space provided by the spacer is not big enough to host such proteins. One improvement of the system could be an increase of the submembrane space. Thus, there is a need for a family of molecules to study the influence of spacer length on the membrane properties, as well as on protein incorporation.

Our approach was to design molecules keeping the same components as DPTL, that is lipoic acid as an anchor group, archaea analogues as lipid headgroup to retain the quality of the bilayer and to use oligoethyleneglycol in different lengths to increase the spacer beneath the bilayer (see Figure 31).

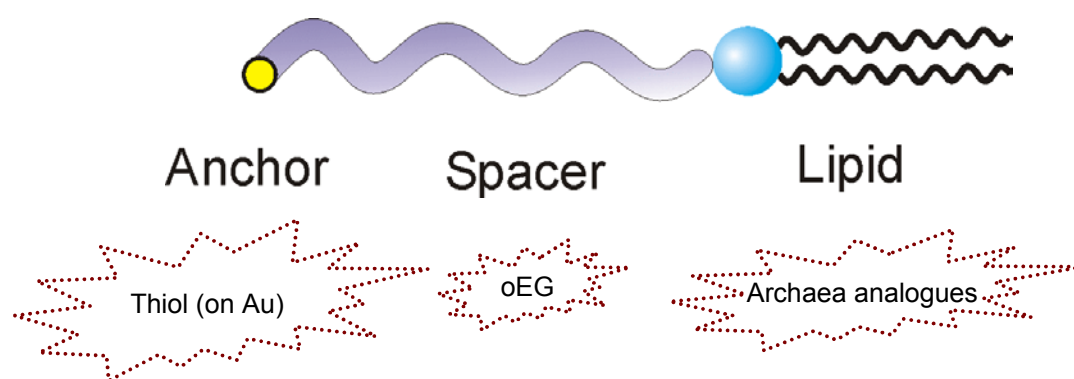


Figure 31: Strategic synthetic plan

Two different strategies were employed: polymerisation leads to longer spacer molecules, however, with large polydispersity. A second approach, the synthesis of defined oligoethyleneglycol spacers proved to be more promising. Both strategies will be subsequently described.

3.2.2. Polymerization

In this chapter, we describe the first route explored to synthesize thiolipids possessing longer spacers: anionic polymerisation. In principle, this approach should have many advantages: the polymers should be synthesized with low polydispersity under very mild conditions in a one-pot process. Furthermore, it allows the functionalization of the spacer differently with the lipid headgroup and the anchor group. The narrow distribution of the molecular weights should be suitable for the formation of a membrane and the presence of different lengths could, to a certain extent, contribute to the compensation of roughness effects of the surface.

To ensure the reproducibility of the synthetic conditions, the only necessary condition is in the use of a dry solvent. The synthetic procedure reported here is particularly promising for generating polymeric amphiphiles because the scheme does not require complicated purification or workup steps.

3.2.2.1. Anionic polymerisation

An anionic polymerisation is a chain reaction: monomers are continuously added to a growing chain. The principal characteristic is a high degree of polymerisation with a very low polydispersity.

The polymerisation occurs in three steps: initiation, propagation and termination as can be seen in Figure 32.

The anionic polymerization process is started by an *initiator*. In the case of anionic polymerization, the initiator is an anion. To obtain this molecule, it has to be activated and in most of the cases in anionic polymerization, this step is a deprotonation of a hydroxy group. The initiator attacks the monomer to open the ring and transfers its charge to the oxygen atom, to form a carbanion.

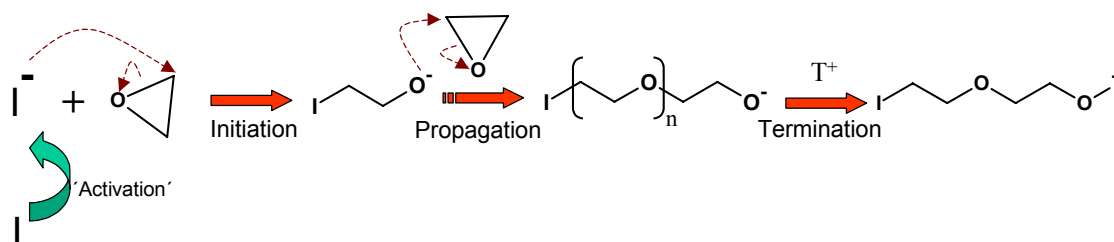


Figure 32: Polymerisation of ethylene glycol

The carbanion now reacts with a second monomer molecule in the same manner as the initiator reacted with the first monomer molecule, a new carbanion is generated. The addition of monomers continues, and each time another monomer is added to the growing chain, a new anion is generated allowing another monomer to be added. In this way the polymer chain grows. This stepwise addition is called *propagation*.

When all monomers have reacted, the polymerisation is on standby. In this case, if more monomer is added, the polymerisation goes on: the reaction is considered as a “living polymerisation”. This feature of anionic reaction is used in the case of block copolymers AAAAABBBB. Once the first monomer A is polymerised, the second monomer B is added and polymerises on the A chains.

The propagation does not stop until a termination reaction occurs. This happens when the active centre of the growing chain is neutralized by a terminating agent, for example, water. Therefore, if high molecular weights with narrow polydispersity are wanted, it is necessary to avoid termination too early, and so, avoid all traces of water.

Anionic polymerisation is commonly used for the polymerisation of ethylene oxide^[65], moreover it allows a functionalization of both ends of the polymer by carefully choosing the initiator and the terminating agent. Therefore, anionic polymerisation should be a method of choice for the synthesis of the targeted thiolipids.

3.2.2.2. Synthesis of oligoethyleneglycol via anionic polymerisation

Our target molecule can be decomposed into three parts: the oligoethylene glycol in the center, linked on one side to the lipid head and on the other to the anchor group (see Figure 31). This can lead to two different strategies for the anionic polymerisation: it is possible to start the polymerisation from the lipid head and terminate it with the anchor group, we will name this “head to tail strategy”. In the “tail to head strategy”, ethyleneglycol will be polymerised starting from the anchor group and a lipid derivate will be used to terminate the reaction. These two strategies, shown in Figure 33 and explained later in this chapter, were tested for a proof of principle of this concept.

There are many challenges in this synthesis. First, the ethylene glycol oligomer is required to have a low molecular mass, which is against all concepts of polymerisation, used normally to obtain the highest molecular masses possible. In the literature, there are no good examples for such low molar masses. Moreover, the initiating molecule has to fulfill some polymerisation conditions: it should not be polymerizable, otherwise it will contaminate the polymer and it should possess only one active centre where the polymerisation can start. Finally, the terminating agent should allow for the attachment of the molecules to a gold surface. To achieve this, there are two possibilities, either a sulfur group is used, with the risk that it also polymerizes, or a precursor that allows a further functionalization.

Both strategies named above were investigated but with only small success. GPC, NMR, Mass spectrometry and elementary analysis were used to characterize the polymers obtained. GPC had to be taken as a qualitative method. Indeed, our oligomers cannot be compared to the product used for the calibration (polystyrene) but qualitatively, it can be observed if the molar mass distribution keeps the same shape, or becomes larger. NMR and mass measurements will help to determine the real molar masses obtained.

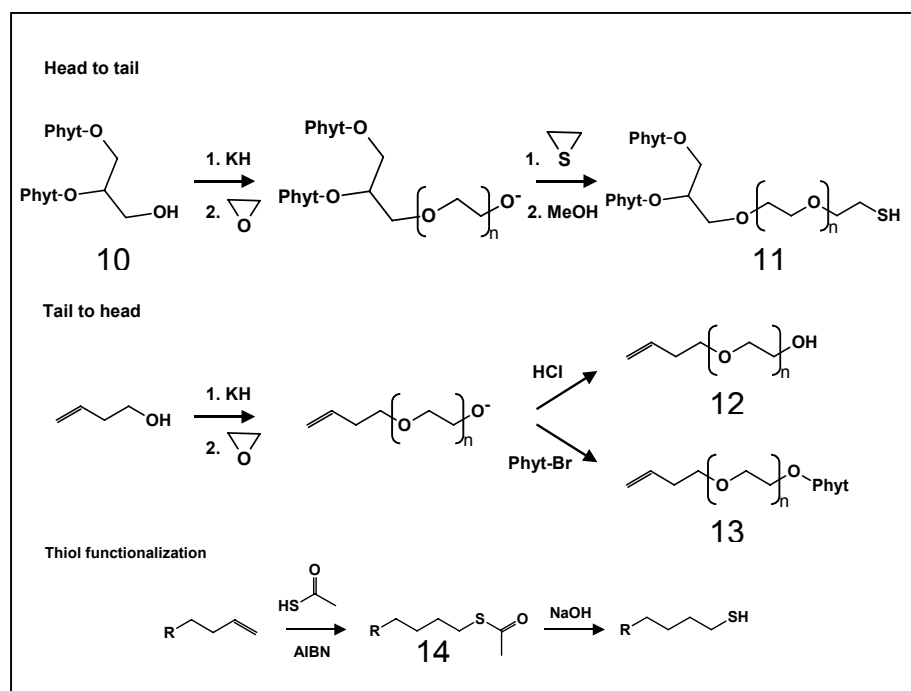
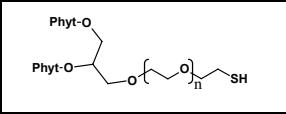


Figure 33: Schematic view of the two polymerisations strategies

- **Head to tail**

The head to tail strategy was conducted starting with DiPhytanylGlycerol (DPG) as shown in Figure 33. To be activated, it was deprotonated with potassium hydride. Then ethyleneglycol was added to produce the ethylene glycol part. Finally, to get a thiolated anchor group, thiirane, a compound similar to ethyleneglycol but containing sulfur instead of oxygen, was added to the growing chain, hoping that it would continue to polymerize on the ethylene glycol moiety, using the strategy of block copolymer synthesis.^[66]

The polymer obtained was in the THF filtrate, it was actually a side product of the polymerization of thiirane (very unexpected exothermic reaction when added to the reactor). The polymer obtained has the following characteristics:

	Ethylene Glycol Units	Mn	Other info
NMR	16-20	1505	1 thiol group
Elementary analysis/Maldi	12-40 max 24	1748 g/mol	0,5-1 thiol group
GPC	30	2038 g/mol	d = 1,16

*Table 2: Characterization of thiolipid 11
(the orange fields were deduced by calculation)*

According to GPC, the molar mass distribution is broad as compared to usual anionic polymerization products, it can have two reasons: first, this polymer was only a side product of the polymerization of thiirane, and this may perturb the polymerization (very exothermic reaction). Second, the polymerization was only conducted to obtain an oligoethyleneglycol, and this may not have the same characteristics as longer chains.

This polymer was used for the formation of a membrane. The results are shown in chapter 4.3.1. These first experiments allowed us to test the concept, and to discover the techniques to be used for the preparation of tBLM systems.

- **Tail to head**

The tail to head strategy has the advantage that it allows the preparation of a precursor, which can be modified for a whole series of different surfaces. This work was the first steps for this project, leading to a more generic synthetic approach in our group^[33].

This strategy, shown in Figure 33, uses the anchor group as an initiator. We want to attach our tethered lipid on gold, the anchor is therefore composed of thiols. However, a thiol can be an initiating site during the polymerization, which can compete with the hydroxy group. Therefore, a precursor strategy was used. In this case, a precursor containing a hydroxy group and a double bond on the other end proved to be suitable to start a polymerization. First, at low temperatures, and using anionic polymerisation, there is a very small chance that the double bond becomes an active site. Second, by implementing a double bond in the molecule, it allows a further functionalization to a broad variety of anchor groups, which can immobilize the molecules on different substrates like gold, metal oxides or silicon.

Two different anchor precursors were used, decenol and butenol, the only difference being the length of the hydrocarbon chain.

Decenol EG Phyt

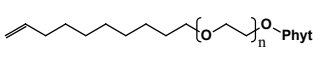
	Ethylene Glycol Units	Mn	Other info
NMR	32-34	1904	
Elementary analysis/Maldi	22-29	1412	
GPC	31	1811	d = 1,136

Table 3: Decenol lipid characterization (the orange fields were deduced by calculation)

Decenol was available in the institute. To terminate the polymer, phytanylbromide was added to the reactor. This compound resembles DiPhytanylGlycerol (synthetic pathway described in chapter 3.2.4.1.), but is faster to synthesize (only two steps described in 3.2.2.3.).

The advantage of decenol resides mainly in the fact that the long C10 chain induces a packing of the monolayer very easily due to the strong Van der Waals forces involved. However, a long hydrocarbon chain close to the gold may influence the electrical properties of the system, which would require a new model circuit.

To be suitable for a gold surface, the double bond of the anchor precursor was transformed into a thioacetate moiety. In the presence of a base, the thioacetate turns into thiol and can attach on the surface. In the literature, it is even reported that thioacetate moieties also bind to the gold surface.^[67]

The thioacetate formation was performed on this polymer. It was possible to monitor the reaction by NMR (see NMR spectrum of **14**), seeing the growth of the peak of the methylene group neighboring the thioacetate function. However, it was not possible to push this reaction to high yields. Starting material bearing a double bond was still present. Therefore, this compound was not used for membrane formation.

Butenol EG Phyt

The butenol moiety should be a more convenient anchor group for our purpose since it still has a hydrocarbon chain influencing the packing, but not long enough to induce a considerable change in the electrical properties of the monolayer.

The living character of the anionic polymerization should allow to synthesize a range of compounds in a one pot synthesis, by taking a small amount out of the reactor, refilling the reactor with monomer to increase the length of the chain and repeat this process. It would also allow one to obtain each time, a spacer group and a lipid functionalised oligoEG with exactly the same chain length. Furthermore, by using two different terminating agents, the characterization of the spacer is simpler because it is closer to a regular oligoethyleneglycol, and though it can give information about the lipid functionalised molecule.

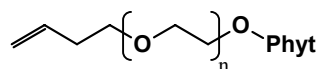
The test reaction for this process was followed via GPC. Samples were taken out of the reactor one day after the addition of monomers, and this was repeated three times. An increase in the polydispersity can be observed. The first polydispersity was determined by comparing the spectrum shape to the spectrum obtained in step 2. Indeed, it was not possible to deduce it

directly from the GPC curve because the peaks were out of the calibration range : the chains are too short.

Step 1 : >1,15

Step 2 : 1,16

Step 3 : 1,19



The distribution is already broad from the beginning. So this method, although very useful in the case of long chains, was abandoned. It does not seem to be suitable for the desired short and defined chains.

A polymerisation using naphthalene potassium as initiator was performed. Half of the ethylene glycol polymer (lipid polymer) was functionalised with a lipid head (phytanyl) and the other half (spacer) was quenched with acid to obtain a hydroxy ending group. The polydispersity for both products is encouraging: 1,11 and 1,07 respectively, with a degree of polymerisation of 10-14 units.

There were attempts to precipitate the polymer to purify it, but it only slightly reduced the amount of naphthalene. The polymer lipid was purified via column chromatography, however separation of the different products was not possible.

3.2.2.3. Experimental

Anionic polymerisation protocol

For an anionic polymerisation, it is crucial to avoid any moisture in the reactor since water will deactivate the anion and therefore stop the reaction.

Typically, the starting molecule (either head or tail) is dissolved in THF (anhydrous) and left under argon in a special reactor designed for anionic polymerisation. Then, 1 equivalent of the initiating agent is added (typically KH) and the mixture is left stirring overnight. Ethylene oxide is added and the reaction is followed via GPC. Typically after some days, the reaction is quenched either by adding a terminating agent like HCl or MeOH if the end should be a hydroxy group, or by adding a functional group such as Phytanylbromide (head) or tosylated butenol (tail).

Synthesis of phytanyl bromide

Phytanol **1** (8g, 27 mmol, 1eq, 296.5 g/mol) and triphenylphosphine (8 g, 30.5 mmol, 1.15 eq, 262.3 g/mol) are dissolved in 80 ml dichloromethane. The mixture is cooled down to 0°C with the help of a water bath. N-Bromosuccinimide (5 g, 28.1 mmol, 1.06 eq, 177.99 g/mol) is added in small portions to the reaction mixture. The mixture is left stirring overnight at room temperature.

The solvent is removed under vacuum and the remaining sticky oil/solid is washed 4 times with hexane. The solvent is removed under vacuum to obtain a colorless oil.

The product was purified via column chromatography with Hexane as eluent to give a colorless oil.

M = 7.43 g ($\rho = 77\%$)

Ref NMR **PhytBr** (Figure 80)

Synthesis of thioacetate from a double bond according to Oliveira et al^[68]

In a 100 ml three necked round bottom flask, decenol PEG was dissolved in 40 ml toluene and cooled down to 0 °C. One spatula of AIBN was added. Thioacetic acid was dissolved in 10 ml toluene and very slowly added dropwise to the reaction mixture. The solution is heated to 70 °C for 1 h. The reaction was followed via TLC. When the reaction is over, the mixture is poured into methanol and washed one time with methanol. Then the solution is filtered and the solvent is removed under vacuum.

Ref NMR **14** (Figure 81)

3.2.1.4. Conclusion

The anionic polymerisation of functionalised oligoethylene glycol molecules was investigated using two different strategies. The polymers obtained were characterized and used on surfaces to build up membranes. Because of time constraints, and after the first surface analysis results, this route was abandoned to the profit of more efficient strategies for our purpose.

It seems that to obtain a oligoethyleneglycol (a short one in comparison with polyEG) it is very difficult to obtain a narrow distribution, despite the use of anionic polymerisation which is associated with a low polydispersity. In our opinion, a narrow distribution may help the formation of the membrane.

3.2.3.1. Experimental

Protection/Deprotection of the Benzyl group

- **Monoprotection of a tetraethyleneglycol moiety**

See procedure in chapter 3.1.2.1.

Tetraethylene glycol (70 ml, 79.1g, 407 mmol, 4 eq, 194.2 g/mol), NaOH 50% in H₂O and Benzyl Bromide (12,178 ml, 17.4g, 102 mmol, 1 eq, 171.04 g/mol) were introduced in a 3 necked bottom flask and refluxed for 24h at 100°C. T_{bath} = 130°C

After 24h, the mixture was cooled, diluted with water and the aqueous layer was extracted 4x with Et₂O. The organic extracts were combined, dried over MgSO₄ and filtered. The solvent was removed under vacuum. The product was purified via flash chromatography with dichloromethane/acetone as eluent to give a yellowish oil.

M = 20,38 g (ρ = 72 %)

Ref NMR **4₄** (Figure 72)

- **Deprotection of a tetraethyleneglycol moiety**

Same procedure as in the next paragraph

Protection/Deprotection of pyran

- **Preparation of THP protected diethylene glycol **15_y****

3,4-dihydro-2H-pyran (3.55 g, 42.3 mmol, 1.2 eq, 84 g/mol) was added dropwise to a solution of 2-(2-chloroethoxy)ethanol (4.4 g, 35.3 mmol, 1 eq, 124.5 g/mol) and the mixture was stirred for 4 h at room temperature. Solid NaHCO₃ was added. The reaction mixture is filtered and washed with ether. The solvent is removed under vacuum. The product is purified via flash chromatography with Petrole ether/THF to give a colorless oil.

M = 6 g (ρ = 82 %)

Yield up to 80% for **15₂**, up to 85 % for **15₃**

Ref NMR **15₃** (Figure 82)

- **Cleavage of THP protected oligoethylene glycol**

16₈ (2g, 3.67 mmol, 1eq, 544 g/mol) was introduced in a schlenk flask, dissolved in a mixture of DCM/MeOH 1/1. 15 drops of HCl 37% were added and the reaction mixture was left stirring overnight under Ar. When solid NaHCO₃ was added, it started bubbling. The solution is filtered over a fritte then the solvent is removed under vacuum.

m = 1,8g (ρ = 100 %)

Ref NMR **4₈** (Figure 83)

Coupling of two protected oligoethyleneglycol moieties

Procedure : NaH (0.30 g, 12.6 mmol, 1.8 eq, 24 g/mol) was placed in a 3 necked round bottom flask of 250 ml, and 15 ml THF was added to form a suspension, under argon.

A solution of **4₄** (2 g, 7 mmol, 1 eq, 284 g/mol) in 15 ml THF was added dropwise and the reaction mixture was stirred under argon at RT for 24h.

A solution of **15**₂ (1.46 g, 7 mmol, 1 eq, 208,5 g/mol) in THF (15 ml) was then added to the solution via cannula. The resulting mixture was stirred at RT for 72h.

The excess of NaH was carefully destroyed by the addition of MeOH at 0°C. The solution was then concentrated under vacuum.

The resulting precipitate was then partitioned between EE/H₂O.

The aqueous layer was then extracted with EE. The combined organic layers were washed with water and brine. Dried on Na₂SO₄ filtered and solvent removed under vacuum.

The product is purified via flash chromatography with ethylacetate to give a colorless oil.

M = 0,94 g (ρ = 29 %)

Ref NMR **16**₆ (Figure 84)

3.2.3.2. Results and discussion

Protecting groups.

The *protecting groups* used here are the benzyl group and the THP group according to Coudert et al.^[69] Because the protecting groups should be removed quantitatively and selectively, they should have different cleavage conditions, and also withstand the cleavage conditions of the other. This is the case for the two chosen groups. Benzyl is cleaved using Pd/C in methanol, whereas THP is removed with acid in dichloromethane.

Moreover, they should be easy to detect via UV and NMR to facilitate the monitoring of the synthetic progress. In the case of THP and Benzyl, NMR will tell very clearly if these groups are present or not. Indeed, Benzyl peaks appear around 7.2 and 4.6, THP peaks are in the 1-2 ppm range, whereas ethylene glycol appears around 3.5.

According to our results, it was possible to obtain **4**₄ and **15**₂ with very good yields (70% and 85% respectively). The cleavage of the pyran protecting group was quantitative, whereas the cleavage of the benzyl group only reached 40% yield. The reaction performed here was not 'pushed' to its end, and since this protecting group had to be used in the next strategy, the reaction conditions were optimised.

Synthesis of unsymmetrical oligoethyleneglycols.

After protecting the oligoethylene glycol moieties **4**₄ and **15**₂, they react with each other to form a longer chain via a nucleophilic substitution reaction. The mechanism will be described in more details.

Nucleophilic Substitution (Second Order)

In a nucleophilic substitution, a nucleophile (Nu:) replaces a leaving group (:X̄:) from a carbon atom, using its lone pair of electrons to form a new bond to the carbon atom. The abbreviation S_N2 stands for Substitution, Nucleophilic, bimolecular. The term bimolecular means that the transition state of the rate-limiting step involves the collision of two molecules.

Mechanism.

An example is the reaction of an alkyl halide with a compound bearing a deprotonated hydroxy group. The product is the corresponding ether.

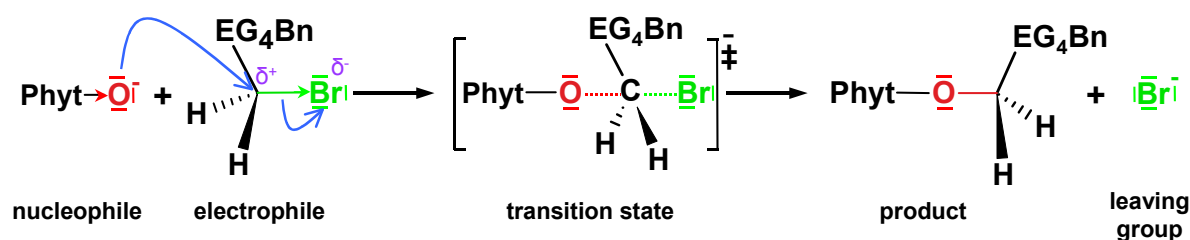


Figure 35: the S_N2 mechanism. The S_N2 reaction takes place in a single (concerted) step.

The O^- ion is a strong nucleophile (donor of an electron pair) because the oxygen atom has unshared pairs of electrons and a negative charge. The alkyl halide is called the substrate, meaning the compound that is attacked by the reagent. The carbon atom of the alkyl halide is electrophilic because it is bonded to an electronegative halogen atom. Electron density is drawn away from carbon by the halogen atom, giving the carbon atom a partial positive charge. The negative charge of the hydroxide ion is attracted to this partial positive charge.

Hydroxide ion attacks the back side of the electrophilic carbon atom, donating a pair of electrons to form a new bond, as shown in Figure 35. Carbon can accommodate only eight electrons in its valence shell, so the carbon-halogen bond must begin to break as the carbon-oxygen bond begins to form. The halide ion is the leaving group, it leaves with the pair of electrons that once bonded it to the carbon atom.

The mechanism in Figure 35 shows attack by the nucleophile (hydroxide), the transition state, and the departure of the leaving group (halide).

This reaction is a concerted reaction, taking place in a single step with bonds breaking and forming at the same time. The middle structure is a transition state, a point of maximum energy, rather than an intermediate. In this transition state, the bond to the nucleophile is partially formed, and the bond to the leaving group is partially broken. This transition state is not a discrete molecule that can be isolated, it exists for only an instant. In the case of an asymmetric carbon atom, the back side attack gives an inversion of configuration, called the Walden inversion.

Unsymmetrical ethylene glycols with six and eight units were obtained, but because of purification problems, there was not enough material to go further with higher molar masses.

Purification.

The major problem concerning this synthesis is indeed the purification step, and this at each stage of the synthetic pathway. Column chromatography is the method of choice to obtain a very pure product, but in this case, with the eluting system chosen, there was a great loss of product, which is decreasing the yields considerably. Moreover, the polarity of the molecules made the separation process long, despite the use of a polar eluting system, THF/Acetone.

Finally, one other difficulty was that despite the use of different developers, the product was hardly seen on the TLC, which made it even more difficult to find the product in the fractions of the column chromatography.

3.2.3.3. Conclusion

The synthesis of antisymmetrical oligoethylene glycol molecules was investigated. It was possible to obtain moieties with 6 and 8 repeat units, functionalised on one side with a benzyl group, and on the other with a THP group. The selective cleavage of the two groups proved to be rather efficient.

Though, the yields obtained are very low, presumably because of the long and tedious purification steps. Therefore, this strategy was abandoned, but the expertise gained about the protecting steps as well as the coupling method was of a great advantage for the pursuit of the new strategy.

3.2.4. Precursor synthesis

Rich from the experience of the former trials, we were able to develop a synthetic pathway that was efficient, relatively simple, and which offers many possibilities to further modify the molecules.

The aims of this synthesis were the following :

- to avoid purification problems by using intermediates which can be seen easily by TLC and are less polar to avoid long separation times
- to be able to obtain any length with the least synthetic steps.

Figure 36 shows a scheme of the synthetic strategy: the concept resides in only 3 reactions that can be repeated to obtain the different chain lengths. The first reaction is the functionalization of the lipid with a small protected spacer moiety. The protecting group is cleaved in a second reaction. There are now two options: either to functionalize the compound obtained with a chosen anchor group, or to pursue the elongation of the spacer chain by adding another small spacer moiety.

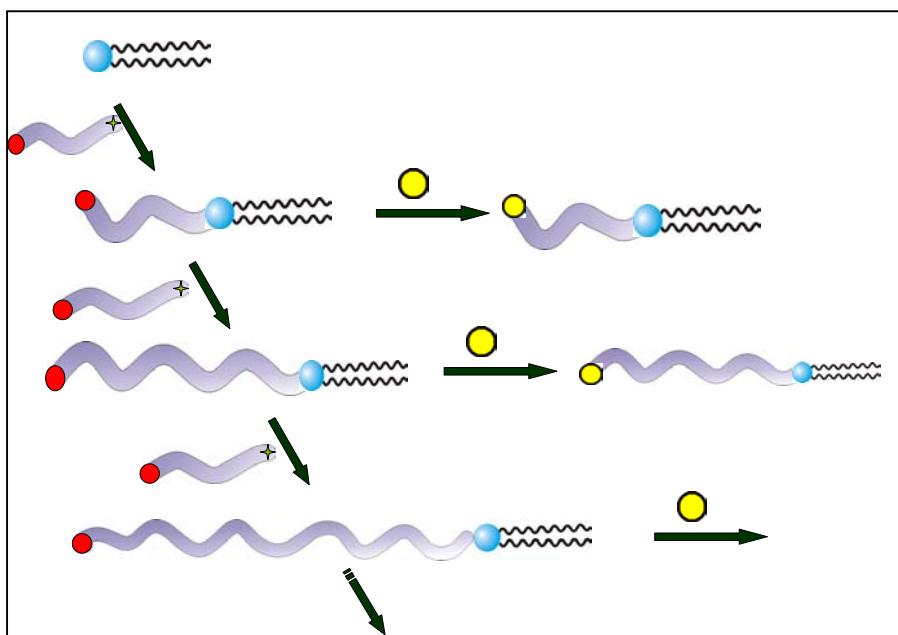


Figure 36: Scheme of the precursor strategy

The fact that archaea analogues are very colourful on the TLC once developed with a “Zuckerreagenz” (see appendix for recipe) will help to track the products more easily. Moreover, these compounds being very apolar, a coupling with ethyleneglycol will reduce the overall polarity of the product, therefore, the problems encountered in the previous synthetic strategy will be avoided. Indeed, as shown in Figure 37, the archaea analogue lipid headgroup reacts with a small monoprotected oligoethyleneglycol to obtain a precursor which is easily identifiable on the TLC. Its polarity allows a fast and problem free purification. A whole pool of molecules with increasing spacer lengths can be obtained very easily by cleaving the protecting group, and repeating the coupling with another ethyleneglycol moiety. Finally, these molecules can be functionalised with an anchor group, for a Au surface, we chose to use lipoic acid. However, this method permits the use of other anchor group to allow the immobilization on various surfaces or even in situ attachment.

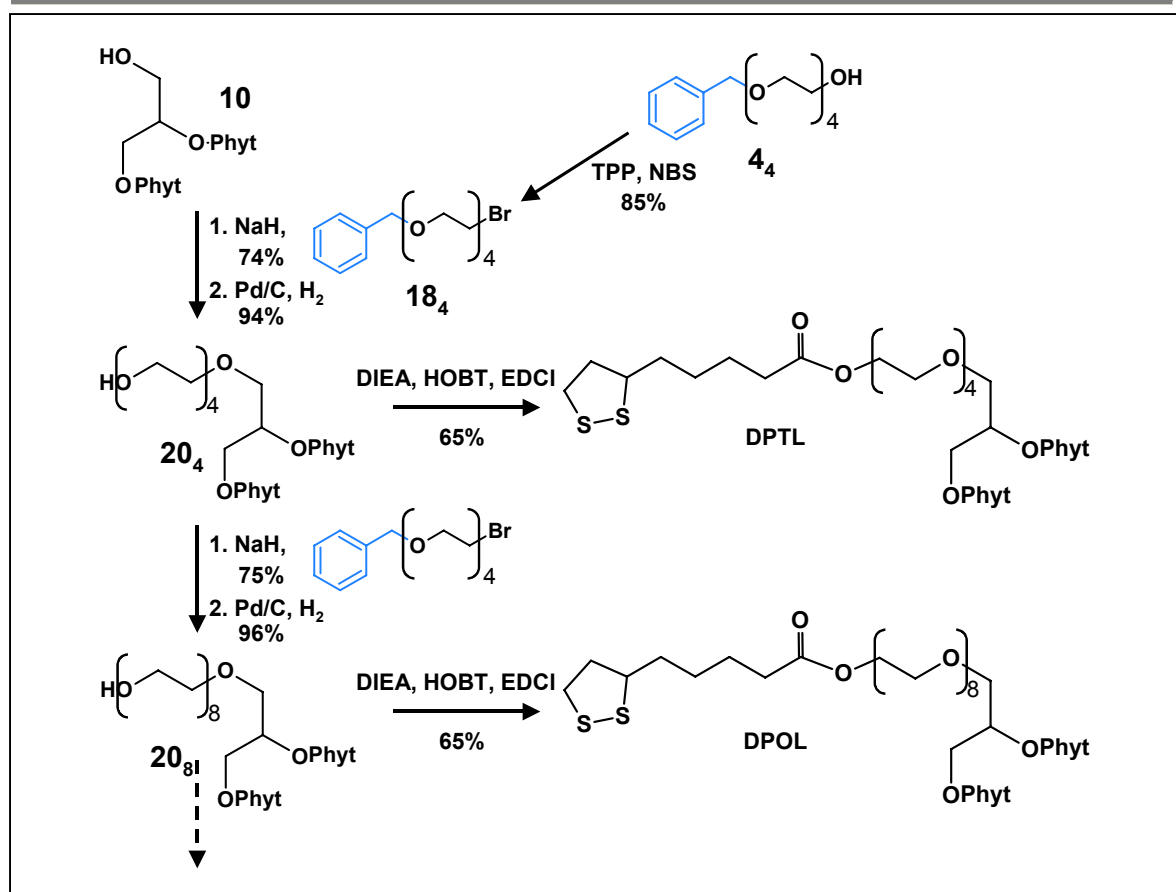


Figure 37: Synthetic pathway using the precursor strategy

Monophytanyl compounds were synthesized the same way and were named after the diphytanyl compounds, adding a “.

3.2.4.1. Experimental

Synthesis of 10: This synthesis was performed in our lab (from and for the whole group of researchers on this topic). It is described in Atanasov et al.^[33]

Phytanbromide was synthesized from phytol according to^[71] (See chapter 3.2.2.3.); c) (+)-3-Benzyloxy-1,2-propanediol 2 (1 eq), NaH (3.1 eq), Phytanbromide 1 (3 eq), THF, 40 °C, 6 d, 86%; d) this step was carried out according to a procedure described elsewhere^[31] and in the next paragraph.

Ref NMR 10 (Figure 79)

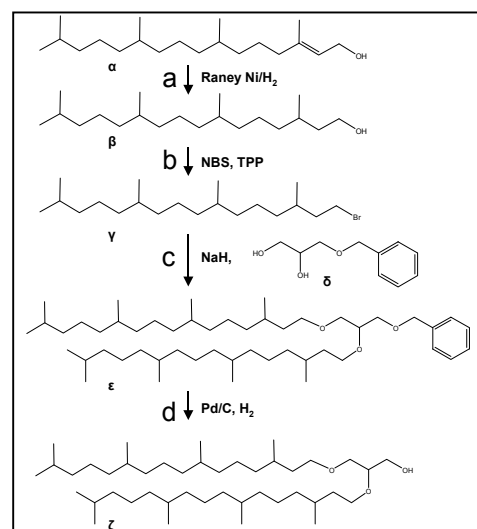


Figure 38: Synthetic route of 10

Synthesis of Monoprotected hexaethyleneglycol

Procedure : NaH (0.19 g, 7.9 mmol, 1.5 eq, 24 g/mol) is placed in a three necked round bottom flask under Ar. THF was added to obtain a suspension. Hexaethyleneglycol (3g, 10 mmol, 2 eq, 282.33 g/mol) is added via syringe in the mixture and it was left stirring for some hours. Benzyl bromide (0.91 g, 5.32 mmol, 1 eq, 171.04

g/mol) in 10 ml THF is added dropwise. After 24h, the reaction is stopped by addition of water to neutralize NaH remainings.

The mixture is washed with THF and centrifuged 5 times at 9000 rpm for 15 min. The solvent is removed under vacuum to give a yellow oil.

The product is purified via flash chromatography with dichloromethane /acetone as eluent to give a colorless oil.

M = 1,33 g ($\rho = 67\%$)

Ref NMR **4₆** (Figure 73)

Synthesis of Brominated benzyltetraethyleneglycol (hexaethyleneglycol)

4₄ (2g, 7mmol, 1 eq, 284 g/mol) is dissolved in 20 ml dichloromethane and then triphenylphosphine (2.12g, 8 mmol, 1.15 eq, 262.3 g/mol) is added. Then the mixture is cooled down to 0°C with an ice bath, and NBS (1.33 g, 7.46 mmol, 1.06 eq, 177.99 g/mol) is added in small portions. The mixture is stirred overnight at room temperature.

The next morning, the dichloromethane was evaporated under vacuum and the remaining powder was washed with hexane. The hexane extracts were collected and the solvent was removed under vacuum.

The remaining colorless oil was usually used without further purification.

M = 2.4 g ($\rho = 98\%$)

After a purification via column chromatography with dichloromethane/acetone as eluent, the product is pure.

M = 1,8 g ($\rho = 74\%$)

Ref NMR **18₄** (Figure 85)

Synthesis of precursors protected lipid-oligoethyleneglycol

a) Procedure for **19₄**

NaH (37 mg, 1.53 mmol, 1 eq, 24 g/mol) was placed in a 3 neck round bottom flask 250 ml, and 15 ml THF was added to form a suspension, under argon.

A solution of **10** (1g, 1.53 mmol, 1 eq, 653 g/mol) in 15 ml THF was added dropwise (via syringe) and the reaction mixture was stirred under argon at RT for 2-4h.

Then the brominated compound **18₄** (1.86g, 5.36 mmol, 3.5eq, 347.25 g/mol) is added dropwise to the mixture. After some time (1 night to one WE) some drops of water were added to hydrolyse the remainings of NaH.

The mixture is washed with THF and centrifuged 5 times at 9000 rpm for 15 min. The solvent is removed under vacuum to give a yellow oil.

The product is purified via flash chromatography with dichloromethane /acetone as eluent to give a colorless oil.

M = 1,04 g ($\rho = 74\%$)

Ref NMR **19₄** (Figure 86)

b) Cleavage of Benzyl group

The compound **19₄** (1.3g, 1.41 mmol, 919 g/mol) is dissolved in 40 ml ethanol and then the catalyst (Pd/C, one spatula) is added and a stream of hydrogen is bubbling until the reaction is over. The reaction is followed via TLC.

The reaction mixture is washed with ethanol and centrifuged 5 times at 9000 rpm for 15 min to remove the catalyst, and the solvent is removed under vacuum to give a colorless oil. It is used without further purification.

M = 1.10 g ($\rho = 94\%$)

Ref NMR **20₄** (Figure 87)

Ester coupling of oligoethylene glycol lipid

Procedure for **DPTDL**

Lipoic acid (260 mg, 1.26 mmol, 1 eq, 206.34) was dissolved in DCM in a 100 mL 3 neck bottom flask under N₂ to give a yellow solution. DIEA (407 mg, 3.15 mmol, 2.5 eq, 129.25 g/mol) was added, and then the solution turned to transparent yellow. HOBT (187 mg, 1.38 mmol, 1.1 eq, 135.13 g/mol) is added and then slowly EDC (266 mg, 1.38 mmol, 1.1 eq, 191.71 g/mol). The mixture was left stirring for 1/2h.

Then, the lipid (0.4 g, 0.3 mmol, 0.2 eq, 1270 g/mol) dissolved in a minimum of DCM was added to the mixture, and it was left stirring over night.

A TLC check showed that the reaction was over.

40 mL DCM were added and the organic layer was washed 3x with sat. K_2CO_3 then 3x with brine. They were dried over $MgSO_4$ and filtered. The solvent was removed under vacuum.

The product was purified via column chromatography DCM/MeOH to give a yellow oil.

M = 0.28 g ($\rho = 64\%$)

Ref NMR **DPTDL** (Figure 88)

3.2.4.2. Results and discussion

This synthetic pathway is very simple, and involves always only three reactions: the nucleophilic substitution of a protected oligoethyleneglycol moiety on the lipid functionalised molecule, the cleavage of the protecting group and finally, the coupling with the anchor group. Table 4 summarizes the yields obtained for the two determining steps, first the synthesis of the precursor, and the ester coupling.

Precursor synthesis	
Compound	Yield
20₄	74 %
20₆	79 %
20₈	75 %
20₁₄	60 %
20''₄	57 %
20''₈	28 %*

Ester coupling	
Compound	Yield
DPHL	55 %
DPOL	21 %*
DPTDL	65 %
MPTL	65 %
MPOL	25 %*

* These yields include the pure fractions. In these separations, there were fractions of mixture, which were not taken into account to calculate the yield.

Table 4: Yields obtained for the precursor synthesis

Monoprotected oligoethyleneglycol

The synthesis of the monoprotected oligoethyleneglycol is a reaction included in the first strategy. It is a crucial one since it determines the length of the spacer and the parity of the chain length. If you use only even numbered chains, then it is not possible to obtain odd chains. Only the introduction of an odd numbered chain will allow to access odd chains. Tetra and hexa ethyleneglycol moieties were synthesized successfully with yields up to 85 %, which gives hope that any small ethyleneglycol will produce a monobenzylated Xethyleneglycol bromide.

Nucleophilic substitution of the monoprotected oligoethyleneglycol on the lipid functionalised molecule.

Similar as in the former chapter, the nucleophilic substitution is the core reaction in this synthetic pathway. It produced very good yields for lengths up to 14 units of ethylene glycol. Moreover, the purification steps are more efficient than in the last synthetic pathway, due to the easy detection of the product on the TLC and the less polar products, even in the case of the longer chains. The eluting system dichloromethane/acetone may also be more adapted to the separation of these products.

Cleavage of the benzyl group

The benzyl group was chosen because of its easy protection/cleavage scheme, which is almost quantitative. Moreover, the benzyl group fluoresces, which allows a very easy detection of its presence on the TLC. This is very useful during the cleavage reaction.

This reaction was optimized by changing the solvent. Our products are not very soluble in methanol, and a small amount of THF is added to help the dissolution. By replacing methanol with ethanol, it was possible to dissolve the product in a single solvent, with comparable yields.

Anchor coupling

In our case, the lipoic acid was the anchor group suitable for gold surfaces, but it is possible to functionalize the pool of molecules obtained with any anchor group. The double bond strategy (see chapter 3.2.2.2.) can also be applied here. The ester coupling was performed, like in the industrial synthesis, with coupling agents EDC and HOBt (see mechanism Figure 30). The typical yields achieved were in the order of 65% and could not be further improved.

3.2.4.3. Conclusion

This last strategy allowed us to synthesize the expected molecules using very simple and efficient reactions that led to the target molecules in a very short time.

With this method, it is possible to get any spacer length by changing the oligoethyleneglycol moiety (even or odd) added, which makes this method very attractive for the synthesis of further molecules. Moreover, because it is the last step, the anchor group can be chosen according to the surface used for immobilization. It may be even possible to use the molecule without any anchor group for in situ attachment on the surface. All molecules that were obtained using this method are summarized in Figure 39.

The yields obtained are quite satisfactory for each step, but they could be improved further by optimising reaction parameters such as time, temperature and stoichiometry between the compounds, which play a crucial role in nucleophilic substitution. However our aim was to obtain enough material to be able to study their properties on the surface, and after this tedious synthetic part, it was at last possible to start real studies of the membrane formation on gold surfaces.

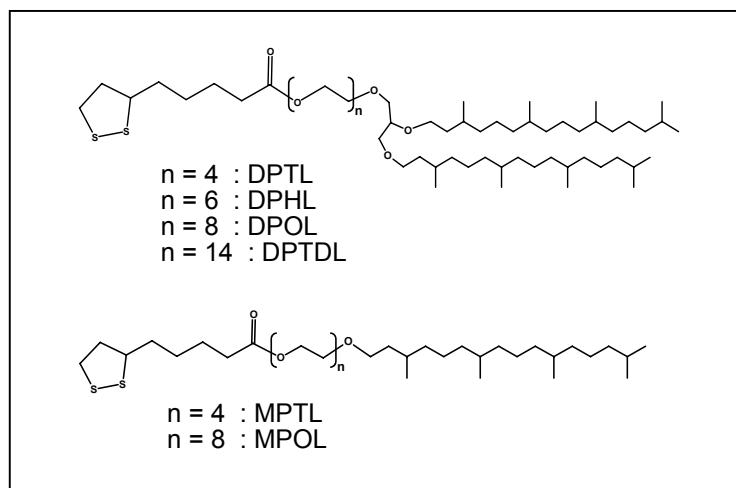


Figure 39: Series of six molecules synthesized

4. Membrane formation, characterization and protein incorporation

4.1. How to build the system

The thiolipids described in chapter 3 were used to form tBLMs. Two aspects of the membrane system were investigated. First, what is the quality of the bilayer and second, how do the different spacer lengths compare to each other. The quality of the bilayer is measured in terms of its electrical sealing properties. The ultimate goal, and therefore, the final test for a “good” tBLM is its ability to functionally incorporate membrane proteins. If the protein behaves as in a natural environment, and this response can be quantified by our measuring tools, the bilayer is suitable for further study. Moreover, since a series of molecules varying only from the spacer length were synthesized, it is also interesting to compare them with each other and see how they differ or behave the same. This will help to get an insight of the influence of the spacer length on the sealing properties of the bilayer. This study will help in choosing a suitable compound to carry on studies on larger proteins: if the sealing properties are kept with a longer spacer, there are many chances that the protein will incorporate and be functional.

To study protein incorporation, the system has to be built in different steps, which are depicted in Figure 40. First, one needs a suitable surface, smooth enough for the monolayer to form. Depending on the length of the molecule, a rough surface would prevent the formation of a lipid monolayer. The second step consists in the formation of the bilayer. This may be one of the most challenging steps. Finally, the incorporation of the protein in the bilayer can be performed in different ways.

This procedure can be monitored by EIS and SPR. The first is to define the electrical properties of the membrane but also to follow in situ the bilayer formation, as well as the protein functioning. The second is to determine the thickness of the system, and check the reaction kinetics.

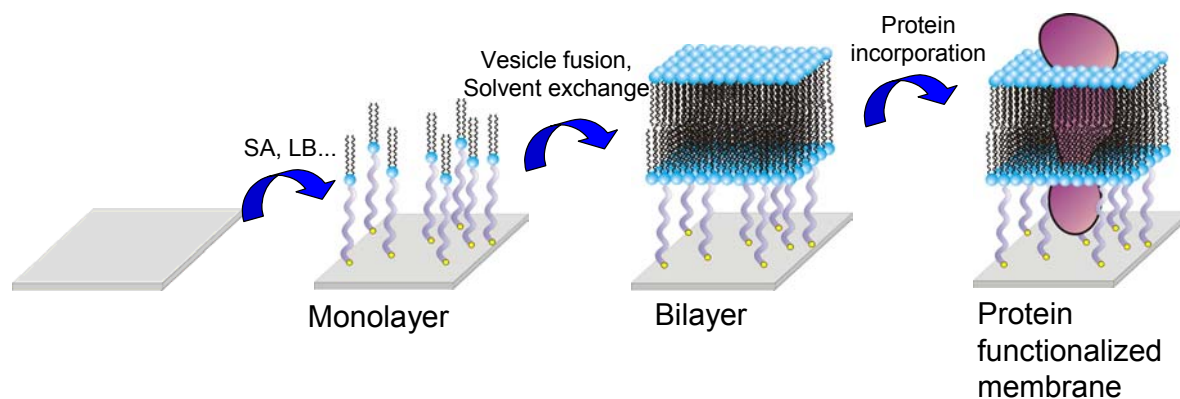


Figure 40: The building steps of a tethered lipid bilayer membrane and protein incorporation

4.2. Procedures

In this part, we will describe in detail the techniques that were used to build up the membrane with the different steps. We will also give an insight into other techniques that we did not investigate.

4.2.1. The substrate

Since the dimensions of the tBLMs are in the nm range, a very smooth surface is needed to prevent surface irregularities in the next steps. To cope with this problem, Template Stripped Gold is used. The low roughness of this substrate allows a good self assembly of the first monolayer.

Preparation. TSG is prepared according to Naumann et al^[72]. A scheme of the preparation is shown in Figure 41.

In short, 60 nm gold films were deposited by electrothermal evaporation on clean Si wafers (CrysteC, Berlin) with a Edwards evaporation machine. The gold surface was then glued with EPO-TEK (Epoxy Technology, USA), an optical glue, to glass slides (BK7, Menzel GmbH, Germany) and cured at 150 °C for 60 min. After letting them cool down, they are ready for use. The slides can be stored for weeks before use. If the Si wafer is stripped from the glass slide, an ultra flat gold surface, templated by the Si wafer, becomes available to form the monolayer.

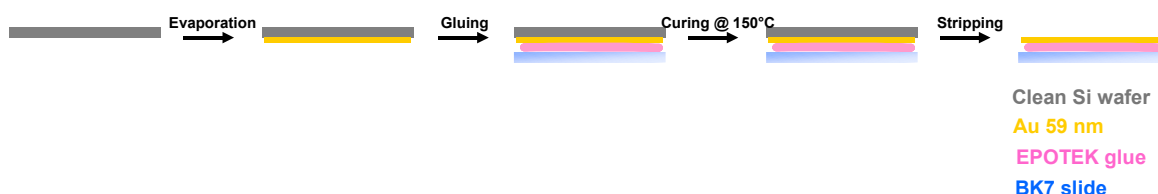


Figure 41: Template Striped Gold fabrication process.

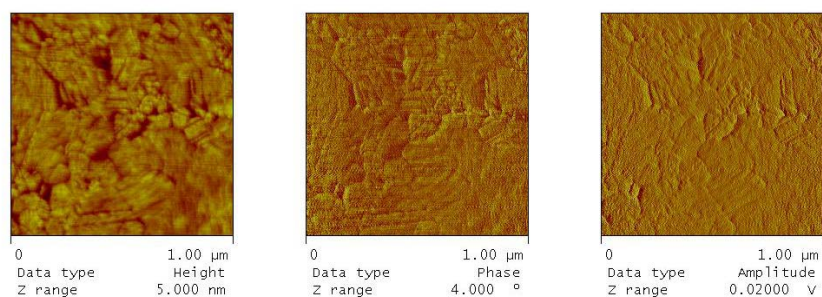


Figure 42: AFM pictures of TSG

The AFM pictures in Figure 42, taken by Inga Vockenroth (MPIP) show the very low roughness (0,36) of the TSG, as well as the large continuous smooth area obtained (see Figure

43). Our measuring cells have an area of at most 0.3 cm^2 , and therefore, the monolayer needs to be homogenous in this area.

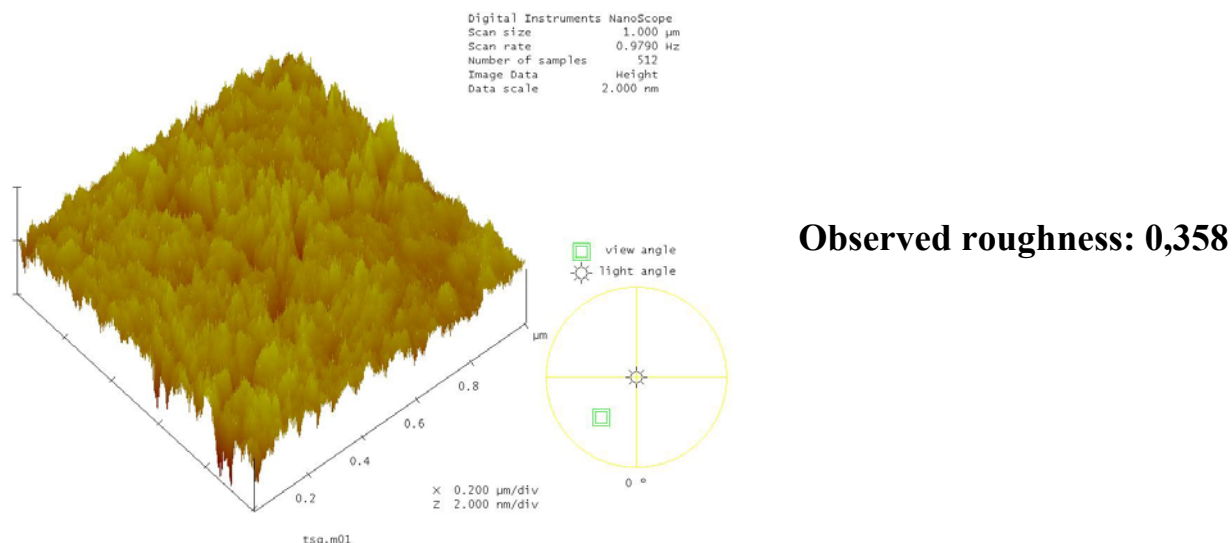


Figure 43: AFM 3D representation of TSG

4.2.2. Monolayer formation

The first step in the tBLM construction consists in the formation of a monolayer. It is crucial to obtain a “good” monolayer on the gold surface, which, in this case, means a densely packed monolayer. Former studies showed that only a densely packed monolayer provides a useful platform to obtain reasonable bilayer properties for the study of membrane proteins. Moreover, only a dense monolayer forms a surface that is hydrophobic enough to allow for vesicle fusion, our method of choice to form a bilayer. There are different ways to obtain monolayers, the following were tested in this work: self-assembly, Langmuir Blodgett transfer and finally lipid-detergent vesicles.

Self-Assembly.

Self-organization, also called self-assembly, is a phenomenon that is not fully understood. It has been studied extensively for the past decade and a lot of definitions can be found in the literature.

For Hamilton et al^[73], self assembly is the “non covalent interaction of two or more molecular subunits to form an aggregate whose novel structure and properties are determined by the nature and positioning of the components”. The non covalent interactions that can come into play at this stage are the following: hydrogen bonding, hydrophobic interaction, charge-charge interaction, Van der Waals attraction, π stacking between aromatic systems and metal ligand binding.

Another definition, given by Whitesides et al^[74], is the “spontaneous assembly of molecules into structured, stable, non covalently joined aggregates”. For Lindsey et al^[75], self-assembly is the “spontaneous formation of higher ordered structures” and Lehn and Pfeil^[76] define it as the “process by which specific components spontaneously assemble in a highly selective fashion into a well defined discrete supramolecular architecture”. All these definitions share the common concepts of interaction, cooperativity and spontaneity. Moreover, self-assembly involves a small group of molecules, not a single molecule, not the bulk, but a defined quantity.

An extensive review of SAMs (Self Assembled Monolayers) on different substrates has been published by Schreiber^[77], using alkanethiols as a model system. In the case of monolayers, the general concept of self-assembly exploits the preferential strong binding of one functional group of a molecule to a substrate (e.g. S-Au), and in principle, it allows the preparation both from solution and from the gas phase. A summary of the interactions taking place in the process are depicted in Figure 44.

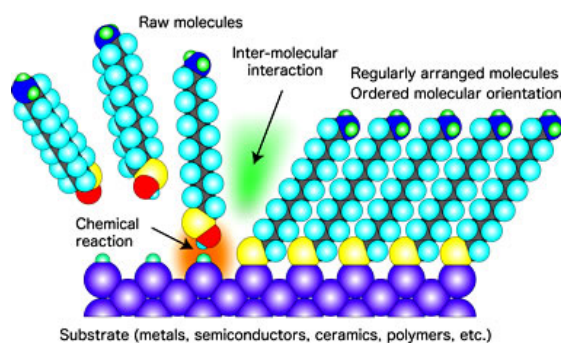


Figure 44: A self-assembled monolayer depicted by a group in Kyoto^[78]

The ease of preparation and the low amount of material needed are important reasons for the popularity of the SAMs. Provided that the substrate has been properly cleaned, in principle, it simply has to be dipped into the corresponding solution for a certain period of time, and the monolayer will assemble. A popular example is alkanethiols in ethanolic solution with concentrations in the micromolar to millimolar range.

Impurities can have a significant impact on the process, and therefore it is very important to carefully control the purity of the solution. Moreover, after completion of the SAM an appropriate rinsing procedure has to be followed.

In our case, like in many other groups, self-assembly was used to create a dense monolayer on the surface. The thiol endgroup allows a chemisorption on gold. Moreover, the hydrophobic forces associated with the hydrocarbon chains of the lipid as well as the hydrogen bonding associated with the headgroup favor an organization of the molecules at the surface. Various parameters such as assembly time or concentration in the assembly container can be varied in order to improve the coverage.

If not stated otherwise, the self-assembly concentration is 0,2 mg/ml of the thiolipid in ethanol, and the self assembly time is 24h. The slide is then dried and introduced into the measurement cell. Buffer is added and the system is ready for the measurement.

Langmuir Blodgett films.

About a century ago, Langmuir demonstrated that monolayers of fatty acids can be ordered on the surface of water. By applying pressure, phase changes from a gaseous state of non interacting molecules to a “solid” state where the molecules interacted in a rigid film can be observed in a phase diagram, the so-called Langmuir isotherm, as schematically depicted in Figure 45. Langmuir and Blodgett realised the transfer of such monolayers from the water surface to a solid substrate by slowly passing an appropriately treated substrate through the air/water interface.^[79, 80]

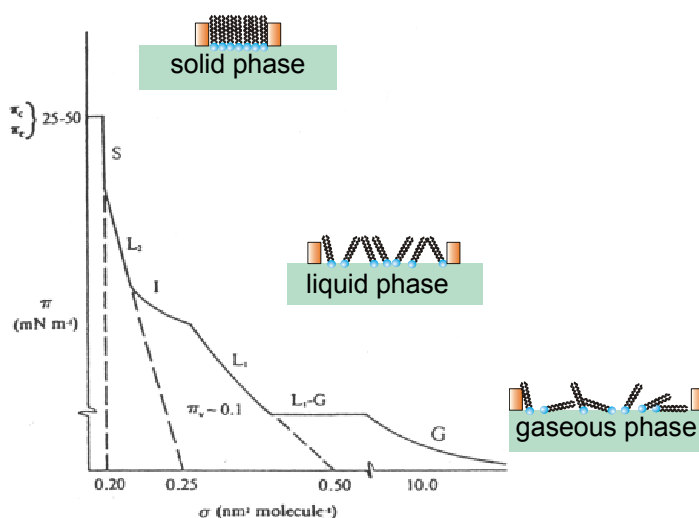


Figure 45: ideal Langmuir isotherm

In practice, films are spread on an ultra clean water subphase in a Teflon trough. The trough has a moveable Teflon barrier straddling the air water interface. This is controlled mechanically to compress the film under servo-control. As the surface area of the film is reduced, the surface pressure of the film increases. The pressure/area isotherm is monitored continuously and at a certain area per molecule, the pressure will begin a rapid increase as the solid phase is reached while the area per molecule remains approximatively constant. If the pressure increases much further, the film will collapse and the molecules will enter the water subphase.

At some predetermined pressure, a substrate may be passed through the air/water interface as shown in Figure 46 and as monolayers are picked up the film area will reduce. The pressure is held constant by feedback from a pressure monitor and the reduction of area is monitored to find a transfer ratio:

$$\text{transfer ratio} = \frac{\text{area of slide covered}}{\text{loss of area from film on trough}}$$

Ideally, this ratio should be 100% but it may be greater (if for example the molecules are slowly dissolving into the subphase) or less if incomplete coverage of the slide is achieved. The first case can be noticed by monitoring the pressure of the film for some time before

attempting to transfer a monolayer. If the pressure is gradually reducing, most probably molecules are either dissolving in the subphase or leaking under the barrier.

Many factors may influence film forming characteristics such as temperature, pH, purity of the subphase. The addition of ions can stabilise the film.

Langmuir-Blodgett transfer is one of the most promising techniques to prepare thin films. It enables

- 1- the precise control of the monolayer thickness
- 2- homogeneous deposition of the monolayer over large areas
- 3- the possibility to make multilayer structures with varying layer composition.
- 4- these monolayers can be deposited on almost any kind of substrate.

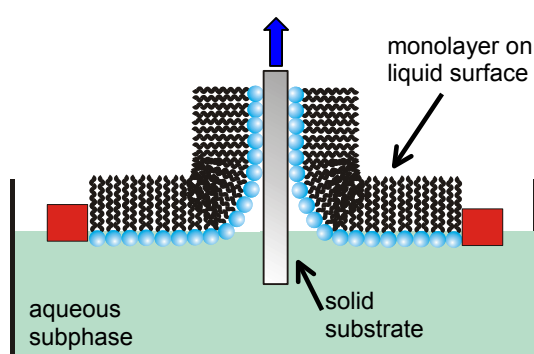


Figure 46: Deposition of a floating monolayer on a solid substrate

In this work, the molecules were dissolved in chloroform at a concentration of 0,5 mg/ml, before being spread on the air/ water interface. The pressure/area isotherms are shown in Figure 47. They show a breakdown of the film above 45 mN/m for both compounds.

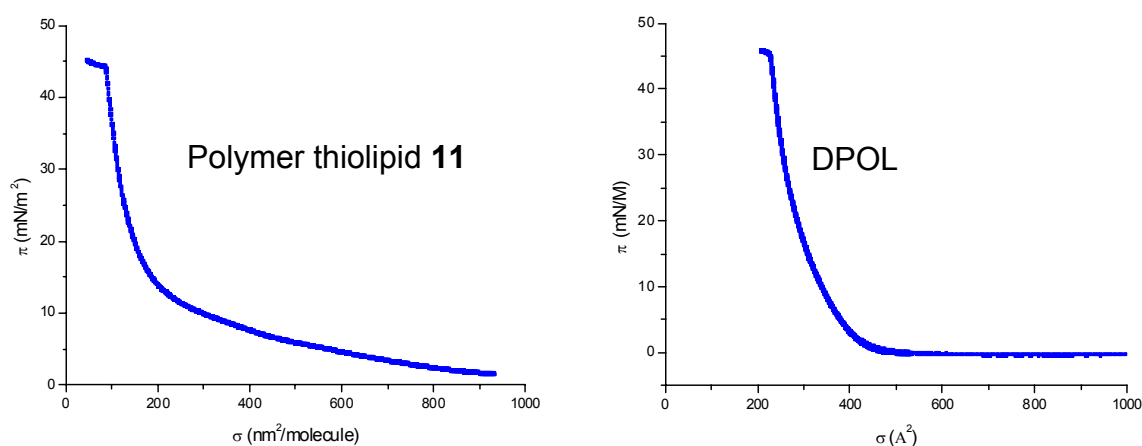


Figure 47: Pressure-area isotherms of **11** and DPOL at room temperature and a compression velocity of 50 mm/min.

If not stated otherwise, monolayers were transferred to solid supports at 40 mN/mm², with a lift-off speed of 0,7 mm/min at room temperature. After the transfer, the slide is directly introduced into the cell and the measurement is started.

Vesicles.

Amphiphiles have the tendency, above a certain concentration (CMC, critical micellar concentration) to form vesicles when dissolved in an aqueous solution. Detergents, for example, assemble very easily into vesicles at very low concentrations. Mixtures of our lipids with detergents in water will form micelles. If a gold substrate is incubated in such a solution, the mixed vesicles may adsorb on the gold surface and the lipids contained in these vesicles may bind covalently to the gold. To remove the detergent molecules, the solution is dialyzed to leave only our lipids to form a monolayer. The different steps are depicted in Figure 48.

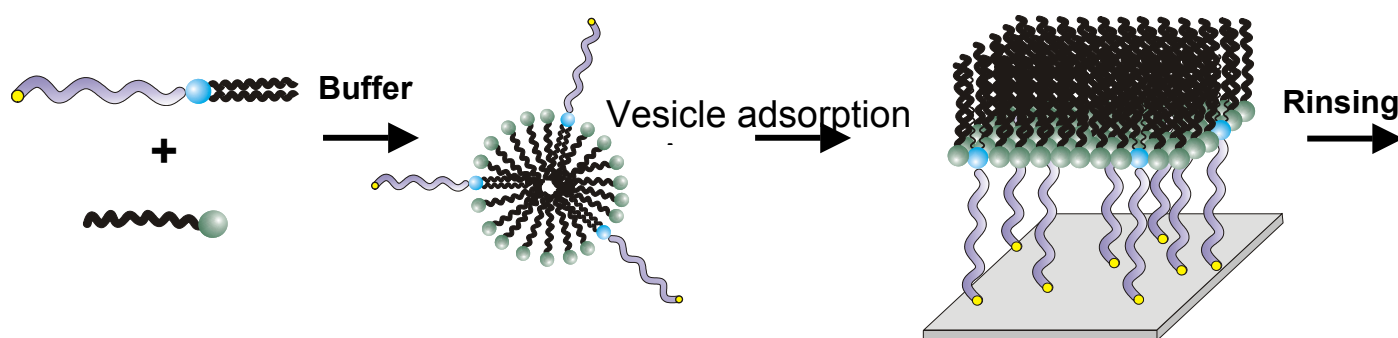


Figure 48: monolayer formation via use of OG detergent.

This well-known technique is used by several research groups to form monolayers^[29]. With the help of detergent, it is very easy to incorporate a lipid in the vesicle. However, the use of a detergent can sometimes lead to solution contamination.

n-Octylglucoside (see Figure 49) was used as detergent to form mixed vesicles. Since it has a very high CMC (20-25 mM) it can be easily removed from solutions by dialysis. Under this concentration, the detergent is not present as micelles but as single molecules dissolved in water.

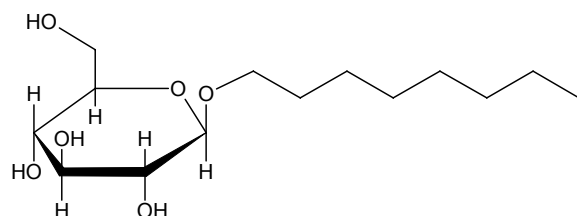


Figure 49: n-Octylglucoside (n-Octyl-beta-D-glucopyranoside)

In practice, a SAM of the polymer thiolipid was formed by incubating a gold electrode in a detergent solution of polymer thiolipid (0.04 mg/ml, 48 mM octylglucoside in HEPES buffer) for 12h, followed by washing with a 48 mM octylglucoside solution in HEPES buffer for 1 h. After characterization of this monolayer by SPR, the surface was rinsed for some hours with pure HEPES buffer to eliminate any traces of detergent.

4.2.4. Incorporation of proteins

After ascertaining the formation of a lipid bilayer, it is important to verify whether this platform is able to host membrane proteins in a functionally active state. Key features are the high electrical sealing properties of the bilayer, to allow for ion transport due only to protein action, and an ion reservoir between bilayer and substrate. A simple, but extremely useful, test consists in incorporating in the lipid bilayer a very simple small protein and in verifying its functionality in this environment. The ion carrier valinomycin and the ion channel gramicidin were used for this test.

The incorporation of a protein into a membrane can follow different pathways. Isolated and solubilized proteins may partition spontaneously into the hydrophobic membrane environment. Most proteins, however, require a membrane-like environment at all times. The easiest way is to fuse proteoliposomes, protein containing vesicles, on the self-assembled monolayer.

Here is a short description of the proteins used for membrane testing and how they function in cells.

Valinomycin.

Valinomycin is a cyclododecadepsipeptide neutral ionophore produced by *Streptomyces fulvissimus*. As a natural ion translocating compound shown in Figure 51, valinomycin^[82, 83] can be used as a model system for electrochemical impedance spectroscopy studies on tBLMs^[84]. It is a cyclic antibiotic consisting of three D-valines, three L-valines, three L-lactic acids, and three D-hydroxyisovaleric acids, forming a highly specific K^+ ionophore^[85], hydrophilic in the inside, and hydrophobic outside. The molecule has a large flexibility in solution but gains marked structure when it complexes potassium with the 6 carbonyl oxygens from the acids; two additional oxygens from water may coordinate with K^+ to give an octahedral coordination. The 9 isopropyl groups and 3 methyl groups contribute to a low solubility in water but relatively high solubility in ether, benzene, chloroform and lipids. The high affinity for potassium gives this compound utility as an antibiotic, an insecticide, a nematocide, and an ionophore in K^+ -specific electrodes.

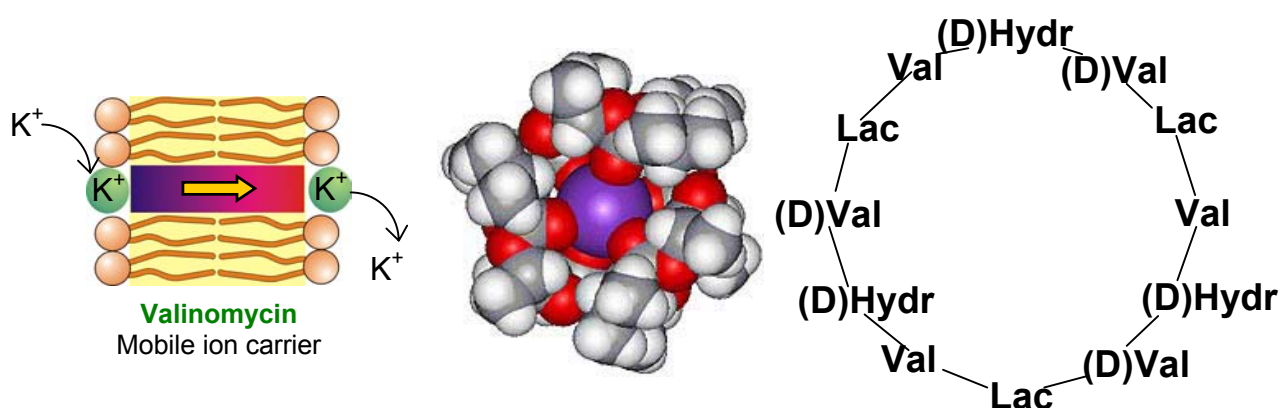


Figure 51: Principle of ion carrier, structure of valinomycin

In practice, valinomycin spontaneously partitions into a preformed lipid bilayer when an aliquot (5 μ l, 17 μ M) of an ethanolic stock solution ($c = 4$ mg/mL) is added to the measurement cell. As a potassium carrier, it transports selectively potassium ions to the

detriment of other ions. The selectivity reaches a factor of 10^4 in the case of Na^+ . In our case, the functional incorporation of valinomycin translates into a decrease of the membranes resistance, and this as function of potassium concentration.

Gramicidin.

This small dimeric protein is a channel-forming ionophore that kills bacteria. It is one of the best characterized and most extensively studied pore-forming compounds^[86, 87]. This linear pentadecapeptide consists of a helical dimer structure^[88] (Figure 53), which produces a continuous channel through a lipid bilayer. In its active form, the resulting dimer has a length of 26 Å, sufficient to span a lipid bilayer, as depicted in Figure 53. The conducting dimer in the bilayer membrane is in equilibrium with non-conducting monomers^[89]. Gramicidin forms a pore of 4 Å in diameter allowing the passage of monovalent cations. The cation selectivity is small but significant and follows^[90]: $\text{H}^+ > \text{NH}_4^+ > \text{Cs}^+ > \text{Rb}^+ > \text{K}^+ > \text{Na}^+ > \text{Li}^+$. Notice with the help of Figure 52, that most of the atoms on the outside of the helix are nonpolar carbon atoms (gray) that interact with the nonpolar interior of the membrane. Viewed end-on, the hole in the center of the molecule through which ions pass is clearly visible (right view). The polar oxygen (red) and nitrogen (blue) atoms exposed in the central hole facilitate the movement of polar ions across the membrane. The ability to generate ion gradients across membranes is essential to the life of a cell. For example, bacterial cells need ion gradients in order to produce ATP. Gramicidin destroys this ability by allowing free movement of ions.

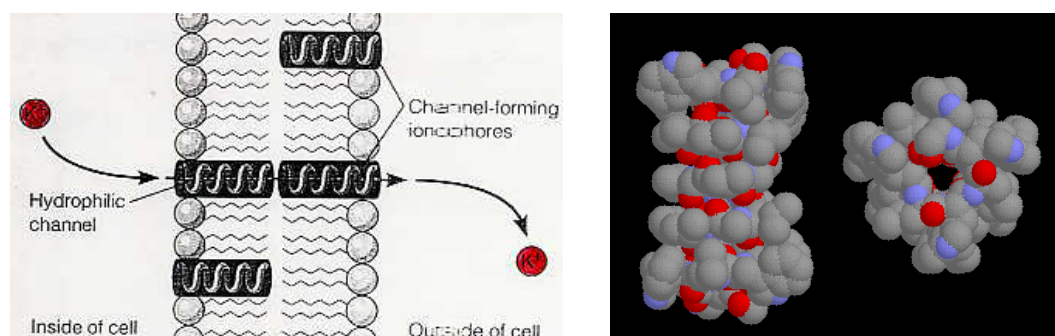


Figure 52: a) Gramicidin channel in a membrane b) Atomistic view

In practice, as in the case of valinomycin, an aliquot (10 µl, 5 nM) of an ethanolic stock solution (5 µg/ml), added in the aqueous bathing solution allows the incorporation of the peptide in the membrane. In this case, the functional incorporation can be shown by exposing the incorporated ion channel to different electrolyte solutions. Due to the size of the pore (4Å) only small monovalent ions can pass through the channel.

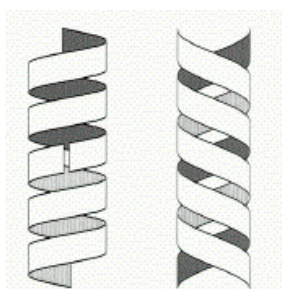


Figure 53: Schematic structure of SS and DS gramicidin dimers

4.3. Membrane formation with our systems

A series of different thiolipids were synthesized. Subsequently, their ability to form “good” tBLMs were investigated. First tests were carried out with the lipids based on ethyleneglycol polymerization as described in chapter 3.2.2. They are characterized with a large molecular weight distribution and an uncertainty concerning the number of thiol functionalities. As results of membrane formation via EIS/SPR measurements were not satisfactory and the defined route adopted, we concentrated on the latter.

When the molecules obtained via defined synthesis were obtained, a quick investigation on membrane formation was completed. Indeed, at that stage of the project, it was important for us to know to which extent this new series of molecules could improve the system in place today (DPTL), as well as become a new tool to study larger proteins. Additionally, from a more fundamental point of view, it is interesting to compare the different spacer lengths obtained with respect to their effect on monolayer formation. Criteria for “good” membranes are their electrical properties of the bilayer with respect to natural ones, and the ability to incorporate small proteins. If this protein behaves like in a natural environment, the tethered membrane possesses good properties to mimic a cell membrane.

A second step would be to optimise the preparative conditions with the ultimate goal to measure single channels events.

The techniques used to characterize the system, Surface Plasmon Resonance (SPR) and Electrochemical Impedance Spectroscopy (EIS) are described in chapter 2.

4.3.1. Polymer membranes

The membrane forming properties of the lipid polymer synthesized as reported in chapter 3.2.2.2.1. were investigated.

As a reminder, the structure of the polymer is shown in Figure 54. The molecules have a rather large polydispersity, and therefore, several attempts were made to improve the monolayer characteristics using different methods of monolayer formation.

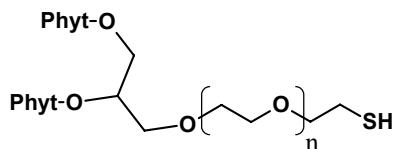


Figure 54: The polymer thiolipid 11

4.3.1.1. Monolayer and bilayer formation

The most straightforward approach is to use the self assembly method. However, first results obtained via this pathway were not satisfactory. So, different parameters as well as different assembly techniques have been screened.

Monolayer formation via SA.

First self assembly parameters optimized for DPTL were used: the slides were incubated in a 0,2 mg/ml ethanolic solution for 24h.

A thickness in air of 14 Å was measured via SPR. The SPR measurements in buffer are shown in Figure 55a. The fitted parameters are listed in Table 5. The thickness of the monolayer is very small as compared to the size of the molecule, suggesting a very diluted surface coverage. When vesicles are added, the thickness increases up to 105 Å. By comparing this to the thickness of a normal bilayer, which is in the order of 70 Å, it seems that the vesicles rather adsorb than fuse on the monolayer.

Upon vesicle addition, the EIS spectrum in Figure 55 does not change significantly. As shown in Table 5, the high capacitance of the layers also corresponds to a lightly packed monolayer. The resistance increases slightly, however, the increase in capacitance also indicates vesicle adsorption. The polymer does not attach on the surface as a dense monolayer, and therefore, does not provide a good hydrophobic platform for vesicle fusion.

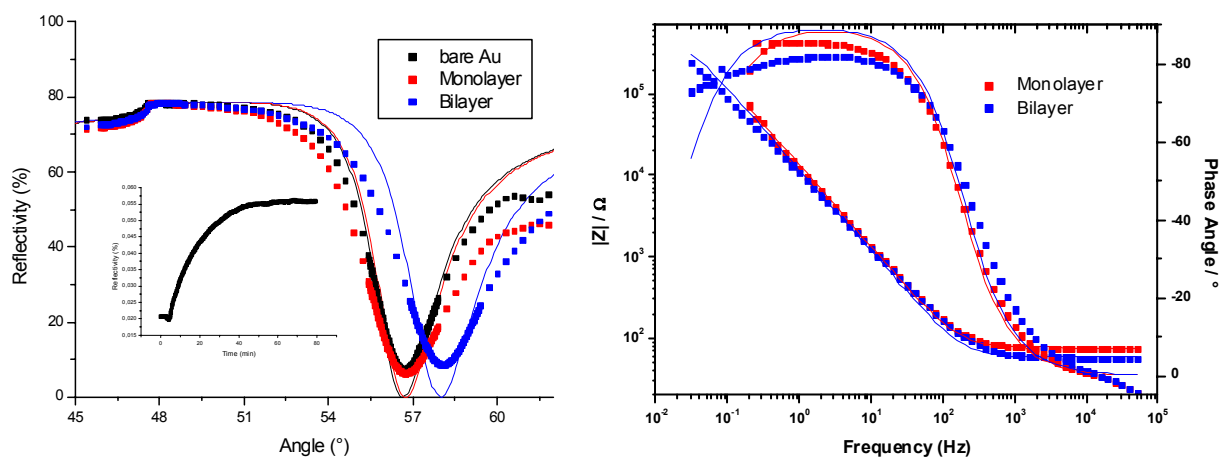


Figure 55: a) SPR data and b) EIS data of bilayer formation via SA

	C_2 (μFcm^{-2})	R_2 ($\text{M}\Omega\text{cm}^2$)	Thickness
Monolayer	15,2	0,3	8 Å
Bilayer	17,6	0,4	105 Å

Table 5: Equivalent circuit values and fitted thickness of bilayer formation via SA for the lipid polymer **11**

To improve the monolayer properties, different parameters were varied. First, an extraction of the slides with ethanol after the SA was considered. In fact, the polymer is a mixture of ethyleneglycol chains terminated by a thiol group, and ethyleneglycol chains with an OH endgroup. The latter do not bind covalently to the surface and occupy space. They may be removed during the wetting of the surface with the buffer. By removing them during extraction, free space is therefore provided for lipids to assemble in the empty spaces.

In Figure 56 the results of a slide after one night of extraction are shown. SPR and EIS data indicate an even more dilute monolayer. But vesicles seem to fuse and bilayer formation can be observed. Indeed, a 20-fold increase of resistance as well as a very obvious decrease in capacitance is observed after the addition of the vesicles to the measurement cell, while the kinetic curve of the vesicle fusion on Figure 56 shows a typical trend for vesicle fusion. Moreover, the thickness simulated for the bilayer (see Table 6) has an increase of 30 Å which is in the range of a lipid upper leaflet thickness. However, the electrical parameters are still insufficient to envisage protein incorporation.

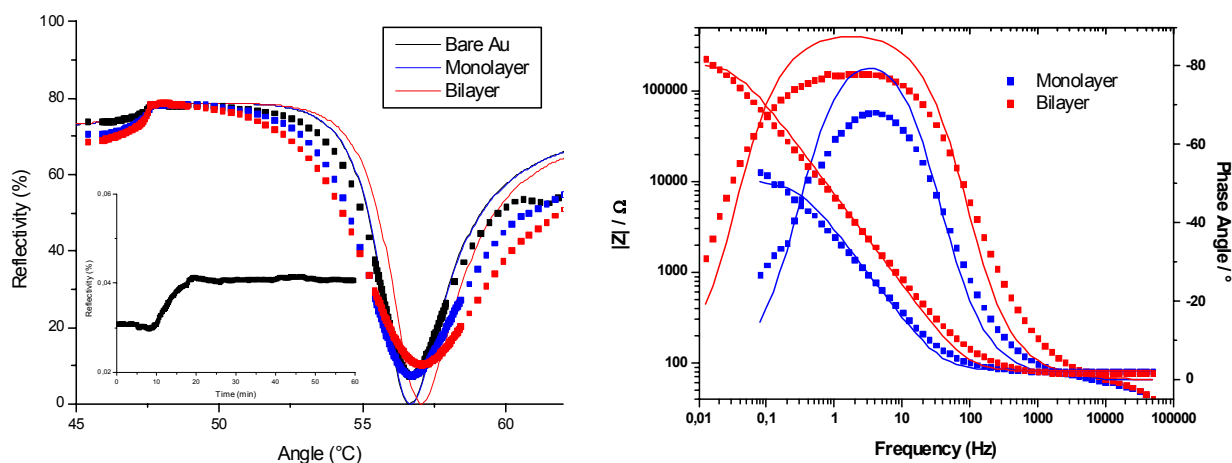


Figure 56: a) SPR data and b) EIS results of bilayer formation after SA and 1 night extraction.

	C_2 (μFcm^{-2})	R_2 ($\text{M}\Omega\text{cm}^2$)	Thickness
Monolayer	67,4	0,007	2 Å
Bilayer	28,5	0,156	32 Å

Table 6: Equivalent circuit values and fitted thickness of bilayer formation via SA and extraction

The concentration is sometimes a parameter that plays a huge role in the self assembly process. Therefore the SA concentration was decreased and the assembly time increased to favor the binding of the molecules with a thiol group against the adsorption of the hydroxy terminated molecules.

Samples were incubated in a solution with a concentration of 0.04 mg/ml for one week. In Figure 57, SPR and EIS hardly show monolayer formation. Therefore, the vesicle fusion should only lead to a supported, partially tethered bilayer.

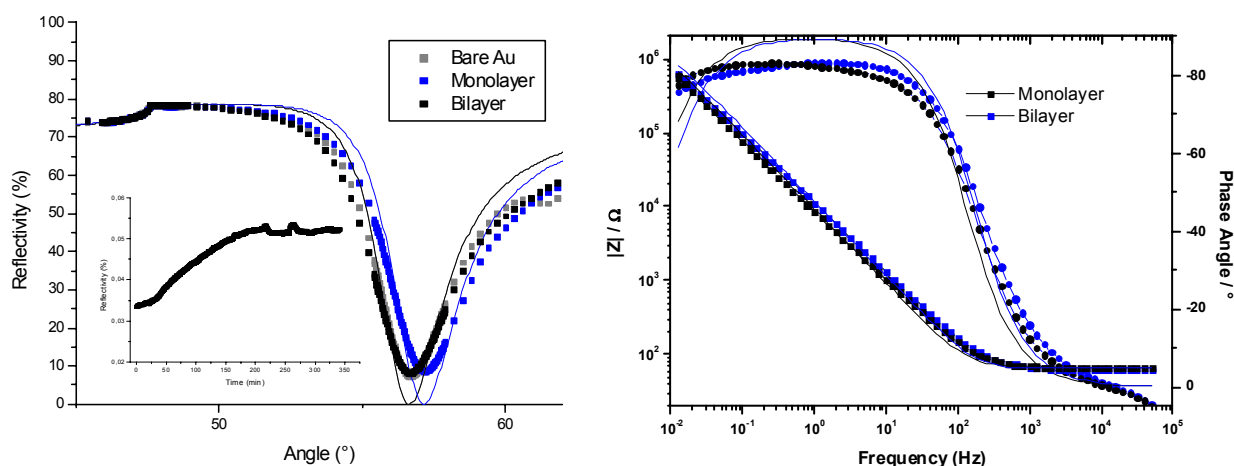


Figure 57: a) SPR data and b) EIS data for SA 0.04 mg/ml, 1 week.

The values shown in Table 7 indicate that a supported bilayer was formed. The thickness increase is about the size of a lipid bilayer, moreover, the formation of a bilayer is translated into a decrease of capacitance.

	C_2 (μFcm^{-2})	R_2 ($\text{M}\Omega\text{cm}^{-2}$)	Thickness
Monolayer	22,4	1,4	0 Å
Bilayer	17,7	1,3	40 Å

Table 7: Equivalent circuit values and thickness of bilayer formation via SA of 0.04mg/ml for one week

As can be seen by the equivalent circuit values in Table 8, the variation of the extraction time did not significantly improve the membrane parameters. The contact angle shows that the surface is very hydrophilic and the absence of vesicle fusion can verify such a hydrophilic surface.

Moreover, the thicknesses simulated according to SPR measurements show that there is definitely vesicle adsorption, and no fusion, the values are far too high.

For 48h extr.	C_2 (μFcm^{-2})	R_2 ($\text{M}\Omega\text{cm}^{-2}$)	Contact A.	Thickness
Monolayer	52,1	0,4	53.6	9 Å
Bilayer	65,2	0,1		Å

For 2,5h extr.	C_2 (μFcm^{-2})	R_2 ($\text{M}\Omega\text{cm}^{-2}$)	Contact A.	Thickness
Monolayer	47,43	0,8	52.7	6 Å
Bilayer	28,34	0,8		159 Å

Table 8: Equivalent circuit values and fitted thickness of bilayer formation via SA 0.04 mg/ml and different extraction times.

According to the thicknesses obtained, and the kinetics observed after addition of the vesicles, it seems that the coverage of the gold surface is very low.

Self assembly does not seem to be suitable for the investigated polymer thiolipid. Therefore, different strategies were used to form a monolayer. In these further experiments, the monolayer only is considered, as a first step of the bilayer construction. Without a monolayer bearing acceptable properties, it is not worth forming a bilayer.

Monolayer formation via LB

The Langmuir-Blodgett method was used to deposit a monolayer on a Au substrate. Subsequently, different treatments were applied to these monolayers as described in the table below.

<i>Name</i>	<i>Treatment after the transfer</i>
LB	Measured directly
LB dried	Dried in air overnight
LB EtOH	Extracted in ethanol for 24h
LB+SA	SA in 0.1 mg/ml polymer lipid in ethanol

Table 9: Treatments after the LB transfer

The SPR and EIS data for the different samples are shown in Figure 58. The corresponding fitted values are listed in Table 10.

According to the thicknesses obtained by SPR and the values for the equivalent circuit, the best monolayer is obtained for the slide LB+SA. The resistance obtained in this case is even better than the one obtained for self assembly alone. The LB transfer alone is comparable to the other treatments performed, and shows impedance spectra much worse than LB+SA.

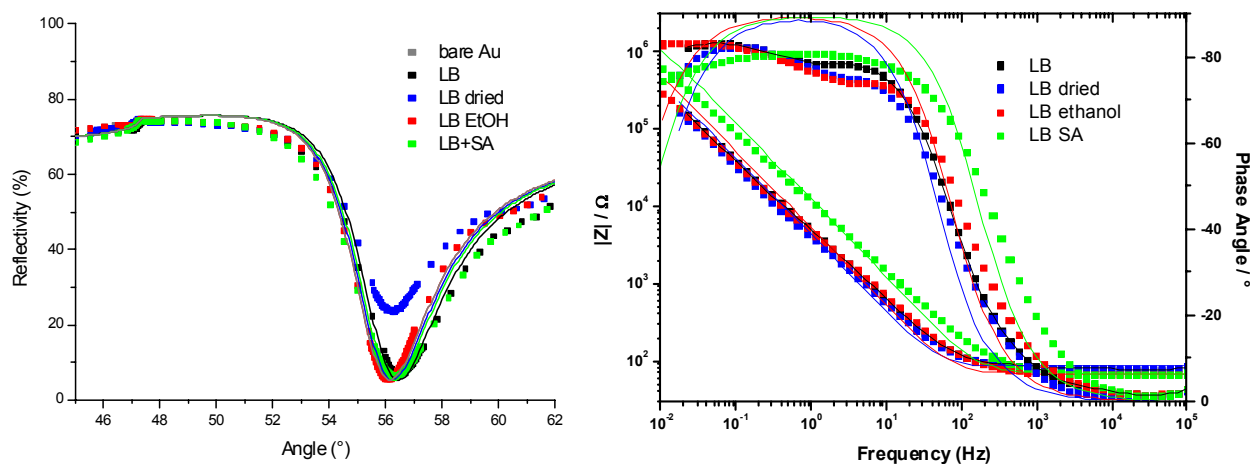


Figure 58: a) SPR data and b) EIS data for the LB transfer experiments

	C_2 (μFcm^{-2})	R_2 ($\text{M}\Omega\text{cm}^{-2}$)	Contact angle	Thickness
LB	40,1	0,5	59,3	24 Å
LB dried	48,5	0,4	70,0	7 Å
LB Ethanol	39,7	0,9	67,6	0 Å
LB SA	17,0	1,3	59,6	13 Å

Table 10: Equivalent circuit values and fit thickness for the different LB experiments.

The results obtained with LB show that LB together with self assembly gives similar results to those obtained with self assembly alone. The most dense packing can be obtained by self assembly. Self Assembly after a previous LB-transfer only adds anchor lipids by filling empty spaces in the monolayer.

LB therefore does not significantly increase the monolayer properties.

Monolayer formation via OG vesicles

Vesicles are used in different ways in bilayers, either to form monolayers, proximal or upper leaflet, or bilayer, like in the group of Chopineau^[91]. So this method was thought to be a promising strategy to build a monolayer with our polymer thiolipid. The detergent/polymer thiolipid mixed vesicles were self-assembled to a surface for 12h and then the slide was measured via SPR and EIS. The values shown in Table 11 are obtained for a monolayer bearing detergent molecules. Then the measurement cell was rinsed with pure buffer to remove the detergent. According to the thicknesses obtained (Figure 59), a monolayer was formed, but the values obtained from the model circuit do not show better properties than the SA slide. Moreover, one has to keep in mind that in this case, one can only guarantee that after the rinsing process, there is less than 0.1 M detergent in the solution, which can still modify the properties of the monolayer.

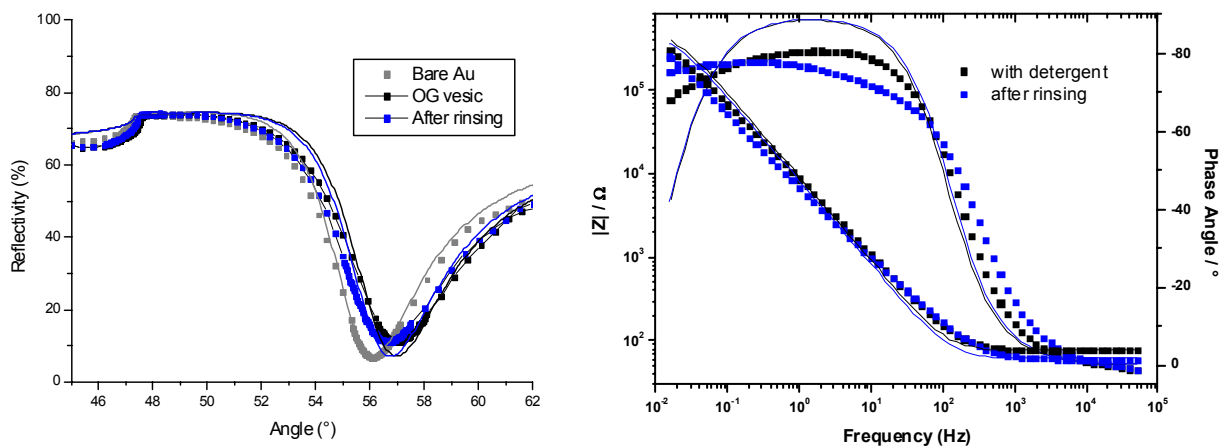


Figure 59: a) SPR data and b) EIS data for a monolayer formed with OG vesicles.

	C_2 (μFcm^{-2})	R_2 ($\text{M}\Omega\text{cm}^2$)	Contact angle	Thickness
With OG	22,6	0,4	38,135	65 Å
After rinsing	25,3	0,4		48 Å

Table 11: Equivalent circuit values and fitted thickness for a monolayer formed with OG vesicles.

4.3.1.2. Conclusion.

Monolayer formation using the polymer thiolipids was investigated using different assembly techniques, namely self-assembly, LB transfer and detergent vesicles assembly. None of the methods led to dense monolayers with sufficient electrical properties.

Similarly, no highly insulating bilayer could be obtained. Most probably, the high polydispersity of the anchor lipids as well as the undefined amount of functional endgroups does not allow dense monolayer formation.

These results show that this molecule is not the best candidate to build these membranes. After these tedious attempts to improve the properties of the polymer, the polymerisation strategy was abandoned, and the project moved on towards a defined synthetic pathway. In the next chapter, we describe the results obtained with these new molecules.

4.3.2. Tether molecules from defined synthesis

A series of anchorlipids has been obtained via defined synthesis. They differ in the length of the spacer unit (4-14) and in the lipid headgroup, i.e. mono or diphytanyl moiety. The different compounds have been tested for their ability to form mono- and bilayer. Furthermore, the obtained tBLMs have been used as a platform for protein incorporation.

4.3.2.1. Monolayer and bilayer formation

Monolayers were obtained by self-assembly. Gold slides were immersed in an ethanolic solution (0,2 mg/ml) of the respective thiolipid for 24h, if not stated otherwise.

- **MPTL**

MPTL differs by one alkyl chain from DPTL, the reference molecule. The influence of the lipid headgroup on the formation of monolayer and bilayer has been investigated.

MPTL coated gold slides give static contact angles around 94° . For a 48h assembled sample, vesicle fusion could be observed using EIS. The spectra are shown in Figure 60, for clarity reasons only, the simulation curves of the SAM and the formed bilayer are shown for the vesicle fusion experiment. The electrical values obtained for the monolayer, shown in Table 12, show a gigaseal, though with a high capacitance, which proves that the coverage of the surface is not complete. These values do only slightly depend on the self-assembly time.

In the impedance spectra shown in Figure 60a), a new shoulder shows the appearance of a new RC element in the model circuit, which can be attributed to the bilayer. The capacitance C_2 decreases, and the resistance R_2 increases. The new RC element may be the indication of the bilayer growth, but this interpretation is not enough to explain the behavior of the membrane.

In order to improve the bilayer properties, the solvent exchange method was used for a monolayer self-assembled for 24h and the results are given in Figure 60b). The formation of a bilayer can be observed by the appearance of the characteristic shoulder. The RC element corresponding to the monolayer does not vary much, but the values obtained for the second RC element show a bilayer, with a capacitance very close to natural membranes.

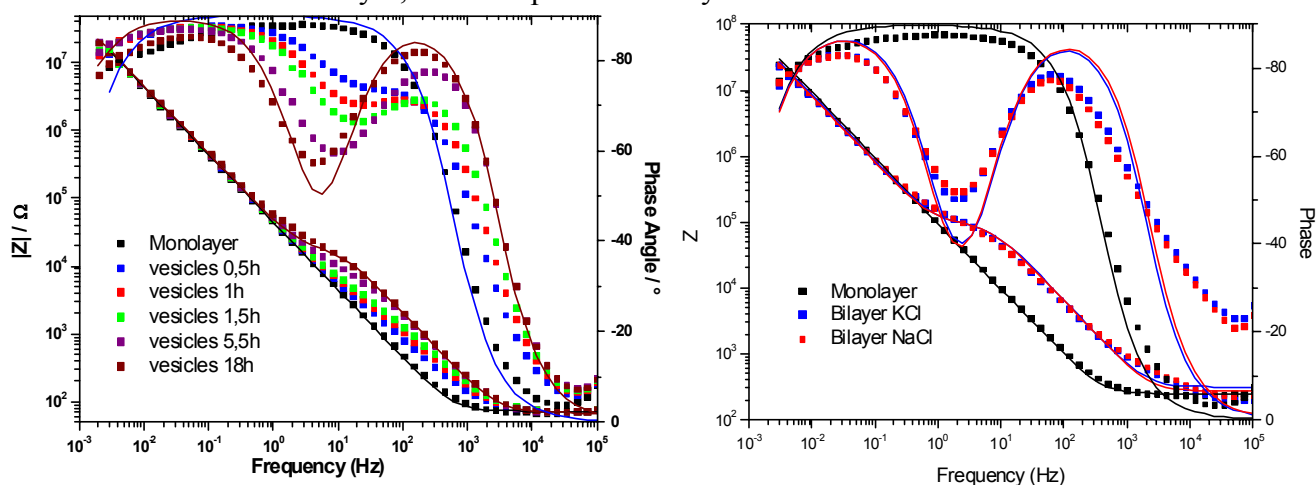


Figure 60: **MPTL** monolayer and bilayer formation via a) vesicle fusion, b) solvent exchange

	C_2 (μFcm^{-2})	R_2 ($\text{M}\Omega\text{cm}^2$)	C_3 (μFcm^{-2})	R_3 ($\text{k}\Omega\text{cm}^2$)
Monolayer	17,9	10,2	-	-
Bilayer VF	16,8	14,2	4,9	3,6
Monolayer	8,3	18,2	-	-
Bilayer SE	9,2	14,4	1,48	14,1

Table 12: Equivalent circuit values for *MPTL* monolayer and bilayer via the two methods.

- **DPHL**

DPHL belongs to the family of DPTL but with a spacer component of 6 ethyleneglycol units. A typical DPHL monolayer has a hydrophobic static contact angle of 97-100°.

As for MPTL, both vesicle fusion and solvent exchange methods were used to form a bilayer.

Figure 61a) shows the in situ formation of the bilayer via vesicle fusion on a DPHL monolayer as monitored by EIS. After 5,5 h, a stable bilayer is formed. Similar to MPTL, the apparition of a second shoulder in the EIS spectrum can be observed, here more pronounced. This is also true for the values obtained for the model circuit, shown in Table 13. The second RC element representing the lipid double layer shows a capacitance very close to those from natural membranes and a resistance in the kilohm range. One can note that, on the contrary to MPTL, a vesicle fusion can be obtained with standard assembly conditions and with a good reproducibility on a DPHL monolayer.

The solvent exchange method gave similar results, but it was abandoned in favor of vesicle fusion, which does not involve incubation of the cell in ethanol.

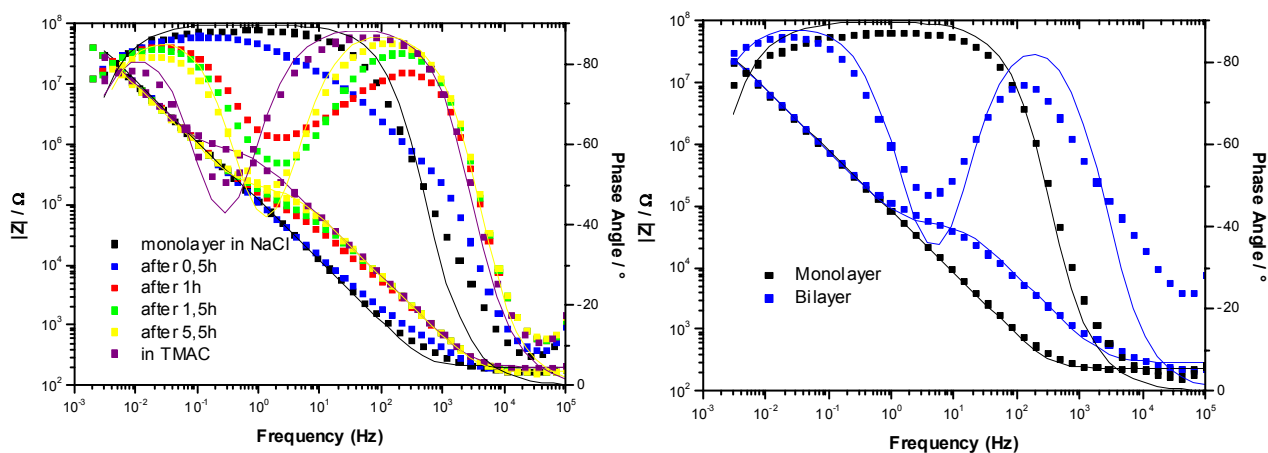


Figure 61: *DPHL* monolayer and bilayer formation via a) vesicle fusion, b) solvent exchange

	C_2 (μFcm^{-2})	R_2 ($\text{M}\Omega\text{cm}^2$)	C_3 (μFcm^{-2})	R_3 ($\text{k}\Omega\text{cm}^2$)
Monolayer	6,87	23,5	-	-
Bilayer VF	8,22	16,3	1,44	31,8
Bilayer VF TMAC	7,30	8,6	1,48	107,6
Monolayer	9,82	13,0	-	-
Bilayer SE	10,3	27,3	1,17	9,2

Table 13: Equivalent circuit values for *DPOL* monolayer and bilayer via the two methods.

One can also observe the role of the size of cations in the electrical properties of the membranes. The bilayer formation experiments were all carried out with NaCl 0.1 M. If this buffer is changed to TMAC (0.1 M), the electrical properties of the bilayer improve. R_3 increases by a factor of 3. In fact, large ions are less permeable than small ions. TMA^+ are very bulky cations which have less probability to go through the membrane than a small Na^+ ion. EIS measuring ion flows across the membrane, the bigger the ion, the better the sealing properties.

• *DPOL*

DPOL has a spacer part of 8 ethyleneglycol units, so the contribution of the spacer component starts to play a predominant role in the system. In this case, the static contact angle measured is about 100° .

Vesicles did not lead to membranes with good electrical properties, only a small shoulder appears in the high frequency range. However, the solvent exchange method proved to be useful as can be seen in Figure 62. Again, the appearance of the second shoulder in the Bode plot can be observed, and fitting to our double RC model circuit shows a capacitance from the fit (Table 14) in the range of a natural membrane and a resistance in the kilohm range. It can be observed that there is a self healing process taking place during the solvent exchange. Indeed, after 4 hours, the electrical properties of the bilayer are better than immediately after the exchange of ethanol against buffer.

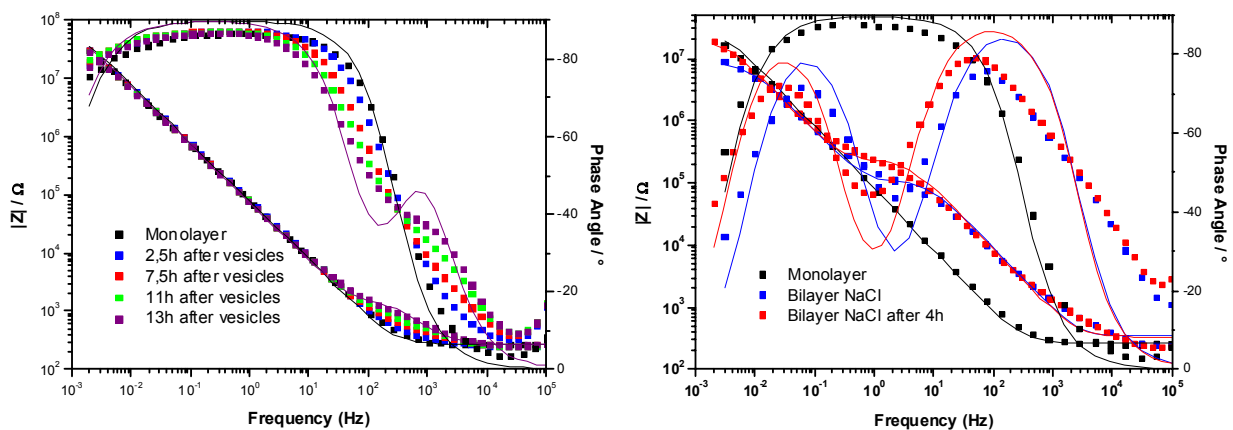


Figure 62: *DPOL* monolayer and bilayer formation via a) vesicle fusion, b) solvent exchange

	C_2 (μFcm^{-2})	R_2 ($\text{M}\Omega\text{cm}^2$)	C_3 (μFcm^{-2})	R_3 ($\text{k}\Omega\text{cm}^2$)
Monolayer VF	10,1	19,1	-	-
Bilayer VF	10,8	20,6	2,21	0,191
Monolayer	9,7	5,5	-	-
Bilayer SE	11,8	1,7	0,93	19,5
Bilayer after 4h	12,1	3,6	0,98	41,6

Table 14: Equivalent circuit values for **DPOL** monolayer and bilayer via the two methods.

Since the molecules now have a longer spacer part, and taking into account that the stretched conformation was maybe not the most stable for the ethyleneglycol part, LB transfer was thought to be a method of choice to produce densely packed monolayers, and maybe force the stretching of these ethyleneglycol moieties to favor a denser packing. Indeed, in a self assembly process, these parameters cannot be controlled and a coiled spacer would maybe occupy more space than a stretched one, which would perturb the monolayer. However, according to the results for LB transfer at different speed and pressures, monolayers obtained via LB transfer have worse properties in comparison to a SAM.

- **DPTDL**

DPTDL is a very long molecule, with a spacer of 14 ethylene glycol units. The static contact angle was about 73° . As shown in Figure 63, no change in the impedance spectrum was observed after 13h vesicle fusion.

Solvent exchange (see on Figure 63) was again a good solution to obtain a bilayer. However, the electrical properties of this bilayer are not comparable at all with the former systems. The shoulder appearing in the high frequencies range does not grow much and it is difficult to fit. Moreover, the self healing properties seen in other bilayers do not take place here. The bilayer is so fragile that after a few hours, the properties degrade. These poor electrical properties, as well as this lack of stability for the bilayer, may be due to the length of the spacer.

However, in comparison to a natural membrane, the DPTDL monolayer has quite promising values: high resistance, and low capacitance.

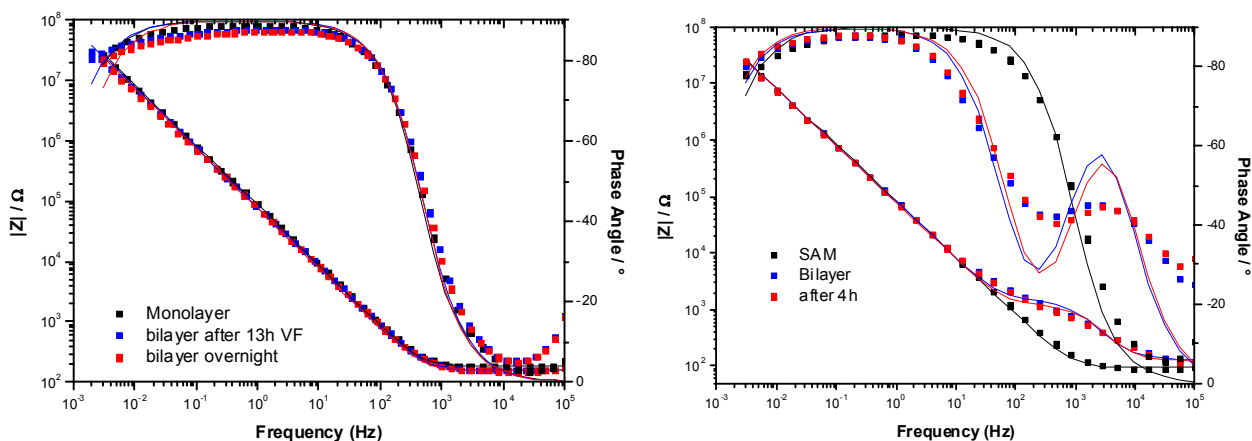


Figure 63: *DPTDL* monolayer and bilayer formation via a) vesicle fusion, b) solvent exchange

	C_2 (μFcm^{-2})	R_2 ($\text{M}\Omega\text{cm}^2$)	C_3 (μFcm^{-2})	R_3 ($\text{k}\Omega\text{cm}^2$)
Monolayer	9,2	37,9	-	-
Bilayer VF	10,4	17,0	-	-
Monolayer	9,4	17,8	-	-
Bilayer SE	9,7	21,6	0,83	1,2

Table 15: Equivalent circuit values for *DPTDL* monolayer and bilayer via the two methods.

It was possible to form a bilayer, with all our synthesized compounds, using different methods. However, these results are not sufficient to consider that our systems are suitable platforms for large proteins. The best test is still to incorporate a small ionophore to see how it reacts in these new constructions.

4.3.2.2. Protein incorporation

Since a bilayer could be obtained for all of our thiolipids, protein incorporation could be tested. As stated in chapter 4.2.5., two different proteins were tested, valinomycin and gramicidin. The results obtained for the different platforms are summarized in this chapter.

Valinomycin

- **MPTL**

As described in chapter 4.2.5., Valinomycin is a ion carrier selective to potassium cations. In the presence of potassium, a membrane containing valinomycin becomes less resistive. Figure 64 shows that a bilayer containing valinomycin is more conductive than without the protein. The values are listed in Table 16. A reversible ten-fold decrease in resistivity R_3 can be observed when exchanging Na^+ against K^+ .

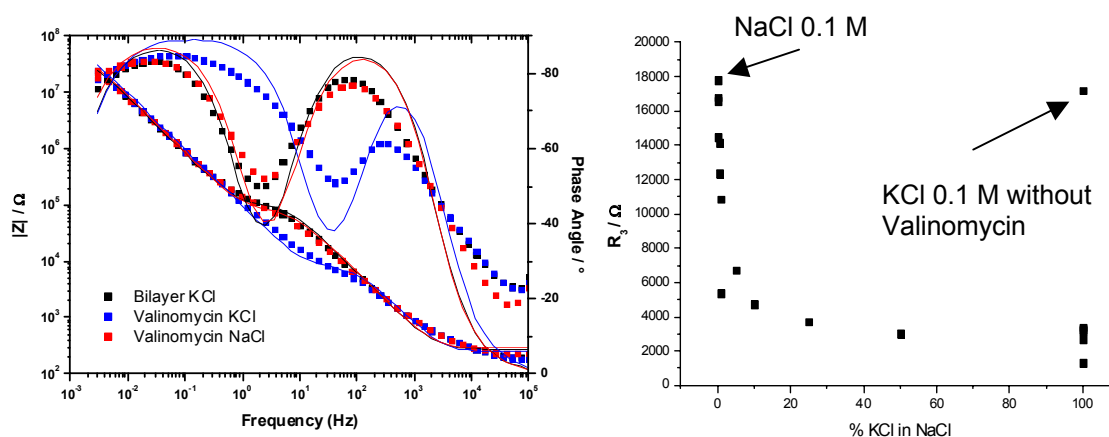


Figure 64: a) Valinomycin incorporation in a **MPTL/DPhyPC** bilayer; b) Exponential behavior of the K^+ transport

Figure 64b shows the membrane resistance as a function of K^+ concentration. The experiment is initially conducted with NaCl 0,1 M. This buffer is exchanged stepwise with buffers with a higher content of potassium ions, while keeping the ionic strength constant. An exponential behavior of the resistance R_3 can be observed while the other components of the equivalent circuit remain rather constant. For concentrations as small as 5mM, the resistivity significantly decreases.

	C_2 (μFcm^{-2})	R_2 ($\text{M}\Omega\text{cm}^2$)	C_3 (μFcm^{-2})	R_3 ($\text{k}\Omega\text{cm}^2$)
Bilayer KCl	9,75	15,1	1,45	17,2
Valinomycin KCl	8,20	17,2	1,16	1,3
Valinomycin NaCl	9,61	19,6	1,43	17,8

Table 16: Equivalent circuit values for Valinomycin incorporation in a **MPTL/DPhyPC** bilayer

- **DPHL**

In a DPHL bilayer, it was also possible to incorporate valinomycin and observe its functionality for several cycles of exchange between NaCl 0,1 M buffer and KCl 0,1 M buffer. The values obtained for the equivalent circuit elements are shown in Table 17. The resistance R_3 is depicted versus the type of buffer in solution in Figure 65.

	C_2 (μFcm^{-2})	R_2 ($\text{M}\Omega\text{cm}^2$)	C_3 (μFcm^{-2})	R_3 ($\text{k}\Omega\text{cm}^2$)
Bilayer KCl	10,1	35,3	1,37	9,1
Valinomycin KCl	9,37	24,9	1,38	2,0
Valinomycin NaCl	10,0	18,5	1,48	21,2
Valinomycin KCl	9,83	17,5	1,35	1,8
Valinomycin NaCl	10,1	16,0	1,51	17,7

Table 17: Equivalent circuit values for Valinomycin incorporation in a **DPHL/DPhyPC** bilayer

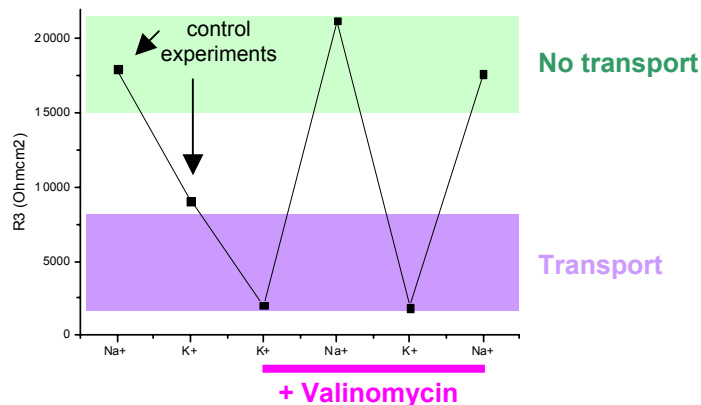


Figure 65: Electrolyte exchange in a **DPHL/DPhyPC** bilayer, in the absence and in the presence of valinomycin

By exchanging the electrolyte composition inside of the flow chamber, it is possible to analyze the altered conductivity of the carrier. In Figure 65, the results of the valinomycin experiment for DPHL are illustrated in terms of the membrane resistance R_3 . To study the selectivity of the protein, impedance spectra were recorded in the presence of two types of electrolytes: KCl 0.1 M, as permeable cations, and NaCl 0.1 M, as non permeable cations. The change in membrane conductivity led to a vertical shift of the plateau-like regime (corresponding to the membrane resistance) of the impedance curves at low frequencies. The first resistances given in Figure 65 are the reference measurements in the two types of

electrolytes before the incorporation of valinomycin. The difference between the two electrolytes is usually not so large, this is yet to be clarified.

After the membrane was doped with valinomycin, the resistance decreased in the presence of potassium ions by a factor of about five, and increases in the presence of sodium ions by a factor of ten. This can be repeated a certain number of times, which shows that the protein is embedded in the membrane and functional.

- ***DPOL***

Similarly, valinomycin could be successfully incorporated in a DPOL tethered bilayer. The values obtained for the equivalent circuit are reported in Table 18.

	C_2 (μFcm^{-2})	R_2 ($\text{M}\Omega\text{cm}^2$)	C_3 (μFcm^{-2})	R_3 ($\text{k}\Omega\text{cm}^2$)
Bilayer KCl	12,7	3,4	1,04	60,4
Valinomycin KCl	11,3	2,3	0,75	1,8
Valinomycin NaCl	14,1	2,3	1,06	40,0

Table 18: Equivalent circuit values for Valinomycin incorporation in a DPOL/DPhyPC bilayer

A 20-fold increase of the resistance can be observed in the presence of valinomycin, when the potassium buffer is exchanged against sodium buffer.

Gramicidin.

The incorporation of Gramicidin in a DPHL/DPhyPC bilayer was successful. Indeed, in Figure 66, the impedance spectra show that for small ions such as Na^+ , the resistance decreases (plateau like region shifts to higher frequencies), so small ions are allowed to move through the pore, while the larger ions TMA^+ , which are larger than the pore, cannot pass. The impedance spectra for TMA^+ is the same before and after incorporation of gramicidin. Moreover, if the solution is exchanged back from NaCl to TMAC, the same phenomenon is observed: the resistance of the bilayer goes back to a level where it was before incorporation of the protein.

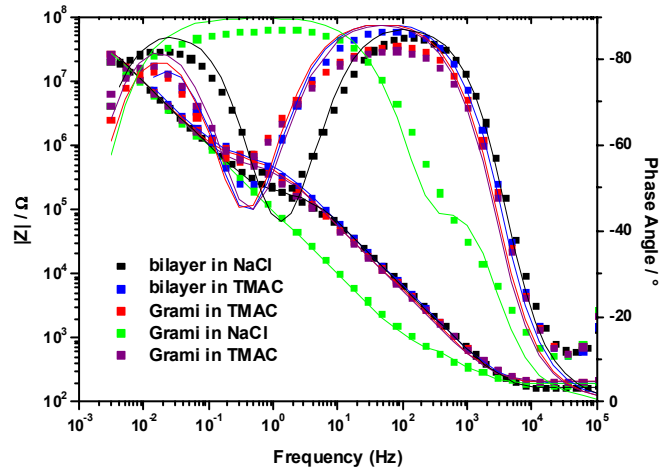


Figure 66: Gramicidin incorporation in a *DPHL/DPhyPC* bilayer

According to the values shown in Table 19, the difference in R_3 between TMA^+ and Na^+ ions is more than 30 fold.

	C_2 (μFcm^{-2})	R_2 ($\text{M}\Omega\text{cm}^2$)	C_3 (μFcm^{-2})	R_3 ($\text{k}\Omega\text{cm}^2$)
Bilayer TMAC	7,3	8,6	1,48	107,6
Gramicidin TMAC	8,23	12,1	1,69	103,4
Gramicidin NaCl	8,39	10,0	4,22	0.070

Table 19: Equivalent circuit values for Gramicidin incorporation in a *DPHL/DPhyPC* bilayer

The selectivity experiment was performed with gramicidin by exchanging the buffer solution several times. In Figure 67, the resistance of the bilayer was depicted versus the ions present in solution. The bilayer has different responses in the presence of different electrolytes. The two first points represent the resistance of the bilayer without protein in the presence of respectively Na^+ and TMA^+ ions. As previously stated in chapter 4.3.2.1., the electrolyte solution has a significant influence on the barrier properties of the bilayer. For TMAC, R_3 is three times higher than for NaCl. The three next points show the resistance of the bilayer with gramicidin. The difference between the two electrolytes used is tremendous, indicating that

gramicidin channels were successfully incorporated in the bilayer. Moreover, it is possible, after back exchange with TMA^+ ions, to reverse the experiment and obtain good sealing properties.

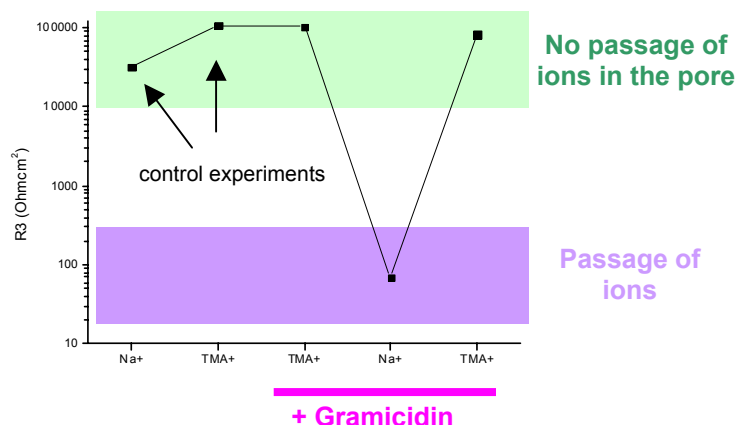


Figure 67: Electrolyte exchange in a *DPHL/DPhyPC* bilayer, in the absence and in the presence of gramicidin

In this chapter, it was possible to show that our thiolipid platforms are suitable for the incorporation of small proteins. A functional valinomycin containing bilayer was observed for three of our systems, as well as gramicidin incorporation in a *DPHL/DPhyPC* bilayer.

4.3.2.3. Comparison between the different systems

We have obtained four different molecules with two different lipid headgroups, di- and monophytanyl by the defined synthesis. All molecules could be used for the formation of a self-assembled monolayer and bilayer.

The equivalent circuit values for the monolayer are shown in Table 20. Very high resistances are observed for all the systems.

Monolayer	C_2 (μFcm^{-2})	R_2 ($\text{M}\Omega\text{cm}^2$)
DPHL	6.87	23,5
DPOL	10.10	19,1
DPTDL	9.43	17,8
MPTL	8.39	10,3

Table 20: Comparison of the equivalent values for monolayers of the different compounds.

The bilayer impedance data could be analysed with the double RC equivalent circuit, the first RC element representing the lipid bilayer, and the second one corresponding to the spacer region. In all cases, highly insulating membranes can be obtained. The capacitances, however, are higher than their natural analogues.

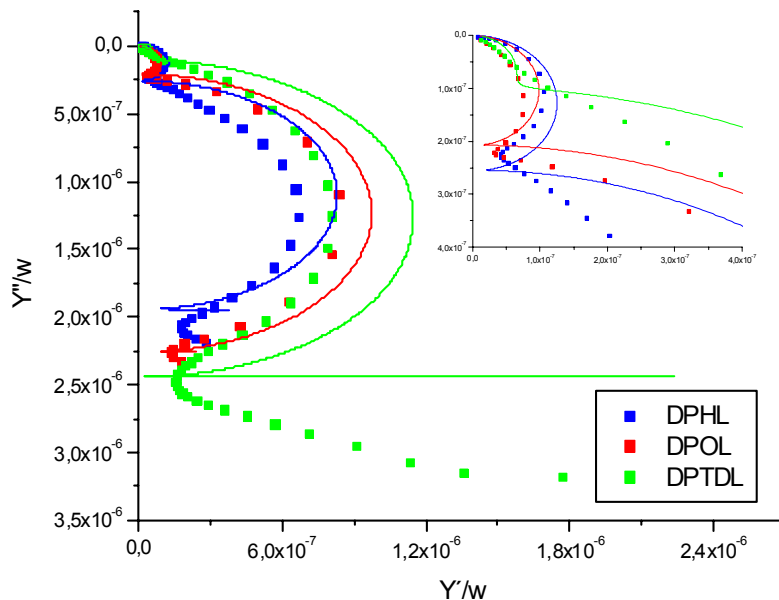


Figure 68: Angular plot of the EIS spectra of bilayers from the different compounds.

In Figure 68, the Nyquist plot clearly shows the two different time constants corresponding to the two capacitances of the system. In this representation, an RC element corresponds to a semi-circle; the radius is proportional to the capacitance. The first, smaller semi-circle corresponds to the lipid bilayer. The inset in Figure 68 shows this region enlarged. The diameter of the circle and therefore the capacitance of the bilayer decreases with increasing spacer length, corresponding to a higher charge separation of bilayer and substrate. On the other hand, the capacity of the spacer region increases with increasing spacer length, indicating that the longer chains allow for more charges to accumulate.

4.4. Conclusion

After the synthesis of a series of compounds, the study of their membrane formation was investigated. Two series of experiments were accomplished using SPR and EIS as analytical tools, first the study of the polymer thiolipid, and then the investigation of a series of defined compounds.

The first study using the polymer thiolipid showed that the monolayer with the best properties was obtained via self assembly. All other attempts to improve the monolayer were in vain. This may be due to the large molecular weight distribution of the polymer, as well as the undefined number of molecules bearing the thiol moiety. After this study, the polymer synthesis strategy was abandoned in favor of a defined synthesis of ethyleneglycol moieties.

The investigation of the defined thiolipids showed the potential of these new compounds. First, monolayers could be formed on TSG using the self assembly process for all compounds. These monolayers have slightly higher capacitances than our model molecules, as well as the natural membranes.

Moreover, it was possible, for each of the compound studied, to form a bilayer using the two techniques described, vesicle fusion and solvent exchange. This bilayer is stable for at least some days.

With MPTL, DPHL and DPOL, it was possible to functionally incorporate proteins, valinomycin and gramicidin. Their functionality could be confirmed by the change of electrical properties when the cations were exchanged.

Finally, the comparison between the different compounds allows for an insight into the role of the spacer length. The longer the spacer, the higher the capacitive contribution to the electrical properties is.

The next step in this project is to further investigate the parameters of the monolayer and bilayer formation to optimise the electrical properties of the system.

A more extensive study of the bilayer formation will also allow to compare the different systems more closely and to look for further understanding of the contribution of the spacer to the electrical properties. Finally, the variation of headgroup in the synthesis allowed us to obtain compounds differing only by the lateral space at the lipid level. This may be of great use for mixed bilayers. The gain in lateral space improved the protein incorporation step.

5. Conclusion & Outlook

Tethered bilayer lipid membranes provide an efficient, stable and versatile platform for the investigation of integrated membrane proteins. However, the incorporation of large proteins, as well as of proteins with large submembrane parts is still a very critical issue and therefore, further optimisation of the system is necessary. Important prerequisites for a “good” membrane are a high packing of the membrane, to avoid defects and provide good sealing properties, and a high fluidity to favor the incorporation of the proteins.

The central element of a tBLM is a lipid bilayer. Its proximal leaflet is, at least to some extent, covalently attached to a solid support via a spacer group. The anchor lipid consists of three distinct parts, a lipid headgroup, a spacer group and an anchor. All parts together influence the final bilayer properties.

In the frame of this work, the synthesis of new thiolipids for tBLMs on gold has been investigated. The aim was to obtain molecules with longer spacers in order to increase the submembrane space. The systems obtained have been characterized using SPR and EIS. The results obtained during this study are multiple.

First, the synthesis of a previously synthesized architecture was successfully scaled up in an industrial lab using a new synthetic approach. The synthesis of large amounts is now feasible.

Then, the synthesis of these molecules were carried out taking into account the following requirements: the increase the submembrane space by having longer ethyleneglycol spacers, the attachment of the molecules to a gold substrate via a thiol bond, and the tunability of the lateral mobility by changing the lipid headgroup. Three different synthetic strategies have been investigated.

The polymeric approach did not prove to be successful, merely because of the broad molecular weight distribution. The synthesis of heterofunctionally protected oligoethyleneglycols allowed to obtain ethyleneglycol moieties with 6 and 8 units, but the tedious purification steps gave very low yields. Finally, the block by block synthesis using ethyleneglycol precursors proved to be an efficient and fast method to synthesize the target molecules. Indeed, these were obtained with very high yields, and the separation was very efficient. A whole family of new compounds was obtained, having 6,8 and 14 ethyleneglycol units and with mono or diphytanyl lipid headgroups.

This new pathway is a very promising synthetic strategy that can be used further in the development of new compounds of the tether system. Indeed, the synthesis of new molecules can be easily transposed into our synthetic pathway. New targets could be molecules having new anchor groups to attach on different surfaces such as silica using the silane chemistry, or new compounds to increase our molecular toolkit, e.g. transmembrane lipids to stabilize the membrane, or lipids bearing different hydrocarbon chains, such as fluorescent tags or polymerizable moieties.

The formation of bilayers was investigated for the different thiolipids, mainly by using EIS. The electrical properties of a bilayer will define the quality of the membrane and allow the study of the functionality of proteins embedded in such a system.

Despite multiple trials to improve the system using self assembly, Langmuir Blodgett transfer, and detergent mixed vesicles, the polymer thiolipid did not show as high electrical properties as tBLMs reported in the literature.

Nevertheless, it was possible to show that a bilayer could be obtained for the different spacer lengths. These bilayers could be formed using self assembly for the first monolayer, and two different methods for bilayer formation, namely vesicle fusion and solvent exchange.

We could furthermore show the functional incorporation of the ion carrier valinomycin: the selective transport of K^+ ions could be demonstrated. For DPHL, it was even possible to show the functional incorporation of the ion channel gramicidin. The passage of small ions is allowed, whereas bulky ions cannot pass through this pore spanning in the membrane.

The influence of the spacer length is translated in an increase of the spacer capacitance, which could correspond to an increase in the capacity of charge accumulation in the submembrane space.

The different systems need to be further optimised to improve the electrical properties of the bilayer. Other techniques can be applied to these new systems to characterize them further, especially FRAP (Fluorescence Recovery After Photobleaching), to measure how the diffusion coefficient varies with the length of the spacer, SPR and QCM-D (Quartz Crystal Microbalance) to monitor the vesicle formation and to obtain information about the thickness of the systems.

Moreover, the incorporation of larger proteins, and proteins bearing submembrane parts needs to be investigated. We assume that the increase of the lateral space should facilitate the incorporation of such compounds. Furthermore, a mixture of different thiolipids, e.g. with different headgroups, may improve the system in combining the properties of both compounds.

Literature

- [1] S. J. Singer, G. L. Nicolson, *Science* **1972**, *175*, 720.
- [2] L. Stryer, *Biochemie*, Verlagsgesellschaft, Heidelberg, **1990**.
- [3] B. Alberts, *Molekularbiologie der Zelle*, VCH, **1995**.
- [4] B. Sakmann, E. Neher, *Single-Channel Recording*, Plenum Press, New York, **1995**.
- [5] K. Kita-Tokarczyk, J. Grumelard, T. Haefele, W. Meier, *Polymer* **2005**, *46*, 3540.
- [6] P. Broz, S. M. Benito, C. Saw, P. Burger, H. Heider, M. Pfisterer, S. Marsch, W. Meier, P. Hunziker, *Journal of Controlled Release* **2005**, *102*, 475.
- [7] C. Nardin, J. Widmer, M. Winterhalter, W. Meier, *European Physical Journal E* **2001**, *4*, 403.
- [8] C. Nardin, S. Thoeni, J. Widmer, M. Winterhalter, W. Meier, *Chemical Communications* **2000**, 1433.
- [9] R. Stoenescu, A. Graff, W. Meier, *Macromolecular Bioscience* **2004**, *4*, 930.
- [10] M. Winterhalter, *Current Opinion in Colloid & Interface Science* **2000**, *5*, 250.
- [11] L. Auvray, in *Summer school "Sensing with ion channels" IUB*, Bremen, **2005**.
- [12] J. J. Kasianowicz, *Nature Materials* **2004**, *3*, 355.
- [13] E. Sackmann, *Science* **1996**, *271*, 43.
- [14] E. Reimhult, F. Hook, B. Kasemo, *Langmuir* **2003**, *19*, 1681.
- [15] J. Jass, T. Tjarnhage, G. Puu, *Biophysical Journal* **2000**, *79*, 3153.
- [16] I. Reviakine, A. Brisson, *Langmuir* **2000**, *16*, 1806.
- [17] E. K. Sinner, W. Knoll, *Current Opinion in Chemical Biology* **2001**, *5*, 705.
- [18] E. Li, K. Hristova, *Langmuir* **2004**, *20*, 9053.
- [19] M. Merzlyakov, E. Li, K. Hristova, *Biophysical Journal* **2005**, *88*, 369A.
- [20] J. C. Munro, C. W. Frank, *Langmuir* **2004**, *20*, 10567.
- [21] J. Zhao, L. K. Tamm, *Langmuir* **2003**, *19*, 1838.
- [22] B. Schuster, P. C. Gufler, D. Pum, U. B. Sleytr, *Ieee Transactions on Nanobioscience* **2004**, *3*, 16.
- [23] P. C. Gufler, D. Pum, U. B. Sleytr, B. Schuster, *Biochimica Et Biophysica Acta-Biomembranes* **2004**, *1661*, 154.
- [24] C. Yoshina-Ishii, G. P. Miller, M. L. Kraft, E. T. Kool, S. G. Boxer, *Journal of the American Chemical Society* **2005**, *127*, 1356.
- [25] A. T. A. Jenkins, J. A. Olds, *Chemical Communications* **2004**, 2106.
- [26] K. Morigaki, K. Kiyosue, T. Taguchi, *Langmuir* **2004**, *20*, 7729.
- [27] V. Subramaniam, I. D. Alves, G. F. J. Salgado, P. W. Lau, R. J. Wysocki, Z. Salamon, G. Tollin, V. J. Hruby, M. F. Brown, S. S. Saavedra, *Journal of the American Chemical Society* **2005**, *127*, 5320.
- [28] B. A. Cornell, V. L. B. BraachMaksvytis, L. G. King, P. D. J. Osman, B. Raguse, L. Wiczorek, R. J. Pace, *Nature* **1997**, *387*, 580.
- [29] S. Terrettaz, M. Mayer, H. Vogel, *Langmuir* **2003**, *19*, 5567.
- [30] S. Schiller, R. Naumann, K. Lovejoy, W. Knoll, *Abstracts of Papers of the American Chemical Society* **2003**, *225*, U539.
- [31] S. M. Schiller, R. Naumann, K. Lovejoy, H. Kunz, W. Knoll, *Angewandte Chemie-International Edition* **2003**, *42*, 208.
- [32] M. R. Moncelli, L. Becucci, S. M. Schiller, *Bioelectrochemistry* **2004**, *63*, 161.
- [33] V. Atanasov, N. Knorr, R. S. Duran, S. Ingebrandt, A. Offenhausser, W. Knoll, I. Köper, *Biophysical Journal* **2005**, *89*, 1780.

- [34] O. Purrucker, A. Fortig, R. Jordan, M. Tanaka, *ChemPhysChem* **2004**, *5*, 327.
- [35] C. Horn, C. Steinem, *Biophysical Journal* **2005**, *89*, 1046.
- [36] W. Romer, C. Steinem, *Biophysical Journal* **2004**, *86*, 955.
- [37] L. J. C. Jeuken, S. D. Connell, M. Nurnabi, J. O'Reilly, P. J. F. Henderson, S. D. Evans, R. J. Bushby, *Langmuir* **2005**, *21*, 1481.
- [38] F. Giess, M. G. Friedrich, J. Heberle, R. L. Naumann, W. Knoll, *Biophysical Journal* **2004**, *87*, 3213.
- [39] www.cis.rit.edu/htbooks/nmr/inside.htm.
- [40] www.chem.arizona.edu.
- [41] H. D. Beckey, *Journal of Physics E-Scientific Instruments* **1979**, *12*, 72.
- [42] www.postech.ac.kr/chem/poly/research.
- [43] www.kruss.info/techniques/contact_angle_e.
- [44] Wikipedia.org.
- [45] W. Knoll, *Mrs Bulletin* **1991**, *16*, 29.
- [46] W. Knoll, *Annual Review of Physical Chemistry* **1998**, *49*, 569.
- [47] C. Gerthsen, *Physik*, Springer Verlag, **1982**.
- [48] M. Kreiter, Dissertation thesis, Johannes Gutenberg Universität (Mainz), **2000**.
- [49] I. Pockrand, *Surface Science* **1978**, *72*, 577.
- [50] G. Kovacs, *Electromagnetic Surfaces Modes*, John Wiley & Sons, New York, **1982**.
- [51] J. F. Tassin, R. L. Siemens, W. T. Tang, G. Hadziioannou, J. D. Swalen, B. A. Smith, *Journal of Physical Chemistry* **1989**, *93*, 2106.
- [52] J. R. Macdonald, *Impedance Spectroscopy*, John Wiley & Sons, New York, **1987**.
- [53] S. Gritsch, P. Nollert, F. Jahnig, E. Sackmann, *Langmuir* **1998**, *14*, 3118.
- [54] M. Stelzle, G. Weissmuller, E. Sackmann, *Journal of Physical Chemistry* **1993**, *97*, 2974.
- [55] supporting information, Fundamentals of Electrochemical Impedance Spectroscopy Gamry Instruments.
- [56] technical support, Princeton Applied Research.
- [57] H. Hillebrandt, PhD thesis, Technische Universität München (Munich), **2001**.
- [58] C. R. Woese, G. E. Fox, *Proceedings of the National Academy of Sciences of the United States of America* **1977**, *74*, 5088.
- [59] J. Lipkowski.
- [60] A. Bendavid, C. J. Burns, L. D. Field, K. Hashimoto, D. D. Ridley, K. Sandanayake, L. Wiczorek, *Journal of Organic Chemistry* **2001**, *66*, 3709.
- [61] L. G. J. Wade, *Organic Chemistry*, Pearson Education, Inc, Upper Saddle River, **2003**.
- [62] W. F. Berkowitz, D. F. Pan, R. Bittman, *Tetrahedron Letters* **1993**, *34*, 4297.
- [63] P. N. Guivisdalsky, R. Bittman, *Journal of Organic Chemistry* **1989**, *54*, 4637.
- [64] M. Makosza, *Pure and Applied Chemistry* **2000**, *72*, 1399.
- [65] R. J. Young, *Introduction to polymers*, CRC Press, **1991**.
- [66] C. Bonnans-Plaisance, M. Jean, F. Lux, *European Polymer Journal* **2003**, *39*, 863.
- [67] J. M. Tour, L. Jones, D. L. Pearson, J. J. S. Lamba, T. P. Burgin, G. M. Whitesides, D. L. Allara, A. N. Parikh, S. V. Atre, *Journal of the American Chemical Society* **1995**, *117*, 9529.
- [68] M. G. Oliveira, B. G. Soares, C. M. F. Santos, M. F. Diniz, R. C. L. Dutra, *Macromolecular Rapid Communications* **1999**, *20*, 526.
- [69] G. Coudert, M. Mpassi, G. Guillaumet, C. Selve, *Synthetic Communications* **1986**, *16*, 19.
- [70] F. A. Loiseau, K. K. Hii, A. M. Hill, *Journal of Organic Chemistry* **2004**, *69*, 639.
- [71] P. G. Schouten, J. F. Vanderpol, J. W. Zwikker, W. Drenth, S. J. Picken, *Molecular Crystals and Liquid Crystals* **1991**, *195*, 291.

- [72] R. Naumann, S. M. Schiller, F. Giess, B. Grohe, K. B. Hartman, I. Kärcher, I. Köper, J. Lübber, K. Vasilev, W. Knoll, *Langmuir* **2003**, *19*, 5435.
- [73] P. Tecilla, R. P. Dixon, G. Slobodkin, D. S. Alavi, D. H. Waldeck, A. D. Hamilton, *Journal of the American Chemical Society* **1990**, *112*, 9408.
- [74] G. M. Whitesides, J. P. Mathias, C. T. Seto, *Science* **1991**, *254*, 1312.
- [75] J. S. Lindsey, *New Journal of Chemistry* **1991**, *15*, 153.
- [76] A. Pfeil, J. M. Lehn, *Journal of the Chemical Society-Chemical Communications* **1992**, 838.
- [77] F. Schreiber, *Progress in Surface Science* **2000**, *65*, 151.
- [78] www.mtl.kyoto-u.ac.jp/english/laboratory/nanoscope/images/image_1.jpg.
- [79] G. L. Gaines, *Insoluble monolayers at liquid-gas interfaces*, Interscience, New York, **1966**.
- [80] H. Möhwald, *Annual Review of Physical Chemistry* **1990**, *41*, 441.
- [81] C. Miller, P. Cuendet, M. Gratzel, *Journal of Electroanalytical Chemistry* **1990**, *278*, 175.
- [82] H. J. Freisleben, D. Blocher, K. Ring, *Archives of Biochemistry and Biophysics* **1992**, *294*, 418.
- [83] B. C. Pressman, E. J. Harris, W. S. Jagger, J. H. Johnson, *Proceedings of the National Academy of Sciences of the United States of America* **1967**, *58*, 1949.
- [84] B. Raguse, V. Braach-Maksvytis, B. A. Cornell, L. G. King, P. D. J. Osman, R. J. Pace, L. Wiczorek, *Langmuir* **1998**, *14*, 648.
- [85] S. Kim, S. Morimoto, E. Koh, Y. Miyashita, T. Ogihara, *Biochemical and Biophysical Research Communications* **1989**, *164*, 1003.
- [86] S. B. Hladky, D. A. Haydon, *Biochimica Et Biophysica Acta* **1972**, *274*, 294.
- [87] W. Veatch, L. Stryer, *Journal of Molecular Biology* **1977**, *113*, 89.
- [88] D. W. Urry, *Proceedings of the National Academy of Sciences of the United States of America* **1971**, *68*, 672.
- [89] J. A. Killian, *Biochimica Et Biophysica Acta* **1992**, *1113*, 391.
- [90] V. B. Myers, D. A. Haydon, *Biochimica Et Biophysica Acta* **1972**, *274*, 313.
- [91] C. Rossi, J. Homand, C. Bauche, H. Hamdi, D. Ladant, J. Chopineau, *Biochemistry* **2003**, *42*, 15273.

Appendix

Materials & Buffers

All the chemicals were purchased from Sigma (Steinheim, Germany) and were used without further purification.

DPhyPC is a commercial lipid from Avanti Polar Lipids (Alabaster, AL, USA)

Acetic acid was distilled before use.

AIBN was recrystallized in ethanol.

THF was dried over potassium benzophenone complex.

The following TLC developers were used throughout this work :

- "Zuckerreagenz": Resorcinmonomethylether and sulphuric acid mixture in ethanol 1/1
- Phosphomolibdic acid

For all aqueous solutions throughout the second part of this work, water from a Millipore purification system (Millipore GmbH, Eschborn, Germany) was used, which had a specific resistance of $> 18 \text{ M}\Omega\text{cm}^{-1}$.

In this study, several electrolyte compositions were used as buffer solutions:

NaCl buffer, a 0.1 M aqueous solution of sodium chloride

KCl buffer, a 0.1 M aqueous solution of potassium chloride

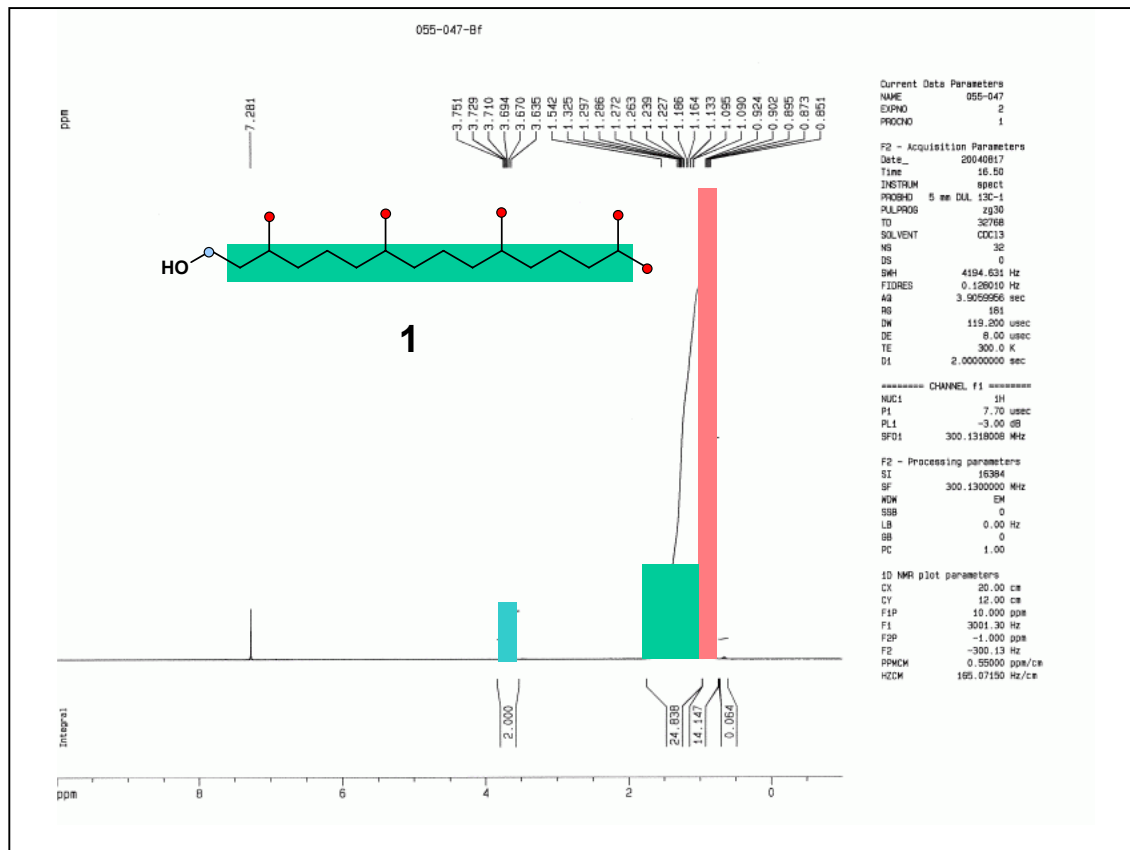
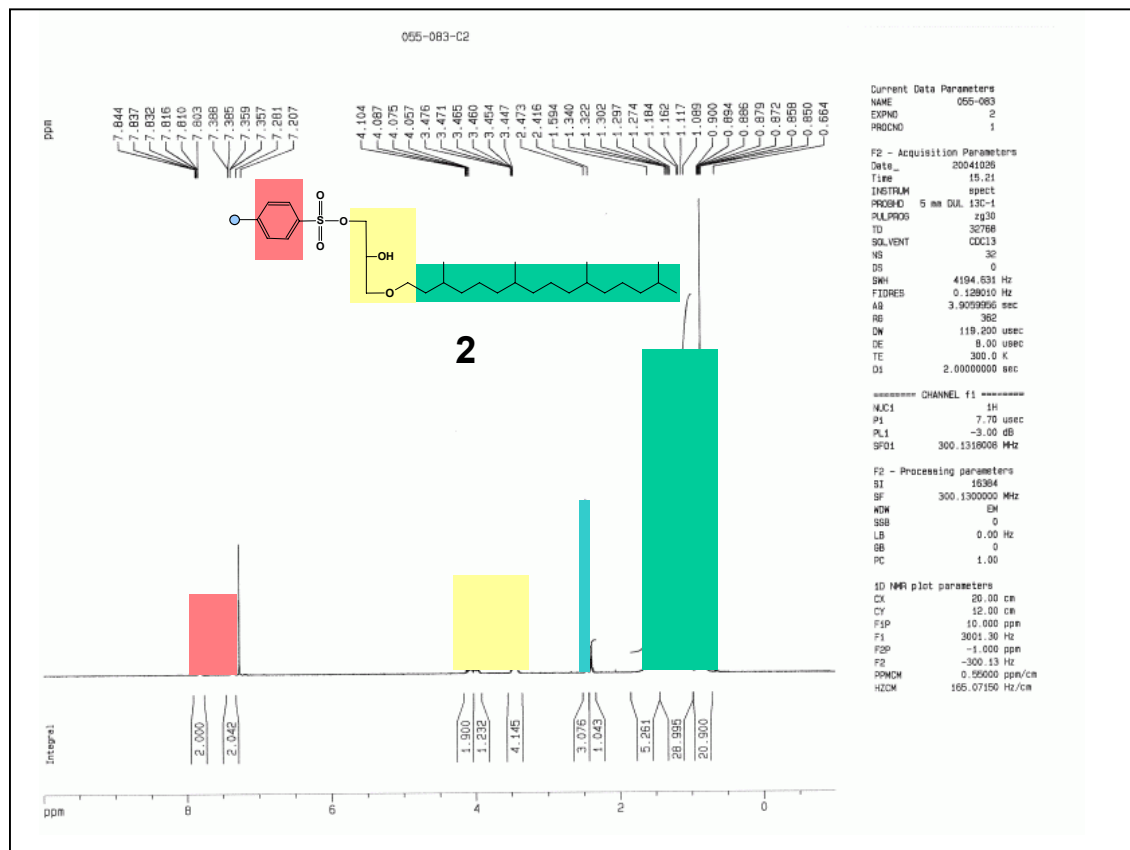
TMAC buffer, a 0.1 M aqueous solution of tetramethylammonium chloride

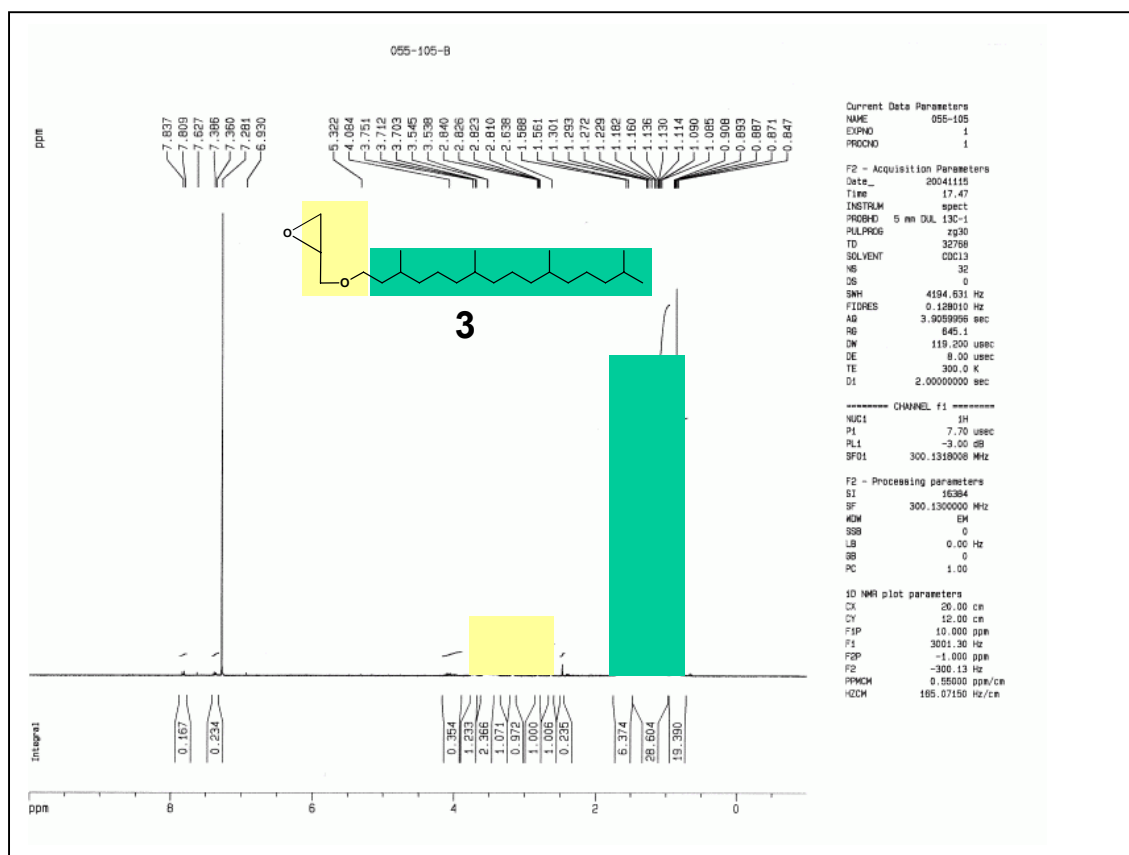
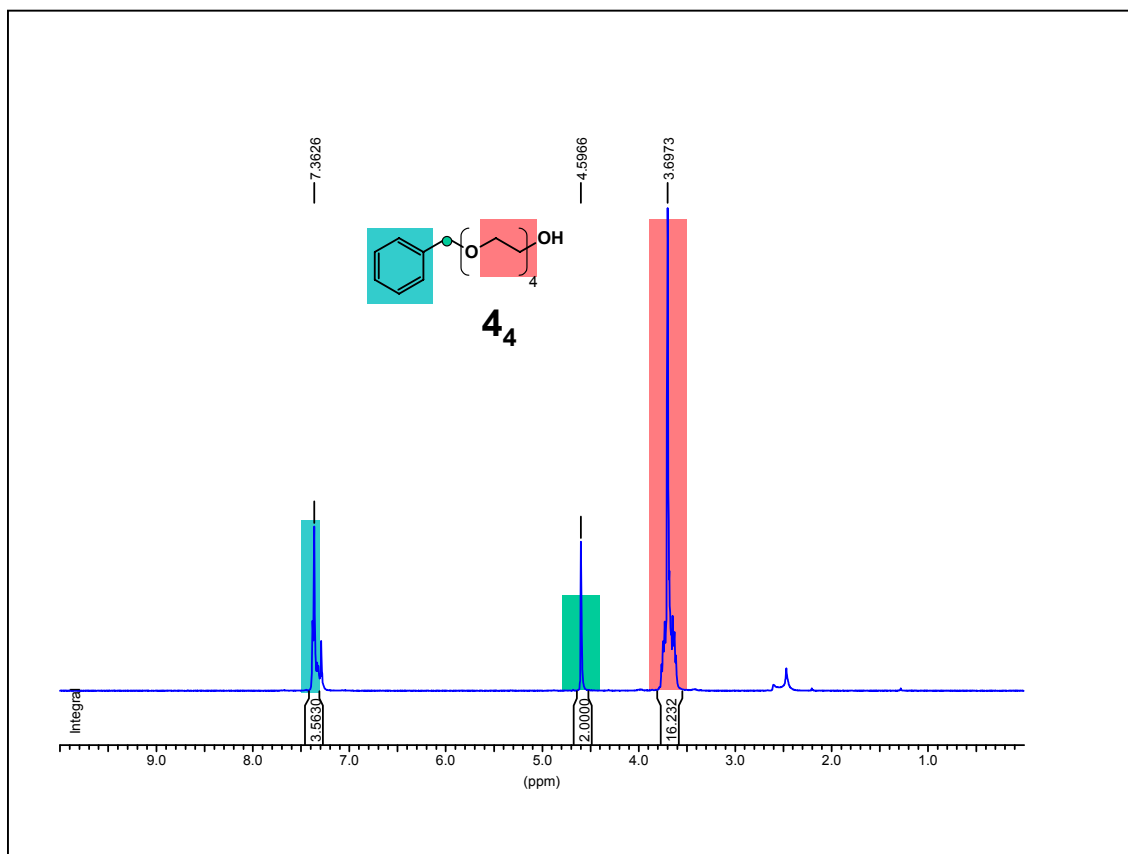
HEPES buffer, 0,1 M HEPES, and 0,04 M KCl at pH = 7,4

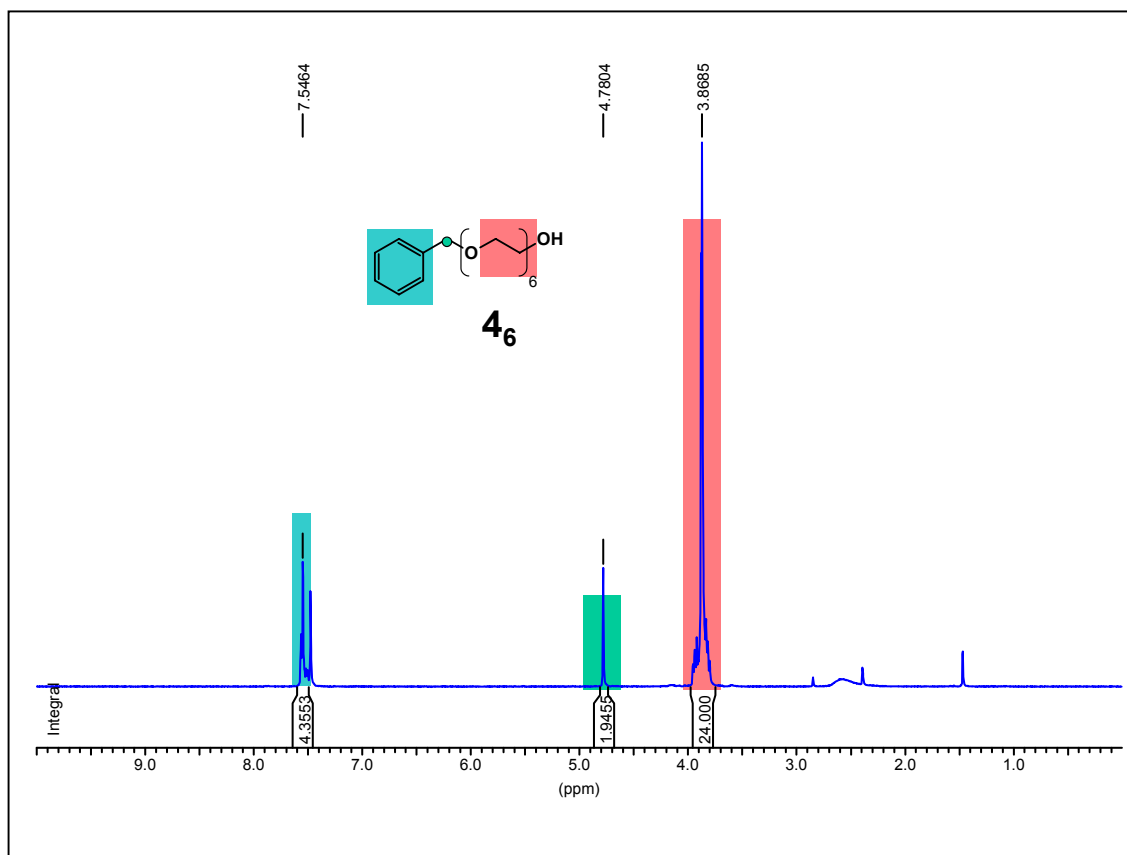
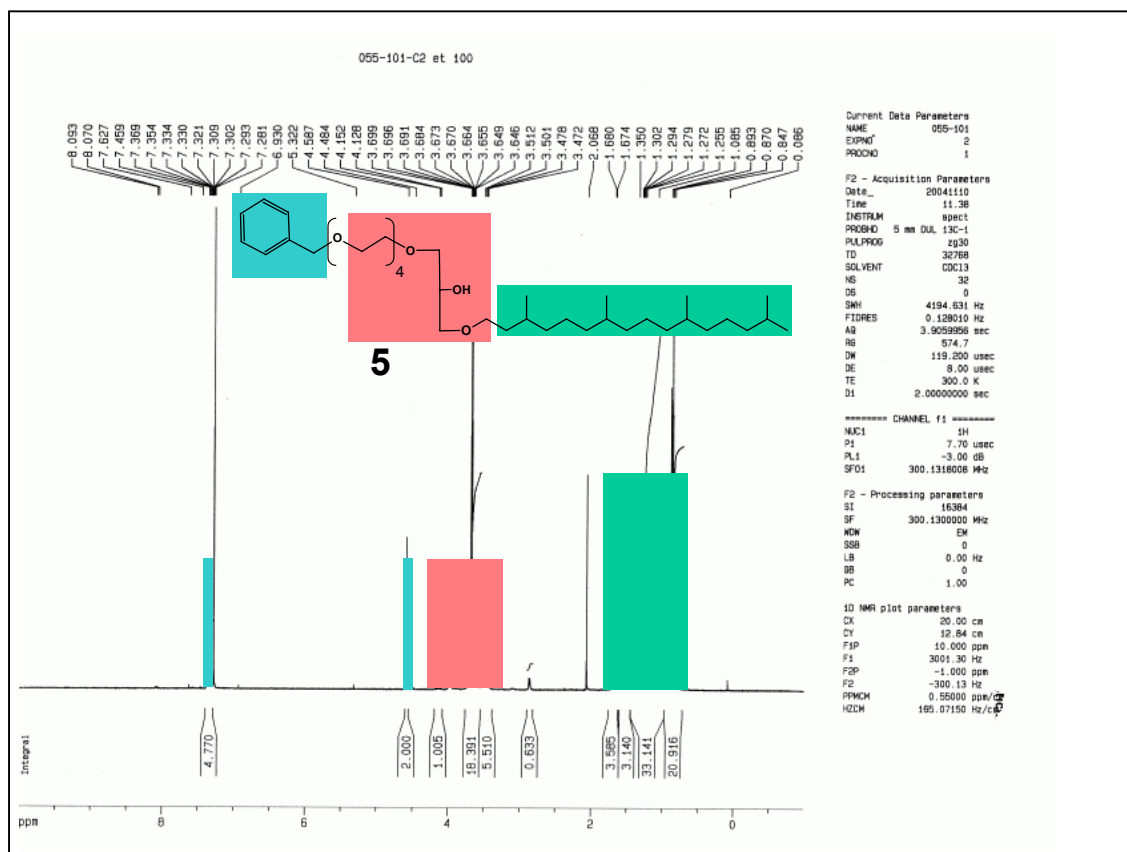
FD-MS/NMR spectra

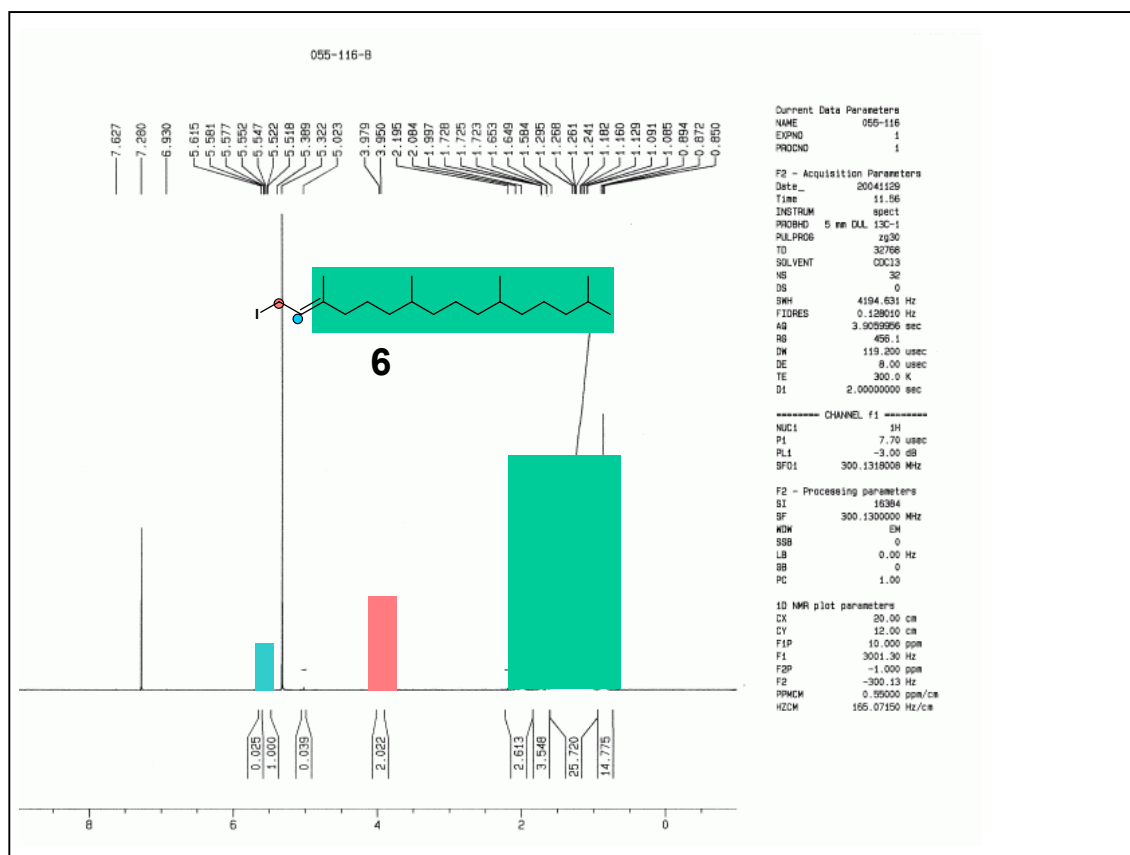
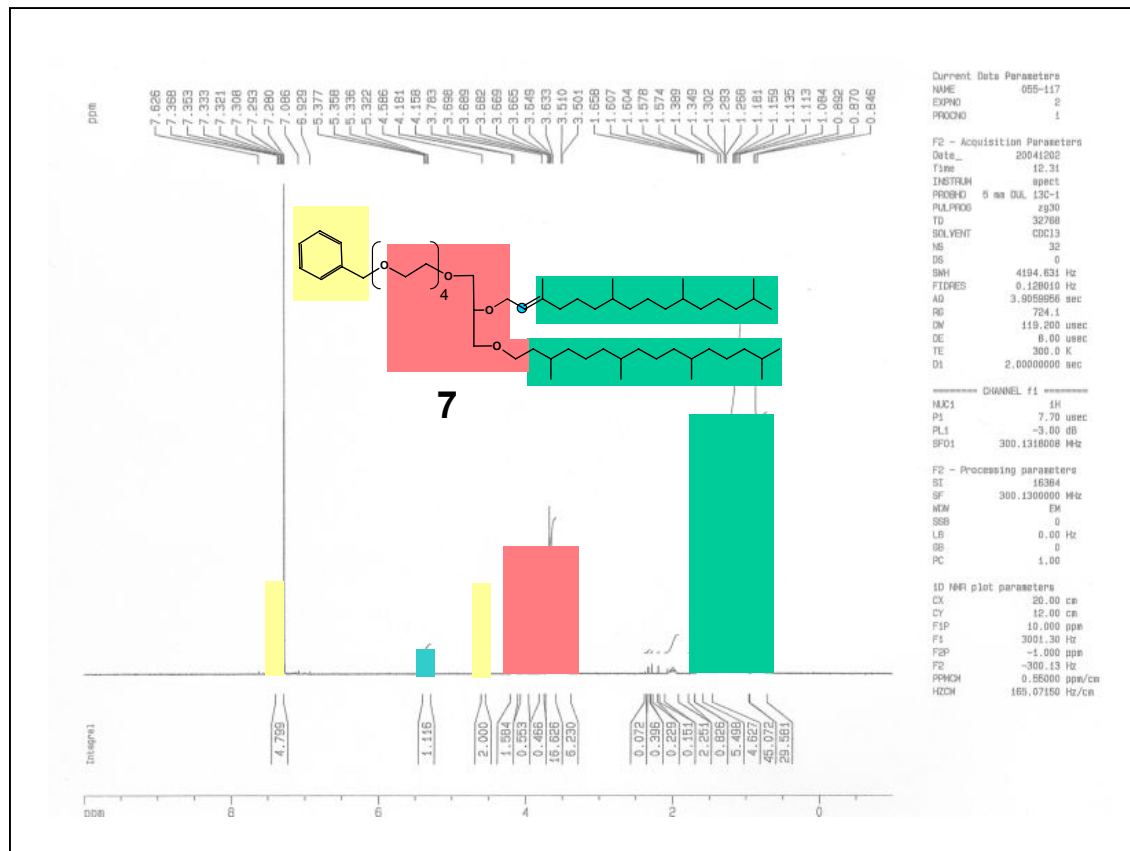
In the following NMR spectra, the attribution of the peaks is shown via a color code. For each different series of products, only one NMR spectrum is shown. The spectra obtained for the different products in a series are similar.

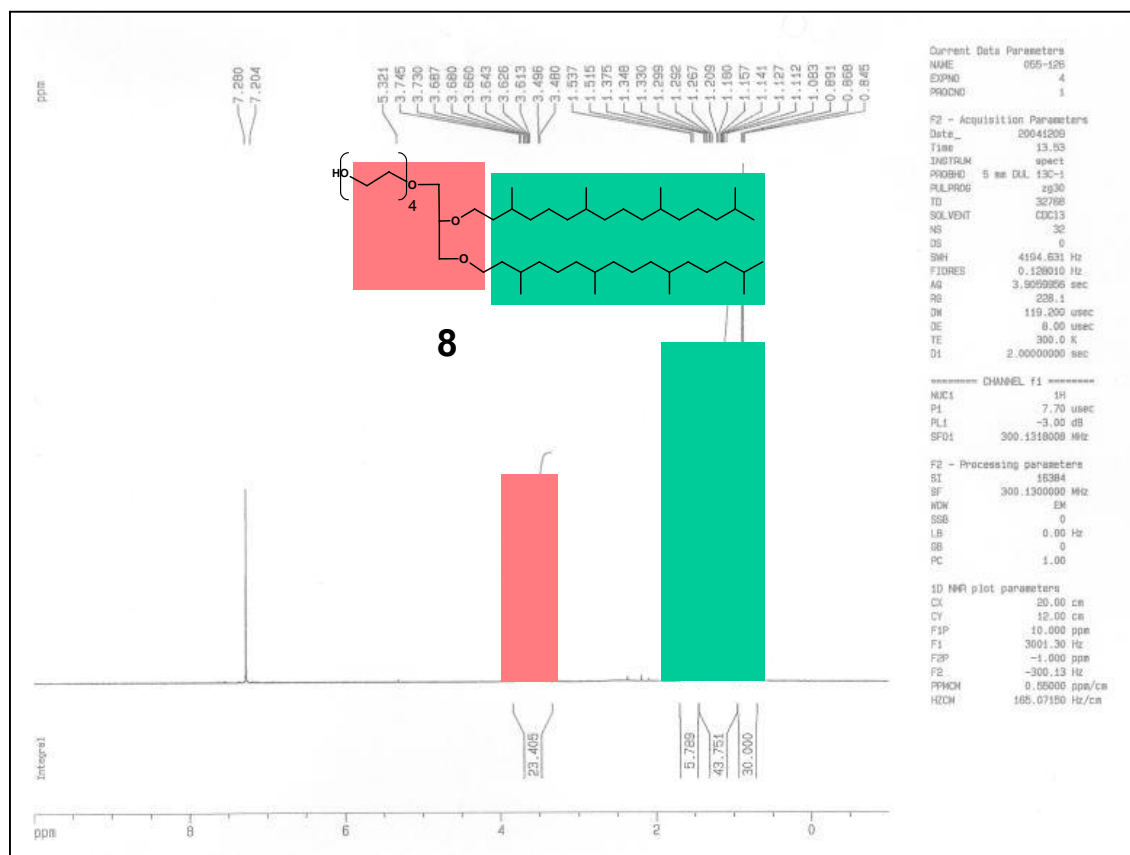
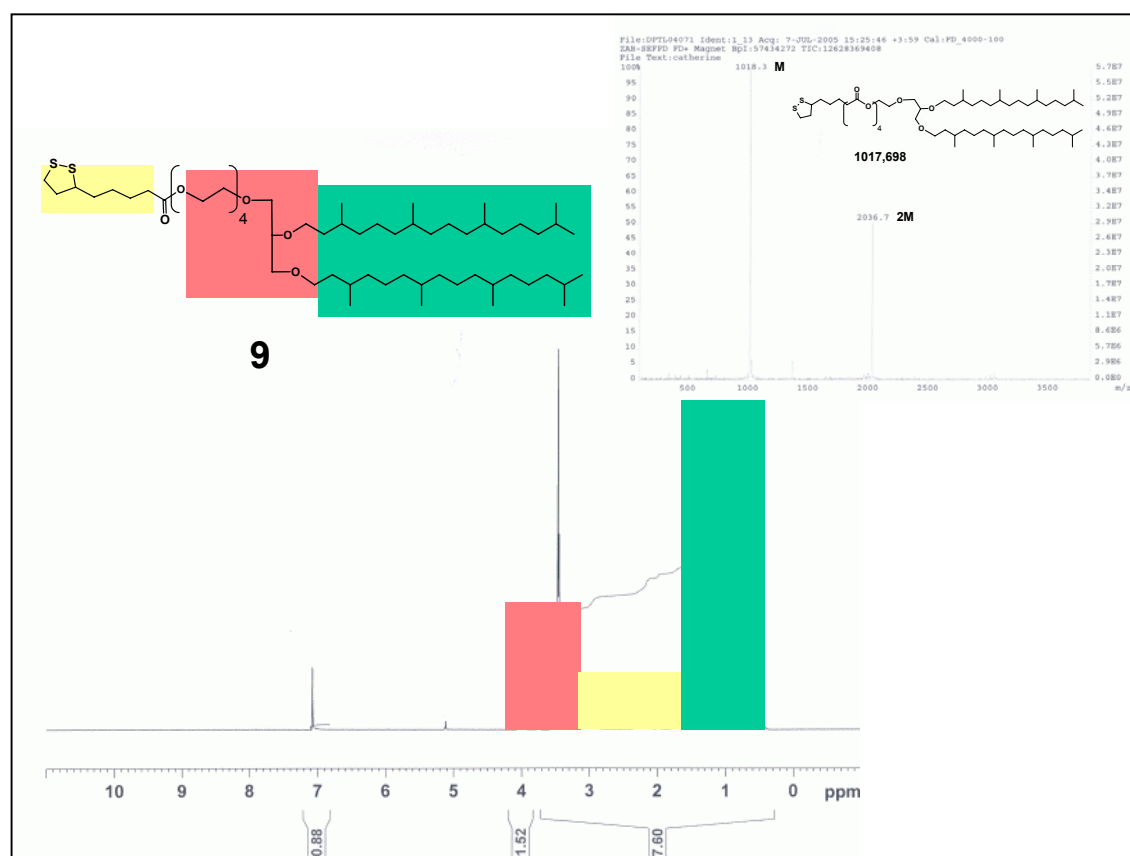
For the products synthesized in Diverchim, no FD-MS spectrum is available.

Figure 69: ^1H NMR spectrum of Phytanol 1.Figure 70: ^1H NMR spectrum of 2

Figure 71: ^1H NMR spectrum of **3**Figure 72: ^1H NMR spectrum of **44**

Figure 73: ^1H NMR spectrum of **4**Figure 74: ^1H NMR spectrum of **5**

Figure 75: ^1H NMR spectrum of 6Figure 76: ^1H NMR spectrum of 7

Figure 77: ^1H NMR spectrum of **8**Figure 78: ^1H NMR and FD-MS spectra of **9**

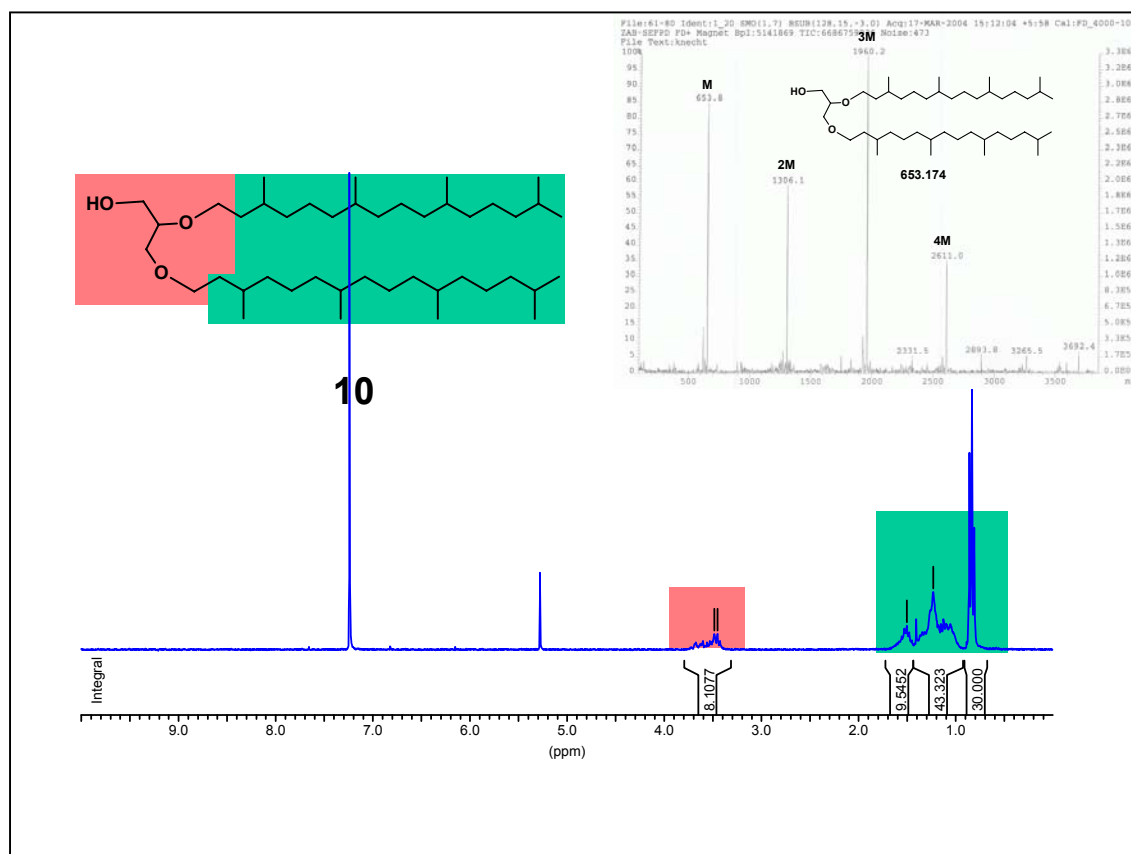


Figure 79: Synthetic route and ^1H NMR and FD-MS spectra of **10**

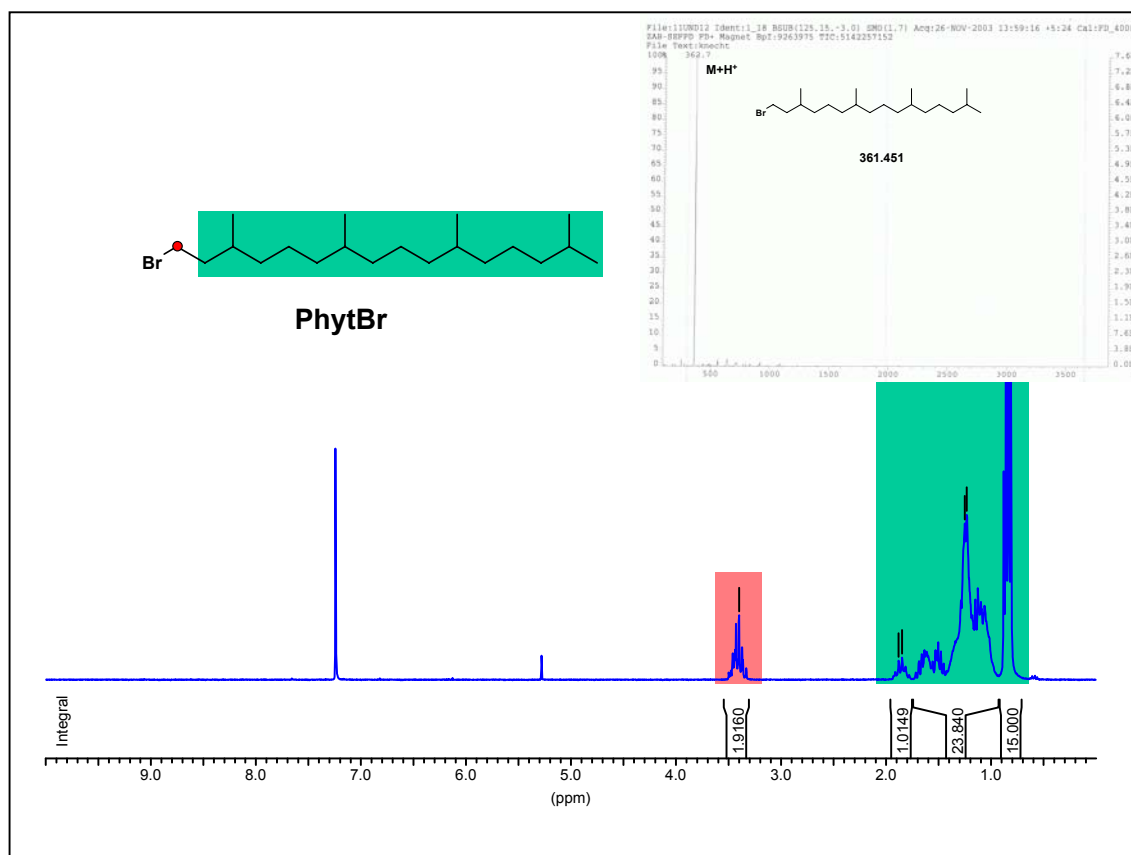


Figure 80: ^1H NMR and FD-MS spectra of Phytanyl bromide

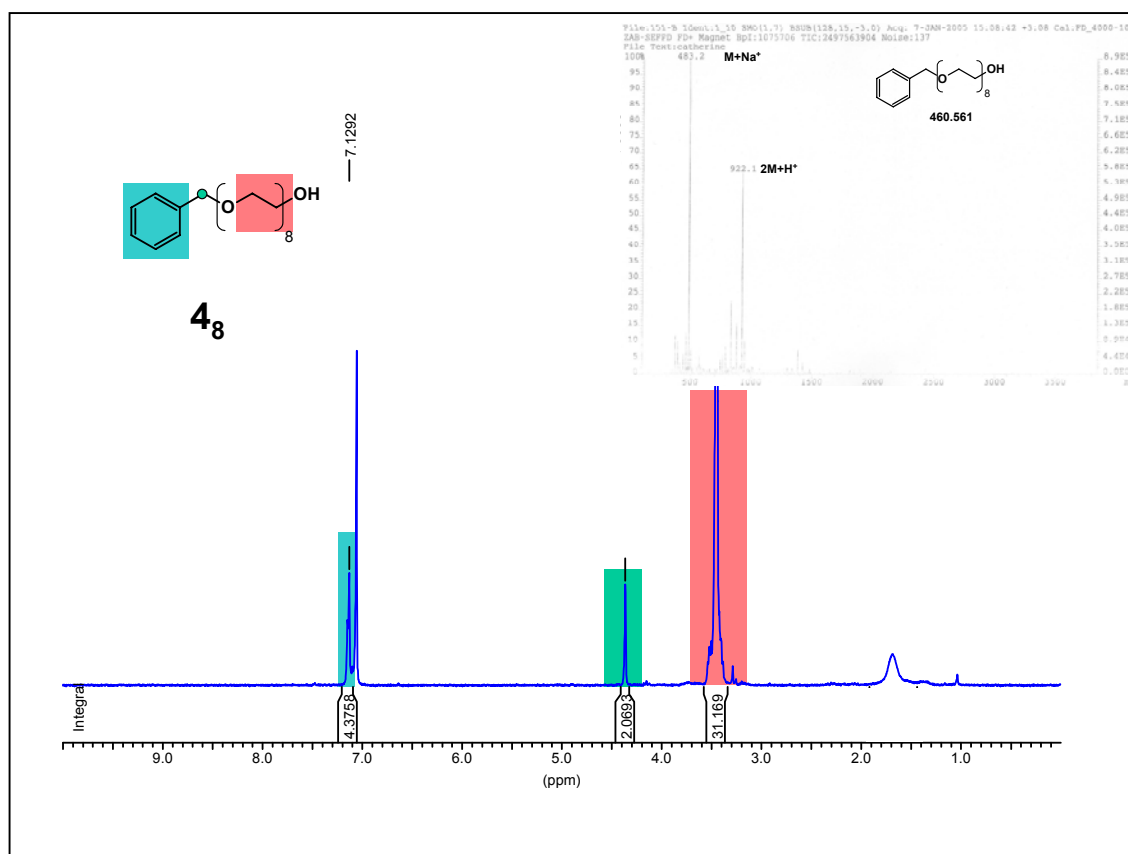


Figure 83: ^1H NMR and FD-MS spectra of 4_8 via deprotection of THP group

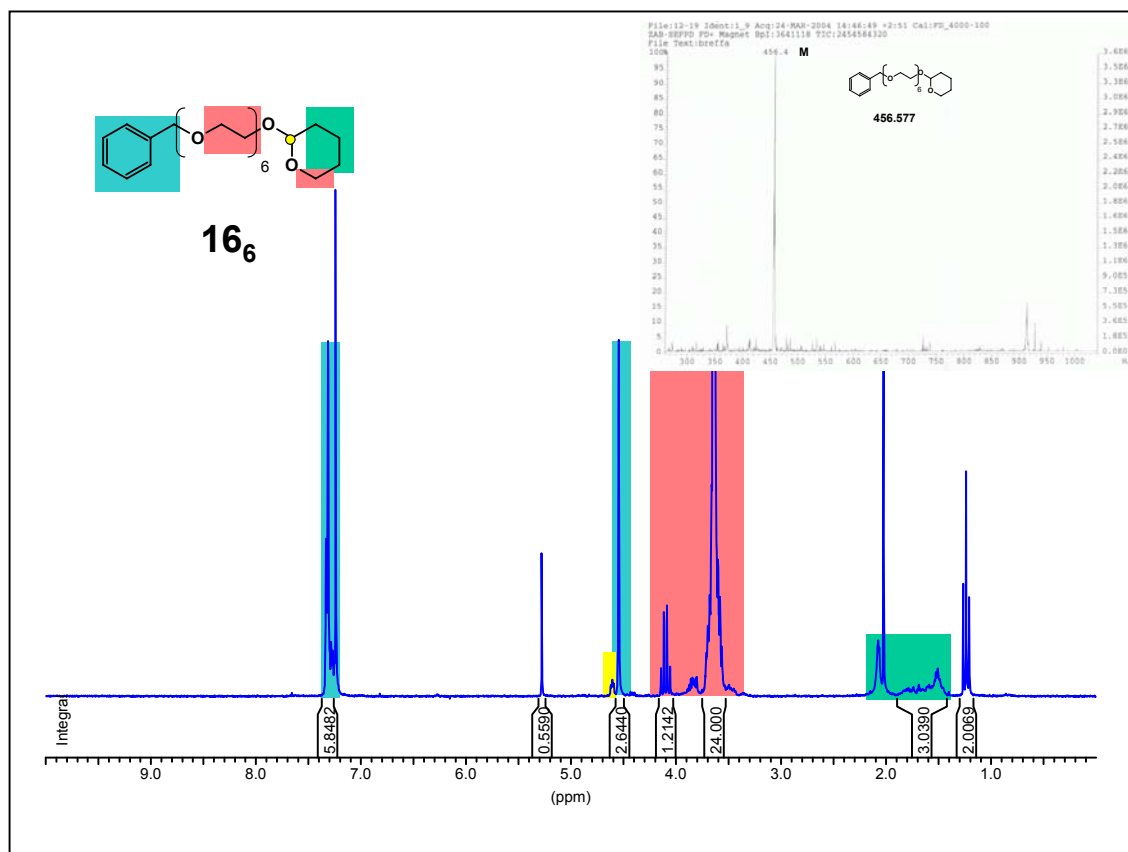
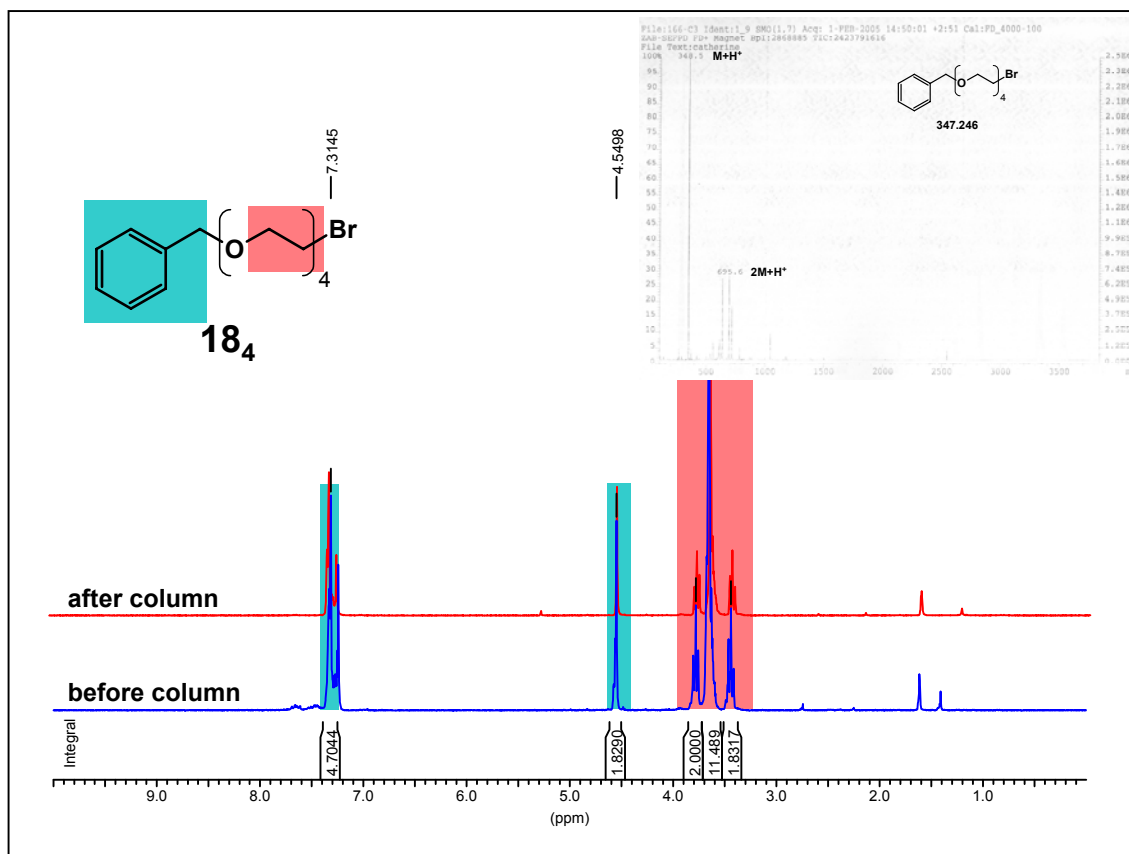
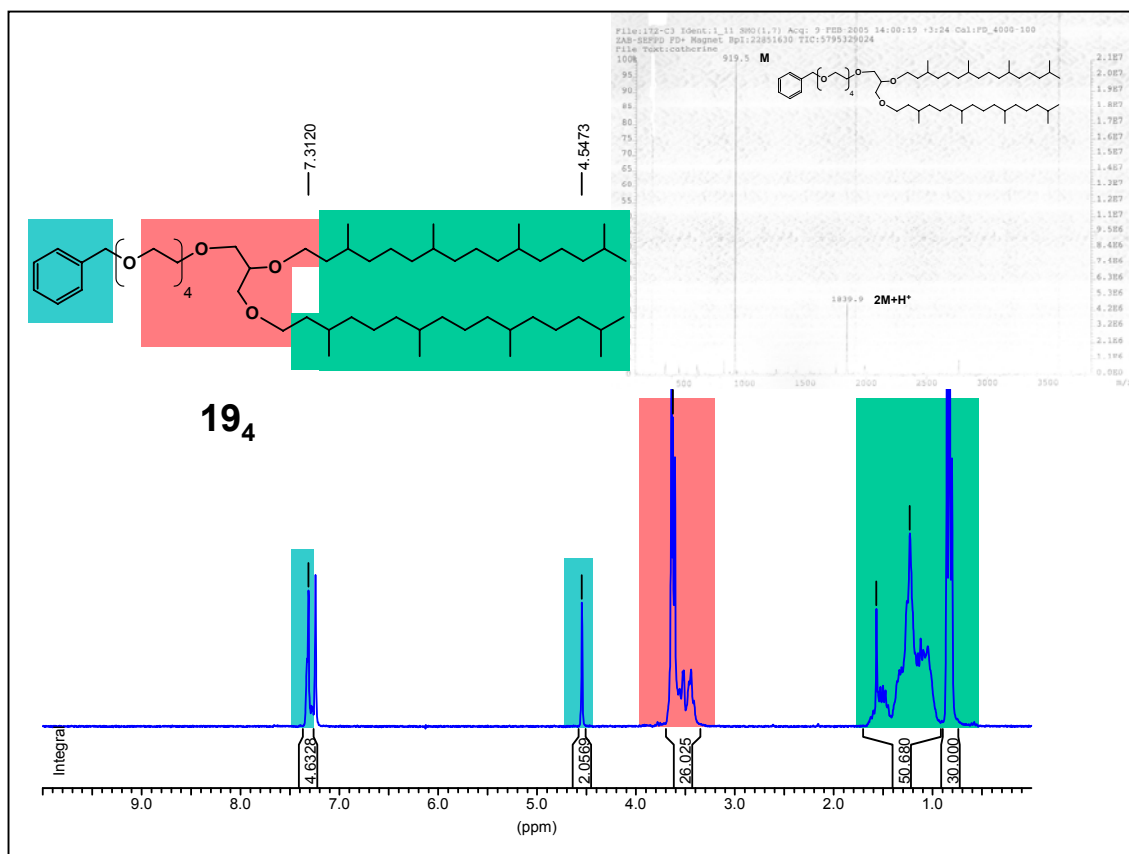


Figure 84: ^1H NMR and FD-MS spectra of 16_6

Figure 85: ^1H NMR spectrum of 18_4 Figure 86: ^1H NMR spectrum of 19_4

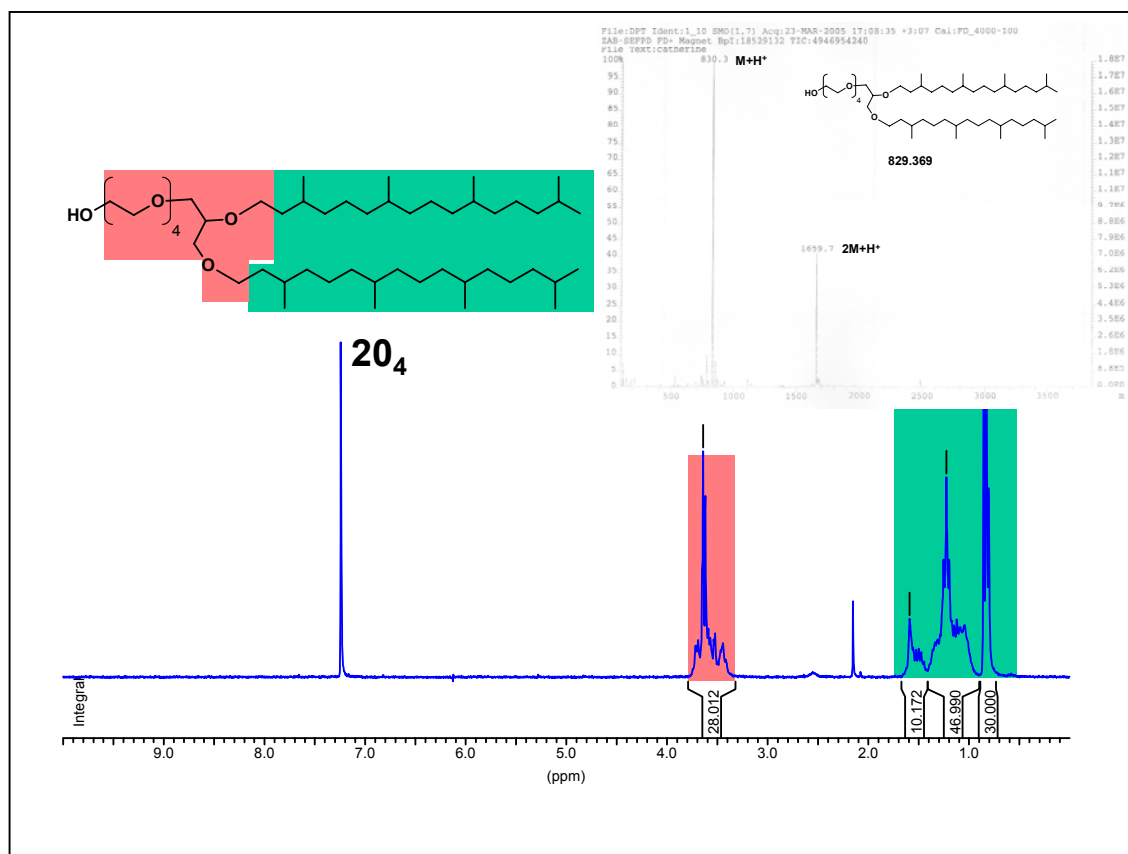


Figure 87: ^1H NMR spectrum of **204**

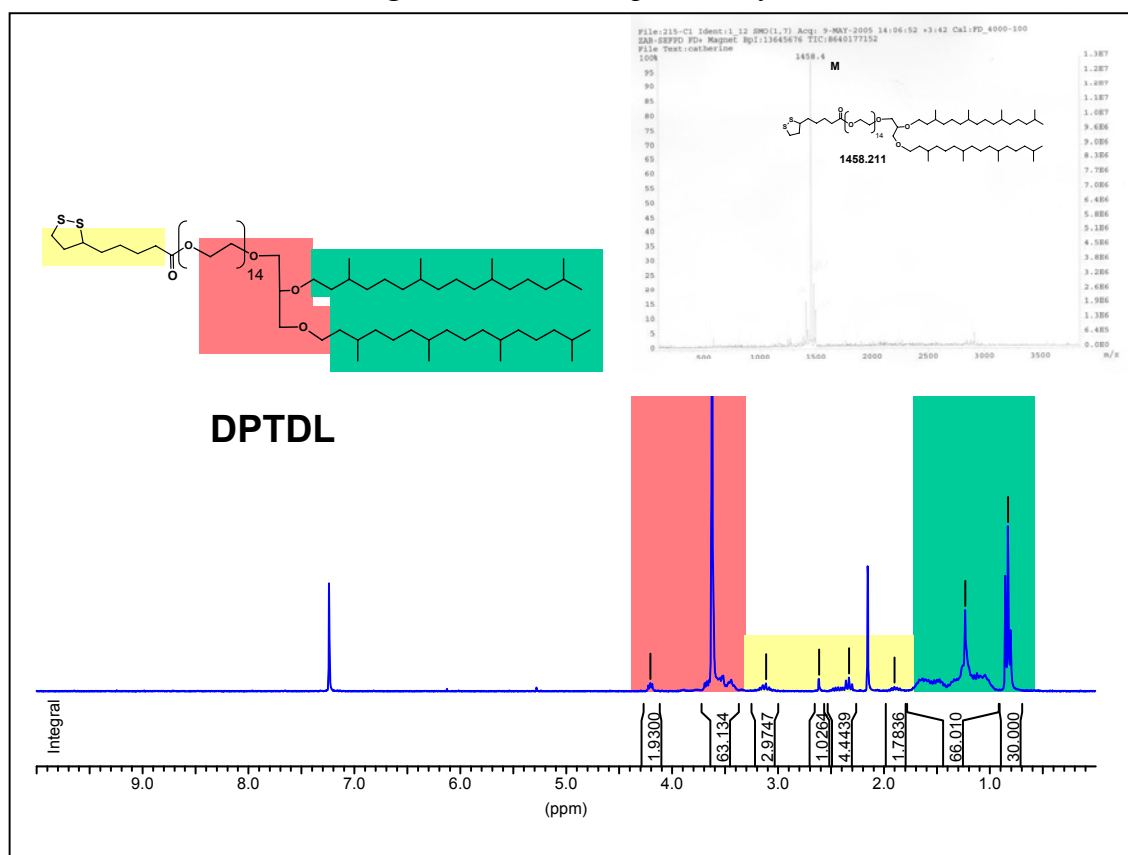


Figure 88: ^1H NMR spectrum of **DPTDL**

Curriculum vitae

Personal Data

Name: Catherine Breffa
Date of Birth: March 24, 1979
Nationality: French

Education

- 2002-2005** **PhD in Chemistry**
Max Planck Institute for Polymer Research, Mainz, Germany
Johannes Gutenberg Universität, Mainz, Germany
- 2001-2002** **DEA (Diplôme d'Etudes Approfondies) in Physics and Chemistry of Surfaces, Colloids and Polymers**
Institut Charles Sadron, Strasbourg, France
Université Louis Pasteur, Strasbourg, France
- 1999-2002** **Diplôme d'Ingénieur Chimiste**
MSc Chemical Engineering, specialty Material Sciences
ECPM (Ecole Européenne de Chimie, Polymères et Matériaux) Strasbourg, France

Publications

1. "In situ investigations of the formation of mixed supported lipid bilayers close to the phase transition temperature", Seantier B, Breffa C, Felix O, Decher G, *NANO LETTERS* 4 (1): 5-10 **2004**
2. "Spacer length variation on tethered bilayer lipid membranes: synthesis and influence on the electrical properties", Breffa C, Koeper I, Knoll W, *in preparation*

Acknowledgements

Many thanks to Professor Knoll for allowing me to perform my research in his group, and giving me the opportunity to enlarge my horizons. I really appreciated his trust in me and the fact that I was allowed to go all over the world to present my results.

Thanks to Ingo and Stefan for the help with the difficult scientific questions, and the others. Special thanks to Ingo for his support and his advice while reading my thesis.

Thanks to the Knoll group, with a special thought for my colleagues in office 1.503 (the office of the year 2005), for being my family during these three years, and for feeding, entertaining, and bothering me when I needed it.

Thanks Amel and Danica, who were so kind to read this work and help to improve the English level and to clear the concepts described here.

Merci à Jean-Louis Brayer et son équipe pour l'accueil chaleureux que j'ai reçu pendant mes quatre mois à Diverchim, ainsi que les précieux conseils au labo.

Thanks to Guillaume, Anton, and others for making my life brighter in the moments of weakness.

Merci à mes parents et à mes soeurs chéris, ainsi qu'à Mamema et Babeba pour leur soutien inébranlable.

Merci Seb, pour tout.

Vielen Dank, Mariuzs, dass Du soviel Zeit mit mir auf verschiedenen Tanzflächen geschwitzt hast.

Merci à tous ceux qui ont croisé ma route et ont contribué à ce que je devienne celle que je suis.

And finally, thanks to all people who changed my life, for the better, or for the worse.